AD-A130 508 PROCEEDINGS OF THE SYMPOSIUM ON FLUID-SOLID SURFACE INTRACTIONS (2ND) HEL..(U) DAVID W TAYLOR NAVAL SHIP RESEARCH AND DEVELOPMENT CENTER BET.. H J LUGT

1/2

UNCLASSIFIED 29 NOV 74 F/G 5/2 NL

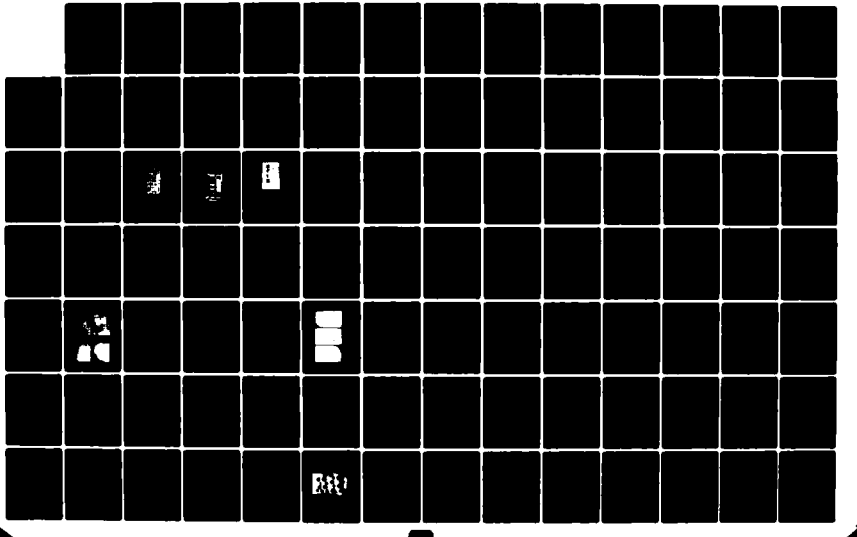

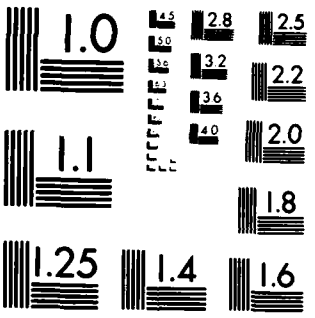

Proceedings

Second Symposium

FLUID-SOLID SURFACE INTERACTIONS

June 5-6, 1974

NAVAL SHIP RESEARCH AND DEVELOPMENT CENTER
Bethesda, Maryland

PROCEEDINGS

SECOND SYMPOSIUM
FLUID-SOLID SURFACE INTERACTIONS

Sponsored and Hosted by

Computation and Mathematics Department
Naval Ship Research and Development Center

June 5--6, 1974

Hans J. Lugt
Editor

LIBRARY OF CONGRESS
Number 75-602584

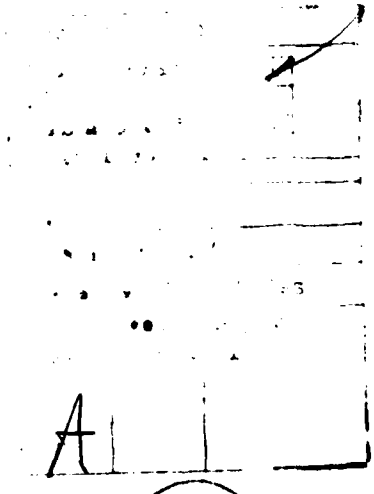

NAVAL SHIP RESEARCH AND DEVELOPMENT CENTER
Bethesda, Maryland

PREFACE

The Second Symposium on Fluid-Solid Surface Interactions was held at the Naval Ship Research and Development Center, Bethesda, Maryland on June 5-6, 1974. This symposium also represented the first official meeting between the U.S. Navy and the Ministry of Defense of the Federal Republic of Germany on the Data Exchange Agreement on "Fluid-Solid Surface Interactions." The first symposium on this subject took place at Meersburg, Germany on May 3-5, 1972, sponsored by the German Ministry of Defense and organized by Dornier System, GmbH, Friedrichshafen. The encouraging results of the Meersburg meeting resulted in a recommendation that an exchange agreement be established to coordinate, intensify, and exploit the research effort directed toward future engineering applications of solid-surface treatment.

The increasing interest in fluid-solid surface interactions is due to the rapid progress in the physics and chemistry of solid surfaces over the last decade. This progress was, in turn, made possible by advances in vacuum technology, in methods of obtaining clean surfaces, and by development of improved measuring techniques such as low-energy electron diffraction (LEED) and Auger spectroscopy. In addition to the sciences of surface physics and surface chemistry, the sciences of rarefied gas dynamics, hydrodynamics, rheology, solid-state physics, and biophysics all share a common interest in fluid-solid surface interactions.

The theoretical approach to the understanding of such interactions is different for the gaseous and the liquid phases. The bulk of the literature is concerned with gas-solid surface interactions, but relatively little work has been published in the field of liquid-solid surface interactions. The possible engineering applications with enormous potential benefits range from heterogeneous catalysis, wettability, prevention of corrosion and biological deposits to drag reduction and heat-transfer

control. The involvement of such a variety of research fields and the wide area of applications demand that an inter-disciplinary approach be taken. The two symposia and the establishment of the Data Exchange Agreement were, therefore, attempts to bring together some of these wide-spread areas so that each working group could benefit from the experience of others in the various specialized fields.

In these Proceedings the historical background of the Data Exchange Agreement is outlined in the article by Professor A. Walz. The symposium itself was divided into two sessions. The first dealt with the molecular interactions of gases and solids; the second was devoted to the continuum aspect of fluid-solid surface interactions and to the problems of liquid-solid interactions. The seeming dichotomy between these two sessions was bridged by the common effort to study the properties of solid surfaces and to develop techniques for treating solid surfaces.

I would like to thank Mr. G. Gleissner, Head of the Computation and Mathematics Department, and Mrs. J.W. Schot, Head of the Fluid Flow Applications Branch, for their support before and during the symposium. I am grateful to Mrs. A. Phillips for her assistance in editing the Proceedings. Thanks are also due to Mrs. B. Schultz, Mrs. A. Centineo, and Miss E.A. O'Bryant who did the bulk of the organizational work.

Hans J. Lugt

November 29, 1974
Naval Ship Research and Development Center
Bethesda, Maryland 20084

CONTENTS

LIST OF PARTICIPANTS

Gronau, K.H. Von Halem, H.	Bundesministerium der Verteidigung, RüFo 4, 53 Bonn 1, Federal Republic of Germany
Walz, A.	Technische Universität Berlin, 1 Berlin 10, Federal Republic of Germany
Bärwinkel, K. Hoff, G. Rieger, H. Seidl, M.	Dornier System GmbH, 799 Friedrichshafen, Federal Republic of Germany
Bossel, U.G. Geissler, W. Meier, H.U. Rotta, J.C.	Deutsche Forschungs - und Versuchsanstalt für Luft - und Raumfahrt, AVA, 34 Göttingen, Federal Republic of Germany
Papenfuss, H.D.	Ruhr - Universität Bochum, 463 Bochum, Federal Republic of Germany
Wirz, H.J.	Von Kármán Institute for Fluid Dynamics, Rhode-St-Genese, Belgium
Huth, J.H.	Naval Sea Systems Command Hqs., NC #3, 2531 Jefferson Davis Highway, Arlington, Virginia 20376 USA
Gillerlain, J. McClure, C.F. Rogers, J.	Naval Ordnance Laboratory, White Oak, Silver Spring, Maryland 20910 USA (Now, Naval Surface Weapons Center)
Jarvis, N.L. Ting, R.Y.	Naval Research Laboratory, Washington, D.C. 20375 USA
Lea, G.K.	National Science Foundation, 1520 H St., Washington, D.C. 20550 USA
Frankl, D.R.	The Pennsylvania State University, University Park, Pennsylvania 16802 USA
Cuthill, J. Klein, R. Madey, Th. Oser, H.J.	National Bureau of Standards Washington, D.C. 20234 USA
Park, J.J. Schmid, L.A. Staugaitis, C.L.	National Space Administration, Goddard Space Flight Center, Greenbelt, Maryland 20771 USA

Allen, R.C.
Belt, J.R.
Cuthill, E.H.
Furey, R.J.
Gilbert, D.
Gleissner, G.H.
Granville, P.
Haussling, H.J.
Lugt, H.J.
McCarthy, J.
Nelson, P.W.
Schot, J.W.
Schrader, M.E.
Tai, T.C.
Whitehead, R.E.

Naval Ship Research and Development Center
Bethesda, Maryland 20084 USA

INTRODUCTORY REMARKS

K. H. Gronau
German Ministry of Defense

As the administrative project officer and representative of the German Ministry of Defense I should like to cordially thank first of all Captain Nelson* on behalf of all German participants for the courteous words of his opening address of this symposium. The initiative for the cooperation between the USA and the Federal Republic of Germany in the field of fluid-solid surface interactions was taken in 1971 by Dr. Lugt at the Naval Ship Research and Development Center (NSRDC). On the German side it was primarily the firm of Dornier System which, supported by the Federal Ministry of Defense, organized the first international special symposium on fluid-solid surface interactions at Meersburg/Bodensee in May 1972. On this occasion the NSRDC work was presented for the first time. In Germany work in the field of interface physics and gas-surface interactions has been encouraged by the Federal Ministry of Defense for several years now and has concentrated on aerodynamic friction, heat transition by convection, adsorption of oxygen molecules from the gas phase at the surface of a solid, desorption of gas at surfaces, and the special problems connected with catalysts.

These discussions between representatives of NSRDC and DORNIER SYSTEM gave rise to the wish for closer cooperation in the exchange of research results. Since the appropriate military agencies in the USA and in the Federal Republic of Germany were informed of these exploratory talks, the possibility soon

---

* Commanding Officer, Naval Ship Research and Development Center, who welcomed Symposium participants to the Center.

appeared of concluding, at government level, a military data exchange agreement including additional USA and German research institutes. After a few administrative obstacles had been surmounted, this DEA was signed in 1973 by the responsible government agencies.

I have special pleasure in stating that the first meeting under this DEA takes place at the Naval Ship Research and Development Center, since the initial impulses for the cooperation, too, emanated from this Center.

I hope that this symposium will give you a review of the most recent work and, based on the technical discussion, will have a stimulating effect on the further extension and exchange of research data in this field.

In conclusion let me thank the NSRDC, especially Dr. Lugt for his preparations for this joint symposium which will to a considerable extent contribute to ensuring the anticipated success for all participants.

HISTORICAL BACKGROUND

A. Walz
Technische Universität Berlin

Most known technical problems of fluid mechanics involve a relative velocity between fluid and solid surfaces. The conservation laws of fluid mechanics, however, involve only the properties of the fluid (such as density, viscosity, heat conductivity, and specific heats). The solid surface influences the fluid motion mainly by its displacement effect (its body shape) which is described by potential flow theory. At the beginning of this century Prandtl introduced the boundary layer concept in order to include adhesion at the solid surface as an important additional boundary condition. With the introduction of this parameter of fluid-solid surface interaction within the molecular or atomic contact layer, the theoretical prediction of surface friction drag became possible.

The important question, however, is whether the adhesion and the related friction drag can be reduced by a suitable choice of solid-surface material and/or by a special treatment of the surface. This question could not have been investigated systematically by theoretical or empirical means until a few decades ago.

A research proposal worked out by the firm Dornier System in 1966 for the German Ministry of Defense may be considered typical and basic for further research on the following topic:

> Objective: To find a solid surface material with as large a value as possible for the sound wave resistance $a_s = \sqrt{\rho E}$ (ρ = density, E = modulus of elasticity). In the limiting case $a_s \to \infty$ a total reflection of the gas molecules at the solid surface is expected and consequently the transfer

of tangential momentum (i.e., friction drag) and heat vanishes.

It may be of interest to note here that similar ideas for research have been published almost simultaneously in the USA, France, Italy, and USSR. This basic research idea resulted in a guideline for discovering suitable solid surface materials, especially those with high atomic weight. However, the fact that the surface of all selected materials is contaminated with deposits from chemical reactions occurring between this surface and air components such as oxygen, nitrogen, and carbon dioxide was discouraging. Thus, the fluid-solid surface interaction is not controlled solely by the properties of the metal itself. The gas molecules strike these contamination layers which are characterized by low densities, low values of sound wave resistance a_s, and undesirable roughness. The only way to overcome these difficulties was to find methods of removing these contamination layers and treating the solid surface so that it becomes resistant to chemisorption and physical adsorption.

After this important look into the mechanism of fluid-solid surface interaction, projects were undertaken in solid surface structure analysis and the development of cleaning procedures, especially of mono-crystal surfaces of high molecular weight. Modern physical techniques such as Auger Spectroscopy, Low Energy Electron Diffraction, and Secondary Ion Mass Spectroscopy were used or modified for these purposes.

Simultaneously, theoretical efforts were started by specialists in the field of kinetics of gases and their interaction with well-defined solid surfaces. The aim of this research group was to develop calculation methods for the accommodation coefficients α, starting with special modes of surface structure and molecule interactions. With sets of these α-coefficients the phenomenon of adhesion and slip may be physically described with more or less accuracy. These

theoretical efforts provided necessary support for further empirical work.

These activities in the molecular physics field were accompanied by theoretical investigations in the field of continuum mechanics aimed at developing information about the effects of slip boundary conditions on the continuum flow (i.e., on friction, heat transfer, and pressure distribution). As is well known, such investigations may be performed on the basis of the Navier-Stokes equations, in connection with an energy balance equation if compressibility must be taken into account.

At that time the Computation and Mathematics Department of the Naval Ship Research and Development Center had already done important work on numerical solutions of the Navier-Stokes equations for other projects, such as the DEA "Boundary Layer Effects" Annex No. AF-68-G-7416, 18 June 1968, which is closely related to the present DEA.

During 1972 Dornier System made a survey of interdisciplinary slip-research activities. The encouraging results of this survey led to the idea of an international meeting to promote discussion and criticism by an interdisciplinary audience. This meeting was sponsored and organized by the German Ministry of Defense and Dornier System, and some cooperating international establishments and specialists. It was held at Meersburg, Germany, from 3-5 May 1972. The program of this meeting, now called the First Symposium on Fluid-Solid Surface Interaction, is attached as an Appendix to these Proceedings for information. Some of the papers of that first symposium are characteristic of the state of the art of slip-research at that time. They are listed below as follows:

"Analysis and Cleaning of Solid Surfaces".

M. Seidl (Dornier System) was successful in cleaning a Cu-monocrystal surface approximately one cm square by bombarding it with ions of argon and finally covering

it with a deposit of carbon such that the surface became resistent to contaminating deposits as mentioned above.

M.E. Schrader (Naval Ship Research and Development Center) presented his own experimental results (Journ. of Phys. Chemistry 1970) with gold surfaces which, in conjunction with Seidl's results, may indicate that gold has substantial advantages for realizing slip-surface conditions (see Seidl's paper in these Proceedings which confirms Schrader's conjecture).

"Theoretical Approaches and Experiments on Accommodation Coefficients for Momentum and Energy".

For the special case of Gas-Solid Surface Interaction, W.J.C. Müller and K. Bärwinkel (Dornier System) have developed modes and related statistical theories of adsorption which may permit the calculation of accommodation coefficients. For low values of the accommodation coefficient of energy α_e, the requirement for surface smoothness is far less restrictive than for low values of α_m, the accommodation coefficient of momentum. Measurements of α_e in the order of magnitude 10^{-2} presented by D. Menzel and J. Kouptsidis (Technical University of Munich) may be considered a confirmation of the theoretical values. On the basis of their own measurements, D. Menzel and J. Kouptsidis expected that by further surface preparation an accommodation coefficient of energy in the order of magnitude 10^{-4} would be achievable.

"Investigations based on continuum mechanics of the effects of surface slip on the flow field".

By comparing numerical solutions of the Navier-Stokes equations for the extreme boundary conditions of nonslip and perfect slip, H.J. Lugt (Naval Ship Research and Development Center) proved that, even in the case of

perfect slip, the Kutta-Joukowsky circulation flow necessary for lift is established after a very short time (which is not self-evident).

In addition to these special reports on results of work directed to drag and heat transfer reduction, other research related to fluid-solid surface interaction was discussed in detail. Heterogeneous catalysis, corrosion, anti-fouling, and procedures for construction in sea-water were pointed out as important problems, the theoretical basis and practical solution of which are closely related to those for other fluid-solid surface interaction problems. It was noted, too, that application of these efforts in the physical-chemical field may be achieved in the not too distant future.

With such results, the closing session of the First Symposium underlined the importance and necessity of close interdisciplinary cooperation among the major disciplines such as continuum mechanics, molecular physics, and physical chemistry. Both the organizing authorities and the participants in this symposium recognized these research goals and agreed to plan and propose a Data Exchange Agreement (DEA) between the US Navy and the Federal Republic of Germany. This DEA was realized on 13 April 1973 as Annex No. MWDDEA-N-72-G-4210.

Within this official framework all establishments involved in this DEA have contributed very encouraging results in both the theoretical and experimental fields. Papers on these results are being presented at this first official DEA-Meeting at the Naval Ship Research and Development Center, denoted as the "Second Symposium on Fluid-Solid Surface Interaction".

Some highlights of this Symposium may be briefly reported as follows:

The Research Group of Dornier System was successful in improving the physical background and the accuracy of theoretical prediction methods for the α-coefficients (as already

sketched in the first symposium) and has verified these results by direct measurements.

Neither theoretical nor experimental results for the important case of liquid (water) -solid surface interaction have been reported in this Symposium. Apparently molecular physics has not so far been successful in describing the mechanism of the liquid-solid surface interaction. Conclusions for the liquid case based upon interaction modes developed for the case of gases are obviously misleading. Significant efforts to overcome these difficulties have been started in both the theoretical and experimental fields and there is some hope that novel approaches will be developed before the Third Symposium. For the time being, drag reduction in liquid-solid surface cases can be realized only by damping turbulent motions in the boundary layer with ejection of polymer material or by laminarization with boundary-layer suction control. Information and know-how on these matters was also exchanged.

SESSION I

Chairman:

Hans J. Lugt

Naval Ship Research and Development Center

The Technological Importance of Gas-Solid Surface Interactions

G. Hoff
Dornier System GmbH
799 Friedrichshafen, Germany

Any reasonable investigation of the interaction of gases with solid surfaces requires precise analysis of the chemical and physical structure of solid surfaces in atomic dimensions. The progress of the past 10 years in vacuum technology and physical analysis techniques has led to the industrial availability of testing methods such as LEED*, AUGER-Spectroscopy and SIMS**. These methods make possible for the first time, the adequate analysis of the structure of solid surfaces. Such measurement of gas-solid surface interaction, involving physically and chemically precisely prepared and analyzed solid surfaces, gives quantitative insight into elementary processes in such different areas as

aerodynamic friction
heat transfer gas-solids
heterogeneous catalysis
ultra-high vacuum technology
crystal growth from the gas phase
oxidation.

The transfer of tangential momentum of gas molecules impinging on a moving solid surface determines aerodynamic friction. With appropriately preconditioned solid surfaces (minimal roughness and avoidance of loosely adsorbed layers), it is possible to reach a tangential momentum accommodation coefficient (TAC) below

---

* Low Energy Electron Diffraction

** Secondary Ion Mass Spectroscopy

10^{-1}, which means that less than 10 % of the tangential momentum of the impinging molecules is transferred to the moving surface. The physically determined lower limit for the TAC seems to be of the order of 10^{-2} to 10^{-3}, due to the atomic roughness of even an ideal surface. The reduction of TAC can become technically significant for missiles and aircraft operating at high altitudes. For satellites and reentry vehicles the advantage of such surfaces is evident.

The energy accommodation coefficient (EAC) can be reduced far more than the TAC because the atomic roughness of the surface is unimportant for energy transfer. Measured values of EAC are of the order of 10^{-2}. With suitable preparation of the surface, EAC values of 10^{-4} seem, in principle, attainable. Various technical applications of EAC values of 10^{-4} are to be expected in the military field.

Infrared seeker heads of air-to-air and ground-to-air missiles are limited to velocities of M = 3. At higher velocities the aerodynamic heating of the infrared dome results in such a strong self radiation that the actual target is no longer detectable. However, an increase in velocity of such missiles above M = 3 is an important military objective. For ICBM warheads, extreme velocities are required in order to decrease reaction time for defensive missiles. In the present work on surface layers with small EAC lies the possibility of increasing the present velocity limit. I believe that our knowledge of gas-surface interactions will be most rapidly applied in the problem of handling thermal loads.

Another important problem is the increase in thrust-to-weight ratios of jet engines. Progress in this area depends essentially on an increase in working temperature. The working temperature is limited by the high-temperature strength of turbine materials. Research on gas-surface layers with decreased heat transfer could

allow a higher gas temperature without increasing the temperature of the turbine blades. In addition, structural analysis of the solid surfaces has indicated new ways to develop oxidation resistant materials. Because oxidation resistance determines the limit for high-temperature application of many materials, this represents an additional method of increasing the thrust-to-weight ratio of jet engines.

UHV-technology is another field of application. The problem here is adsorption and desorption of water from the vacuum chamber walls. H_2O-adsorption-free surfaces could make the UHV technique as easily manageable as the HV-technique.

The most important non-military application of gas-surface interactions is in the field of heterogeneous catalysis. Most products of chemical industry are produced by catalytically controlled reactions. However, catalysts are developed in an entirely empirical manner. For important reactions such as the Haber-Bosch process for ammonia synthesis more than 20,000 different catalysts were tested, and still there is no certainty that the best catalyst for this process has yet been discovered.

Catalysts accelerate thermodynamically possible reactions without reacting themselves. They adsorb the reaction partners on their surface, thus concentrating them. The chemical and physical structures of catalytic surface activate the adsorbed molecules which then react. Finally the reaction products desorb from the catalyst surface. Investigations on gas-surface interactions will give research on catalysis a new base in the near future.

Finally, let us consider an example from the materials sector, where unsolved problems in gas-surface interactions and adsorption-layers on solid surfaces are blocking progress. The development of high-strength materials is directed toward composite materials consisting of fibers with a metallic matrix. Carbon

fibers, boron fibers and whiskers qualify for such composites. Al_2O_3 whiskers are the most interesting because they have the best compatibility with high-temperature materials. However, one kilogram of first-class Al_2O_3-whiskers costs several hundred thousand DM and therefore whiskers must be ruled out as a base for future materials, although the material from which they are produced costs only a few DM per kilogram.

Al_2O_3 whiskers are grown from gas-phase reactions. We are engaged in growing such whiskers and we must admit that the process is much closer to an alchemical procedure than to modern chemical engineering. The critical surface physical processes for whisker growth (nucleation, epitaxial growth, and the gas-surface interaction) have not been mastered in such a way as to control such processes. Even when this Al_2O_3 whisker is available and a composite material with an aluminum matrix is to be produced, new interface problems arise. It is not possible to obtain adherence between Al_2O_3 whiskers and the aluminum matrix, although aluminum-oxide that accumulates on solid aluminum displays ideal adherence. The reason for inferior adherence is adsorption layers on the Al_2O_3 whiskers.

The possible technological applications of gas-surface interactions are intriguing and important. This is the attraction as well as the danger. Only when the various disciplines needed for the solution of the problems presented to us, ranging from aerodynamics through theoretical physics to surface and solid state physics, really communicate with each other will we be successful. Symposia such as this one are the most effective way to conduct such discussions among the different disciplines.

Review of the Studies of Gas-Solid Surface Interactions and the Investigations of Marine Fouling at Dornier System

H. Rieger
Dornier System GmbH
799 Friedrichshafen
Germany

This paper gives a short survey of two study areas investigated at Dornier System which fall within the scope of this Symposium.

These areas concern:

1. Gas-solid surface interactions
2. The prevention of marine fouling

I. Investigations of Gas-Solid Surface Interactions

The investigations carried out so far in this field are primarily concerned with the solution of the following two questions:

First, to what extent does the momentum transfer in the collision of gases and solids depend on the structure of the solid surface, and

Second, what surface treatment methods will reduce the momentum transferred from the gas to the solid?

These questions are of fundamental significance in understanding aerodynamic friction, because such friction is caused by the tangential momentum transferred from the gas to the solid.

A further special aspect of gas-solid surface interactions is the aerodynamic heating of flight vehicles as it occurs, for example, on rockets and guided missiles flying at high speeds. This aerodynamic heating is caused by energy transfer from the gas to the solid.

Gas friction and aerodynamic heating of flight vehicles are typical surface effects. It can thus be expected that both effects depend on the characteristics of the gas as well as on those of the solid surface. Experiments have shown, however, that in the continuum flow region both gas friction and aerodynamic heating depend only on the gas and not on the solid.

How can this independence of gas friction and heating of the solid surface be explained? In the continuum flow region, the gas molecules of the free flow do not come into direct interaction with the solid surface but interact with gas molecules which are situated near the solid surface. In this way a maximum amount of momentum and a maximum amount of energy are transferred to the solid. This means that in the continuum flow region a flying body experiences the greatest possible friction and the greatest possible heating.

In the slip flow region, however, a much higher proportion of gas molecules interact directly with the solid. In this flow region it is thus possible to reduce gas friction and heating by means of solid surface preparation. This preparation must be such that the collision of gas molecules with the solid surface is as elastic as possible.

Reduction of friction and aerodynamic heating on flight vehicles by preparation of the solid surface is of great significance for the entire field of aeronautics and space flight. Numerous attempts have been made in the past to investigate the influence of the solid surface on the energy and momentum transfer from gases to solid surfaces. These attempts were unsuccessful because it was not possible (until quite recently) to analyze or prepare the solid surface structure at the molecular level. Such analysis and preparation is, however, the absolutely necessary precondition for a successful investigation. This is the only way to guarantee, for example, that the gas molecules do, in fact, impact

the atoms of the solid and not undefined surface contaminations. Furthermore, only controlled preparation of the solid surface guarantees that the surface characteristics can be varied in a definite way and that the effects of this variation on the momentum and energy transfer can be measured.

Fig. 1 illustrates the necessity for preparation of the solid surface down to atomic dimensions. In this case the chemical composition of the surface of a contaminated and of a clean copper single-crystal was investigated by means of Auger spectroscopy, an advanded surface analysis technique. Auger spectroscopy provides the chemical composition of the solid surface in the first atomic layer, i.e. directly on the surface.

Fig. 1 shows the Auger spectrum of a contaminated copper single-crystal without special surface cleaning. The main contaminants of this surface are sulfur, chlorine, carbon, oxygen and potassium. These contaminations can be removed from the copper surface by vacuum-heating and ion bombardment. Fig. 1 also shows the Auger spectrum of a copper surface cleaned in this way which contains only the copper peak.

By using several analyses and preparation techniques complementing one another, we can be sure that our investigations of gas-solid surface interactions can be performed reproduceably on defined solid surfaces. We can, furthermore, define variations of the surface characteristics.

Table 1 shows schematically the way in which we performed the investigations of the gas-solid surface interaction. The work was subdivided into experimental and theoretical investigations.

Experimental Investigations

Experimental investigations included surface analysis, surface preparation, and molecular beam and friction experiments.

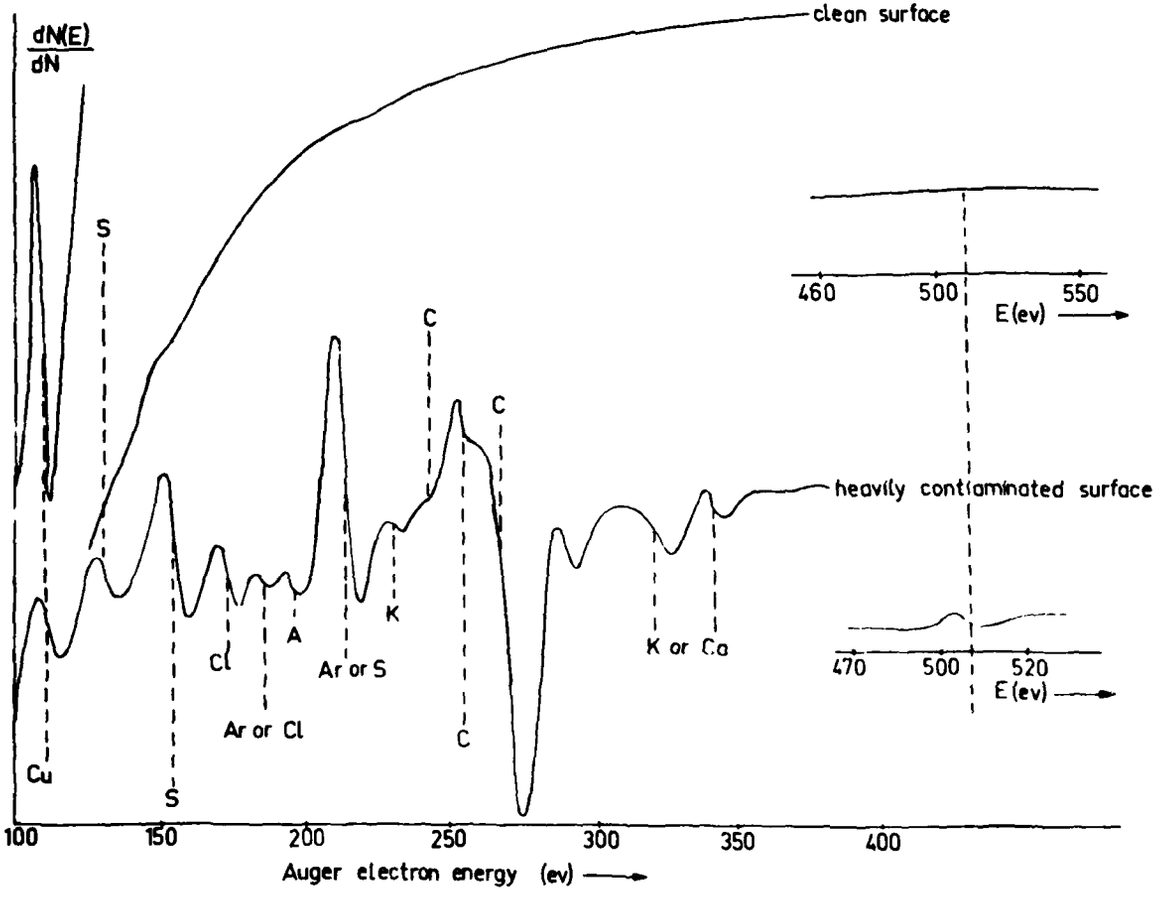

Fig. 1 Auger Spectrum of a Contaminated and of a Clean Copper Surface

Table 1

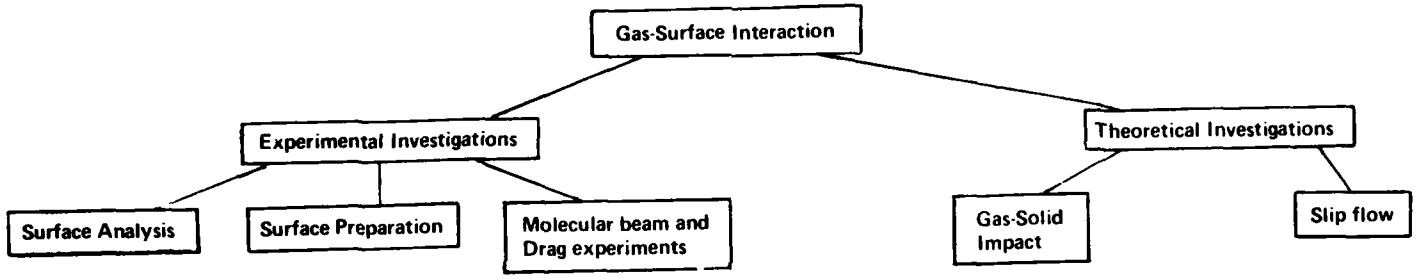

LEED Auger-Spectr. SIMS Microbalance Optical Methods Electronmicroscope	Mechanical, chemical and electrochemical Polishing Vacuumtempering Ion sputtering Vapour deposition	Molecular beam-scattering Momentum-transferexperiments Slip Flow Experiments	Kinetic of the impact in dependence of several parameters	Boundary Conditions Accomodation co-efficients

Surface Analysis

The following methods were used for surface analysis: (LEED) Low Energy Electron Diffraction for determining the crystalline structure of single-crystal surfaces.

Auger spectroscopy (AES) and secondary ion mass spectroscopy (SIMS) for determining the chemical composition of the solid surface.

LEED, AES, and SIMS analyze the first atomic layers of solid surfaces.

Microbalance measurements for investigating absorption and desorption processes.

Optical methods or electron microscopy for investigating thin surface layers such as oxide layers.

Surface Preparation

Surface preparation was accomplished mainly by the following techniques: mechanical, chemical and electrochemical polishing; vacuum tempering; surface cleaning by ion bombardment; and evaporation of special elements.

Measurement of the Gas-Solid Surface Interaction

The gas-solid surface interaction was investigated primarily by molecular beam and friction experiments.

The molecular beam experiments on the interaction of gas beams and defined solid surfaces may be subdivided into two groups: scattering experiments for investigating the angle distribution of the scattered gases, and experiments measuring directly the momentum transfer from the gas to the solid by means of force measurements.

Friction experiments investigated the slip effect by the rotating cylinder method and were performed mainly on technical

surfaces, the structure of which is not well known.

Theoretical Investigations

All experiments were supported and supplemented by theoretical investigations, experimentors and theorists working closely together. The theoretical work centered on investigation of the impact processes of gases and solid surfaces and on investigations of the slip flow region. The investigations of collision processes were mainly concerned with calculating the influence of different parameters on the kinetics of impact. The investigations of the slip flow region centered on the exact description of the boundary conditions of flow using suitable accommodation coefficients.

The results of the investigations performed so far are reported in more detail in the papers of Dr. Baerwinkel and Dr. Seidl. They show that appropriate surface preparation can contribute to considerable reduction of the momentum transfer during the collision of gases and solid surfaces. The limits for a further reduction of the tangential momentum transfer, however, also become evident. These limits are largely set by the surface roughness and are considerably closer for tangential momentum transfer than for energy transfer. It can therefore be expected that the heating of flight vehicles can be much more effectively reduced by suitable surface preparations than can aerodynmic friction.

II. Investigations of Marine Fouling

Finally the investigations performed at Dornier System, covering the fouling behaviour of various materials and of antifouling paints, are summarized. It was the aim of these investigations to prevent the fouling of buoys as well as of optical and acustical sensors of buoy network in the North Sea.

Fig. 2 shows the sample carrier exposed in the North Sea, with samples of different materials and paints.

Fig. 2 - Sample Carrier for Investigating Marine Fouling

Figs. 3 and 4 give an impression of the marine fouling of such samples. In these pictures one can see the heavy fouling on stainless steel after an exposure of five months (Fig. 3) and after an exposure of one year (Fig. 4). In contrast samples of copper alloys and samples sprayed with antifouling paints are still free of fouling or have only small fouled areas after similar exposure.

Fig. 3 - Coated and Uncoated Samples After an Exposure Time of Five Months

Fig. 4 - Coated and Uncoated Samples After an Exposure Time of One Year

Prevention of fouling of glass presents a special problem, particularly significant for optical sensors. One method of keeping glass free is shown in Fig. 3 and 4, where a copper network was applied on the glass plate, giving far-reaching protection against fouling.

Physical Parameters Governing Slip-Boundary Conditions and Their Influence on Momentum and Energy Transfer

K. Bärwinkel
Dornier System GmbH
799 Friedrichshafen, Germany

1. Slip and Nonslip Continuum Flow

According to normal continuum hydrodynamics or aerodynamics the thermal load and the forces exerted on a solid body moving through a fluid are determined by certain details of the flow field surrounding the body. The drag coefficient which is partly due to friction is an example. The friction force amounts to about 80 % of total drag for normal airplanes and may be calculated by integrating the shear stress over the whole surface of the solid body under consideration. The wall shear stress τ_w, in turn, is obtained from the velocity gradient:

$$\tau_w = \eta \left.\frac{\partial u}{\partial y}\right|_{y=0} \tag{1}$$

where y is the coordinate normal to a plane wall. This equation holds if the continuum theory applies as well as the nonslip boundary condition

$$u\ (y=0) = 0\ . \tag{2}$$

The velocity gradient, of course, follows from the Navier-Stokes equations, subject to appropriate boundary conditions.

Eqs. (1) and (2) indicate that in the normal case fluid-solid surface interaction is of no interest. In the slip regime, however, it comes into play via generalized boundary conditions. The flow equations of continuum theory are retained in the slip regime. As we shall see, eq. (1) also remains valid. In contrast,

the velocity boundary condition, eq. (2), is generalized by introducing the slip coefficient ζ:

$$u(o) = \zeta \left.\frac{\partial u}{\partial y}\right|_{y=0} \tag{3}$$

In a wide region of physical cases ζ practically vanishes and the slip boundary condition (3) reduces to the nonslip condition (2). The opposite extreme is $\zeta = \infty$, where a finite velocity may exist at the wall together with a velocity gradient equal to zero.

2. Slip Flow in Liquids and Slip Flow in Gases

Slip flow in gases is a well-established physical phenomenon. It is understood to be a rarefaction effect. The degree of rarefaction required for slip to become evident depends on the specific interaction between the gas and the solid surface. On the other hand, since this interaction can be manipulated (for the time being) to a limited extent only, an appropriate degree of rarefaction is necessary for such manipulations to have an effect.

Clearly the physical origin of slip flow at a liquid-solid boundary must be quite different. It appears that the ratio of the forces between the solid surface and molecules of the liquid system on the one hand and the forces within the liquid on the other should be important. This is the physical quantity which determines the wettability. M.B. Barbin's recent paper [1] claims that slip flow in water was induced by covering a quartz surface with a layer of hydrophobic molecules.

In what follows, considerations will be restricted to the gas-solid surface system.

3. Boundaries to the Slip-Flow Regime

Let us discuss the meaning of ζ for the special case of a linear velocity profile and a given value u at some fixed distance δ from the wall.

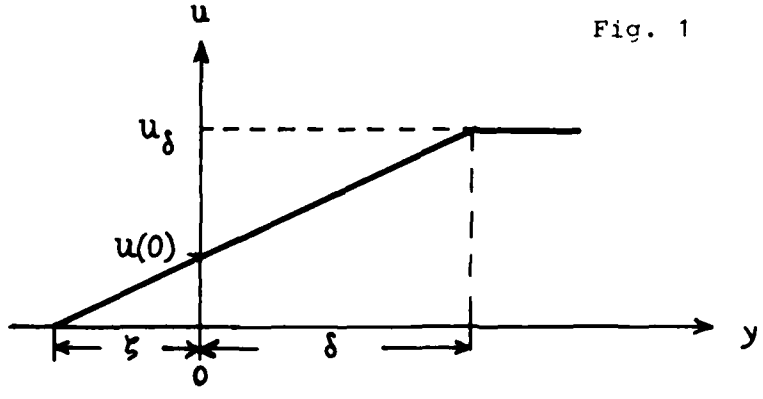

Fig. 1

If the velocity profile is extrapolated beyond the wall, the velocity becomes zero at a virtual distance, equal to ζ, behind the solid surface. A non-negligible slip velocity must be taken into account if ζ cannot be neglected in comparison with δ. It is reasonable to define

$$0.01 < \zeta/\delta \tag{4}$$

as a boundary to the slip flow regime and to take δ as the boundary layer thickness (for flows of high Reynolds number). Another boundary to the slip flow regime is reached if the mean free path ℓ of the gas molecules becomes comparable to the boundary layer thickness. In this case it no longer makes sense to use the continuum flow equations. Thus,

$$\frac{\ell}{\delta} < 0.1 \tag{5}$$

may denote the second boundary to the slip flow regime and eqs. (4) and (5) together define the slip flow regime by

$$\frac{0.01}{\nu} < \frac{\ell}{\delta} < 0.1 \tag{6}$$

with

$$\zeta = \nu \cdot \ell . \tag{7}$$

Whereas ℓ depends only on the physical state of the gas, ν is characteristic of the interacting system made up of a solid surface and a gaseous phase. From a physical standpoint eq. (7) is thus a very reasonable representation of the slip coefficient.

For ordinary surfaces ν is of the order of one and with

$$\ell/\delta \approx M/\sqrt{Re} \tag{8}$$

for $Re \gg 1$ and

$$\nu \approx 1$$

we arrive at the well-known definition [2]

$$0.01 < M/\sqrt{Re} < 0.1 \tag{9}$$

of the slip flow regime for flows of high Reynolds number. With increasing ν the slip flow regime is extended to lower values of $M/\sqrt{Re}$ and thus to higher densities of the gas.

4. Accommodation Coefficients

In gas kinetic theory the state of a gas is generally described by the distribution function $f(\vec{r}, \vec{c}, t)$ where

$$f(\vec{r}, \vec{c}, t)\ d\vec{c}$$

is the number density of particles with a velocity in the velocity-space element $d\vec{c}$ around $\vec{c}$, taken at a space-time point $\vec{r}$, t. It is, however, often sufficient to know a few macroscopic parameters (p, T, $\vec{u}$) characteristic of the physical state. Under this condition, the Navier-Stokes equations apply. One exception is the Knudsen layer of approximate thickness ℓ immediately adjacent to a solid surface. Here the distribution function is affected by the specific interaction of gas particles with the

solid body.

The so-called accommodation coefficients (AC's) are introduced as descriptive parameters of this specific interaction: If ϕ_i is the flux of some physical quantity (energy, momentum, etc.) incident on the wall and ϕ_r the flux reflected from the wall, then

$$AC = \frac{\phi_i - \phi_r}{\phi_i - \phi_{eq}} \tag{10}$$

where ϕ_{eq} is the flux carried by a Maxwellian distribution coming from the wall at the same temperature as the wall.

Let α be the AC of tangential momentum, so that α is just that fraction of the incident momentum flux lost to the wall. The slip coefficient is then simply related to α by

$$\nu = \zeta/\ell = \frac{2-\alpha}{\alpha} \tag{11}$$

This formula was developed by Maxwell and follows from two assumptions (cf.|4|):

1. A fraction α of the atoms incident on the wall leaves it with a Maxwellian velocity distribution and according to the cosine law. The remainder is specularly reflected (Maxwell's model).

2. The distribution function of the molecules approaching the wall does not change within the Knudsen layer (Maxwell's assumption).

Since momentum flux is nothing but a force per unit area, microscales are a possible device for measuring α. Such a device is used at Dornier System |3|. In these experiments particle beams are directed onto the surface under study. It is clear from the definition of the ACs that they depend on the actual distribution of the incident particles with respect to velocity. The ACs determined by our microscales are therefore called beam accommodation coefficients. They are functions of the particles' energy

and of the angle of incidence. Roughly speaking, a weighted average of beam ACs (with respect to energy and angles of incidence) is obtained for α if we calculate it from a measured slip coefficient according to Maxwell's formula (11). A convenient method of measuring ζ involves a friction experiment, e.g. using a device with rotating cylinders, as is done at Dornier System [5].

The evaluation of ζ from a friction experiment is always based on the continuum relation between the wall shear stress and the velocity profile. Now the validity of this relation might be doubted for slip flow because the continuum theory does not describe the Knudsen layer and the macroscopic velocity extrapolated through the layer onto the wall generally deviates from the mean flow speed within the Knudsen layer [4].

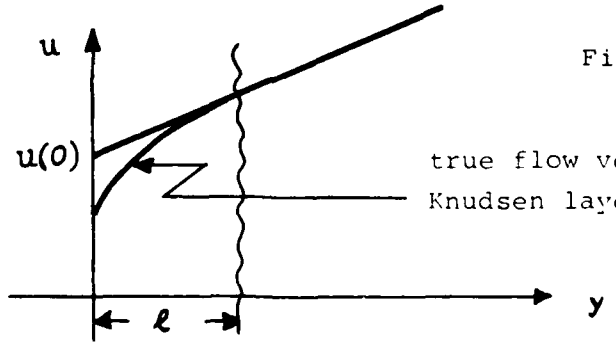

Fig. 2

However, if we take the simple free-path formula for viscosity

$$\eta = \frac{m}{2}\, n \cdot \ell \cdot \bar{c} = \frac{m}{2} \cdot \frac{p}{\kappa T} \cdot \ell \cdot \bar{c} \qquad (12)$$

with the thermal velocity

$$\bar{c} = \sqrt{\frac{8\kappa T}{\pi m}} \qquad (13)$$

we have the same level of description as we have in eq. (11), and eq. (1) can be proved:

The number N of gas particles per unit aera and time incident on the solid surface is

$$N = \frac{p}{\sqrt{2\pi m\kappa T}} \tag{14}$$

and the mean tangential momentum per particle

$$\bar{p}_t = m \cdot u(\ell) = m(u(0) + \ell u'(0)) \underset{(2)}{=} m\, u'(0) \cdot (\zeta+\ell). \tag{15}$$

According to the definition of α the momentum flux lost to the wall is then

$$\tau_w = \alpha \cdot \frac{p}{\sqrt{2\pi m\kappa T}} \cdot m \cdot (\zeta + \ell)\, u'(0) \tag{16}$$

and, making use of eq. (11), we arrive at eq. (1), with η given by eq. (12).

The slip-boundary condition may also be given in the form

$$\tau_w = \frac{4}{\pi} \cdot \frac{\alpha}{2-\alpha} \cdot \frac{p}{\bar{c}} \cdot u(0) \tag{17}$$

Evidently, ζ can be increased by making α small, which means smaller velocity gradients and thus reduced friction. If we manage to realize some low value of α, it will be desirable to judge this achievement in view of the drag reduction to be expected (only the portion due to friction should be taken into account).

Consider again the constant-shear stress layer (linear velocity profile) of section 3. with δ and u_δ fixed. The reduction of frictional drag gained by slippage as compared with the frictional drag in nonslip flow is then R percent* with

$$R = \frac{100}{1 + \frac{\alpha}{2-\alpha} \cdot \frac{\delta}{\ell}} \tag{18}$$

* A similar formula for Couette flow with slippage at both walls is given in [2].

In Fig. 3 R is plotted as a function of α for various values of the parameter δ/ℓ. To get an estimate for situations of practical interest we have introduced the boundary layer thickness [6]

$$\delta = 5.64 \cdot L / \sqrt{Re_L} \qquad (19)$$

for a plate of length L = 50 cm. Fig. 4 then indicates the variation of δ/ℓ with height H and speed of flight u_∞. (For simplicity we have used the barometric pressure formula and a constant temperature T = 293 K.)*

According to Figs. 3 and 4 values of α below 0.01 would be of great interest for fligth applications. Of course this is only a rough estimate. For the study of special systems extensive numerical work seems indispensable. Recent progress in the calculation of flows with slip-boundary conditions is reported by H.J. Lugt and coworkers (e.g. [7]).

5. The Scattering Kernel

Any finite set of ACs yields only a partial description of an interacting gas-solid surface system. Every aspect of such an interacting system is covered only by the scattering kernel P, which relates two branches of the distribution function, namely the distribution function f^+ of incident particles and the distribution function f^- of reflected particles in the manner of a linear integral transform:

$$f^+(\vec{c}) = \int_{-\infty}^{0} dc'_y \left| \frac{c'_y}{c_y} \right| \int_{-\infty}^{+\infty} dc'_x \, dc'_z \; f^-(\vec{c}') \; P(\vec{c}' \to \vec{c}) \qquad (20)$$

---

* In the hypersonic range the boundary-layer thickness is no longer given by eq. (19) so that the determination of δ/ℓ should be modified appropriately.

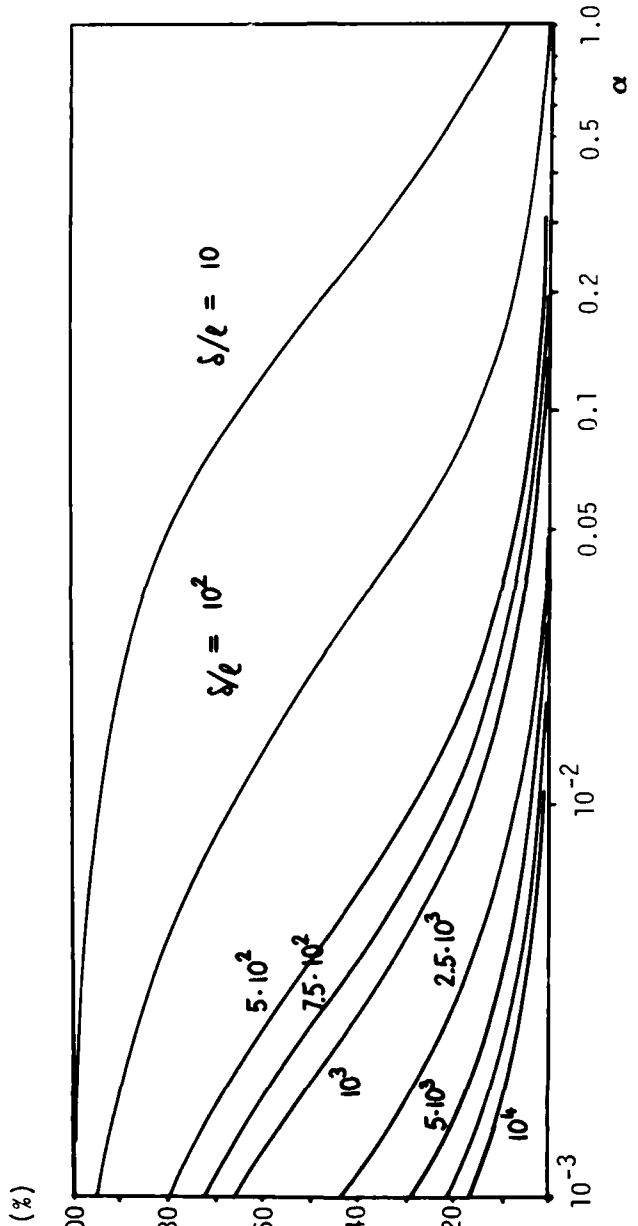

Fig. 3 - Estimated Reduction of Frictional Drag

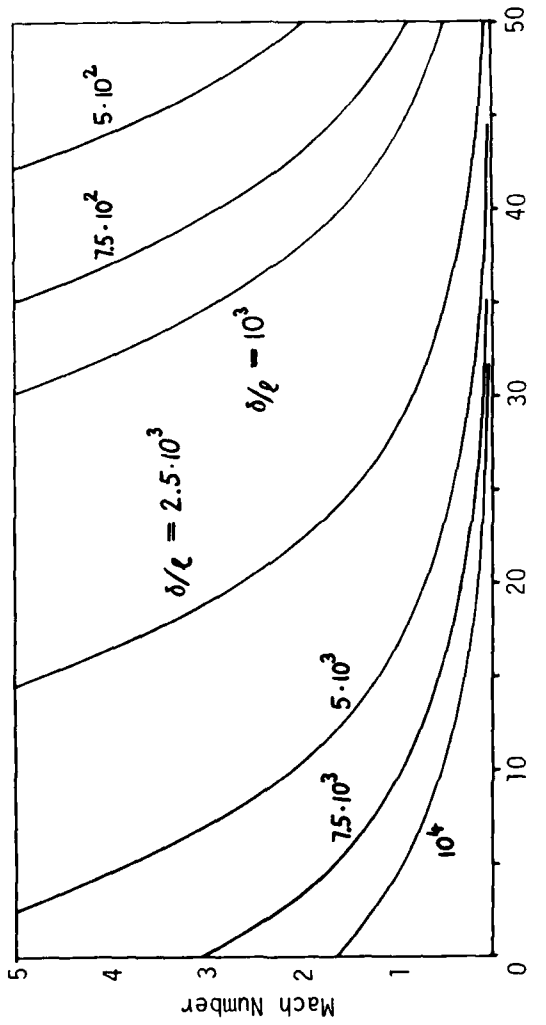

Fig. 4 - Lines of Constant δ/ℓ

Nonlinearity and nonlocality in space and time can be introduced as further complications.

$P(\vec{c}' \to \vec{c})\, d\vec{c}$ is the probability that a gas particle with a velocity $\vec{c}$ in $d\vec{c}$ leaves the surface if one with $\vec{c}'$ hits the surface.

If, using molecular beam techniques, one selects a single velocity

$$f^-(\vec{c}') = \text{const} \cdot \delta(\vec{c}' - \vec{c}_0) \tag{21}$$

the scattering kernel can be obtained from the scattered distribution function

$$f^+(\vec{c}) = \frac{c_{y,0}}{c_y} P(\vec{c}_0 \to \vec{c}) \tag{22}$$

Because of the conservation of particles and the preservation of equilibrium once reached at the solid surface, as well as because of its meaning as a probability density, the scattering kernel belongs to the class of normalized, reciprocal, and non-negative functions:

$$\int_0^\infty dc_y \int_{-\infty}^{+\infty} dc_x dc_z\, P(\vec{c}' \to \vec{c}) = 1 \tag{23}$$

$$\frac{c_y'}{c_y} \exp\left(-\frac{m(c'^2 - c^2)}{2\kappa T_s}\right) P(\vec{c}' \to \vec{c}) = P(-\vec{c} \to -\vec{c}') \tag{24}$$

(for $c_y > 0$, $c_y' < 0$, T_s = surface temperature)

$$P(\vec{c}' \to \vec{c}) \geq 0 \tag{25}$$

Hitherto only a limited number of model functions was known which fulfilled these conditions. The following ones (of which number 5 is a completely new model to be studied) have an intuitive physical meaning:

1) specular reflection:

$$P(\vec{c}' \to \vec{c}) = \delta(c_y + c_y')\ \delta(c_x - c_x')\ \delta(c_z - c_z') \tag{26}$$

2) perfect backscattering:

$$P(\vec{c}' \to \vec{c}) = \delta(\vec{c} + \vec{c}') \tag{27}$$

3) perfect accommodation:

$$P(\vec{c}' \to \vec{c}) = \frac{2}{\tau}\left(\frac{m}{2\kappa T_s}\right)^2 c_y \exp - \frac{mc^2}{2\kappa T_s} \tag{28}$$

4) diffuse elastic reflection with a cosine law

$$P(\vec{c}' \to \vec{c}) = \frac{c_y}{\pi c^3}\,\delta(|\vec{c}| - |\vec{c}'|) \tag{29}$$

5) exchange of an energy quantum ε with preservation of tangential momentum

$$P(\vec{c}' \to \vec{c}) =$$

$$\frac{m\, c_y\, \delta(c_x - c_x')\,\delta(c_z - c_z')}{1 + \exp - \varepsilon/\kappa T_s}\left\{\delta\left(\frac{m}{2}c_y'^2 - \frac{m}{2}c_y^2 - \varepsilon\right) + \exp\left(-\frac{\varepsilon}{\kappa T_s}\right)\delta\left(\frac{m}{2}c_y'^2 - \frac{m}{2}c_y^2 + \varepsilon\right)\right\}$$

$$+ \frac{\Theta\left(1 - \frac{mc_y'^2}{2\varepsilon}\right)}{1 + \exp - \varepsilon/\kappa T_s}\,\delta(c_y' + c_y)\ \delta(c_x' - c_x)\ \delta(c_z' - c_z) \tag{30}$$

Here Θ is the unit step function: $\Theta(x) = 0$ if $x < 0$, $\Theta(x) = 1$ if $x > 0$.

The beam AC of tangential momentum and the relative transfer of normal momentum considered over a sufficiently wide region of incidence angles and energies are very sensitive to variations of the scattering kernel. We therefore hope to extract a lot of information about $P(\vec{c}' \to \vec{c})$ from the measurements with our micro-scales device by fitting to them linear combinations of model

functions. Results for ordinary surfaces are reported by W.J.C. Müller [8].

6. Rigorous Results on Slip-Boundary Conditions in Terms of Knudsen Accommodation Coefficients

The rigorous theory of boundary conditions in the slip flow regime is based on the solution of Boltzmann's equation for the distribution function in the Knudsen layer subject for the boundary condition (20) with an arbitrary scattering kernel [9]. The rigorous theory so far has more or less been confined to the case of near equilibrium flow (low speed of flow near the wall!). Under this condition the velocity-slip coefficient can be expressed in terms of the so-called Knudsen ACs α_{ij} [10]. These are defined as

$$\alpha_{ij} = \frac{\langle Q_i Q_j \rangle - \langle Q_i \hat{P} Q_j \rangle}{\langle Q_i Q_j \rangle - \langle Q_i \rangle \langle Q_j \rangle} \tag{31}$$

Here i and j have no intuitive meaning but only refer to an arbitrary enumeration of polynomials (see below).

The triangular brackets indicate the average over a Maxwellian flux of particles at the temperature of the wall:

$$\ldots = \frac{2}{\pi} \left(\frac{m}{2\kappa T_s} \right)^2 \int_0^{\infty} dc_y c_y \iint_{-\infty}^{+\infty} dc_x dc_z \, (\ldots) \exp - \left(\frac{mc^2}{2\kappa T_s} \right) \tag{32}$$

$\hat{P}Q$ denotes the integral transform performed with the scattering kernel:

$$\hat{P}Q(\vec{c}) = \int_0^{\infty} dc'_y \iint_{-\infty}^{+\infty} dc'_x \, dc'_z \, P \, (\vec{c} \rightarrow \vec{c}') \, Q(\vec{c}') \tag{33}$$

Finally, Q_i are polynomials of the velocity. The first five are needed for the slip coefficient:

$$
\begin{aligned}
Q_1 &= c_y \quad \text{(particle velocity normal to surface)} \\
Q_2 &= c_x \\
Q_3 &= c_z \\
Q_4 &= c^2 \\
Q_5 &= c_y c_x
\end{aligned}
\tag{34}
$$

The result for the slip coefficient is now*:

$$
\zeta = \frac{2-\alpha_{25}}{\alpha_{22}} \left[1 + \alpha_{25} \left(\frac{2}{\pi} \cdot \frac{\alpha_{22}}{\alpha_{25}} \cdot \frac{2-\alpha_{55}}{2-\alpha_{25}} - \frac{1}{2} \right)\right] \ell \tag{35}
$$

with the mean free path determined by viscosity according to eq. (12).

7. The Slip Coefficient Traced Back to Beam Accommodation Coefficients

Admittedly, reliable data on α_{25} and α_{55} are lacking and we might just as well take recourse to eq. (11). It is consistent with the heuristic considerations underlying this simple formula to identify α with α_{22}. Thus

$$
\zeta \approx \frac{2-\alpha_{22}}{\alpha_{22}} \cdot \ell \tag{36}
$$

If we measure the AC of tangential momentum for a thermal beam of particles (at the temperature of the surface but with a well-defined direction) as a function of the angle of incidence ϑ, say $\alpha_{\text{beam}}^{T_s}(\vartheta)$, we have

$$
\alpha_{22} = \frac{1}{4} \int_0^{\pi/2} \sin^3\vartheta \cos\vartheta \, \alpha_{\text{beam}}^{T_s}(\vartheta) \, d\vartheta \tag{37}
$$

---

* The scattering kernel is assumed to be independent of the azimuthal angle.

Thus the beam AC is averaged with a weight function, the maximum of which lies at an angle of incidence equal to 60°.

If we have a beam with a well-defined energy of the particles and not with a thermal distribution, the averaging process (37) must of course be generalized to include the energy variable.

8. The Thermal Slip-Boundary Condition

The thermal slip-boundary condition reads

$$T(0) - T_s = \zeta_\lambda \left.\frac{\partial T}{\partial y}\right|_{y=0} \tag{38}$$

with ζ_λ as the thermal slip coefficient.
The formula for ζ_λ, which corresponds to eq. (35), involves the Knudsen ACs α_{11}; α_{14}; $\alpha_{1,10}$; α_{44}; $\alpha_{4,10}$; and $\alpha_{10,10}$. On the level of Maxwell's heuristic approach a simplified formula comparable with eq. (11) is obtained:

$$\zeta_\lambda = \frac{2\gamma}{(\gamma+1)\,Pr} \cdot \frac{2-\alpha_E}{\alpha_E}\, \ell \tag{39}$$

with $\gamma = c_p/c_v$, the ratio of specific heats, Pr as the Prandtl number, and α_E as the energy AC. The Knudsen AC most intimately related with α_E is α_{44}.

Fig. 5 shows an estimated reduction of heat flow (in per cent) as a function of α_E, compared with the case $\alpha_E = 1$. The heat flow is here due to internal friction in the flow parallel to a flat plate; no slippage of the velocity is assumed. Further assumptions are: $Pr = 1$, $\gamma = 1.4$, and no gradient of pressure or temperature parallel to the solid surface. The calculation is based on the temperature profile (|6| p. 56)

$$T = T_{st} + (T_{st} - T_O)\left(\frac{u}{u_\delta} - 1\right) - (T_{st} - T_\delta)\left(\frac{u}{u_\delta}\right)^2 \tag{40}$$

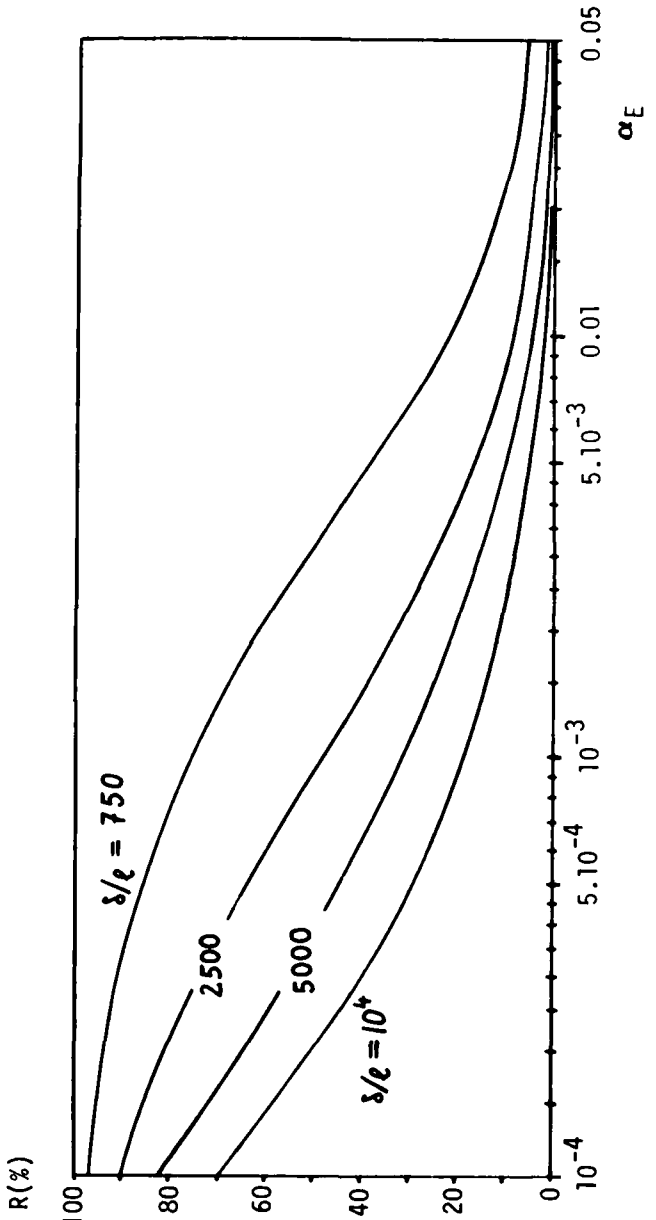

Fig. 5 - Estimated Reduction of Heat Flow

with the stagnation temperature

$$T_{st} = T_{\delta} \left(1 + \frac{\gamma-1}{2} M_{\delta}^2\right) \tag{41}$$

and, again, on the model of the constant-shear stress layer. The result is

$$R_E = 100 \frac{\frac{7}{6} \cdot \frac{\ell}{\delta} \left(\frac{2-\alpha_E}{\alpha_E} - 1\right)}{1 + \frac{7}{6} \cdot \frac{2-\alpha_E}{\alpha_E} \cdot \frac{\ell}{\delta}} \tag{42}$$

The parameter δ/ℓ is the same as that given in section 4. Again, values below 0.01 for the AC would be of practical interest in the nonslip continuum flow and slip flow regime. In view of microscopic roughness, it may be easier to reach such low values for α_E than for the AC of tangential momentum.

9. Some Simple Ideas on Microscopic Parameters

9.1 Roughness on an Atomistic Scale

If a particle is specularly reflected from an idealized rectangular step it transfers twice its tangential momentum, where tangential refers to the average surface plane

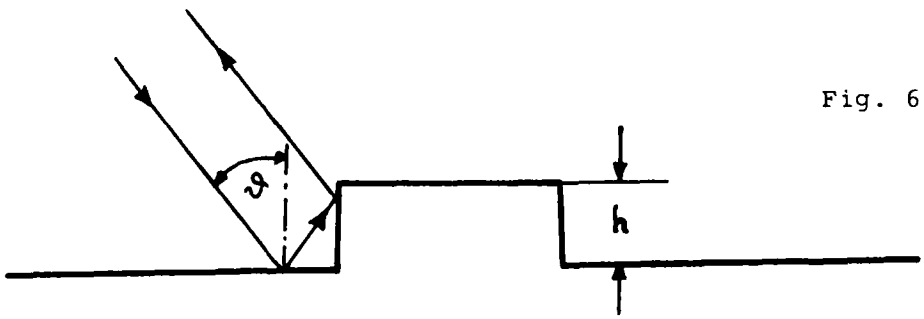

Fig. 6

On the basis of this simplified mechanism, we have calculated beam ACs of tangential momentum for surfaces containing idealized steps. These ACs depend on the angle of incidence, step height, and average distance between steps. The direction of steps on the surface can also be taken into account.

As an example, take a fresh cleavage surface of rocksalt. Details of the surface on an atomistic scale - even the sense of steps - can be rendered visible by decoration techniques. The experimental results of De Wainer [11] indicate that about 30 upward und 30 downward steps must be expected per µm. If the steps run perpendicular to the propagation direction of the arriving gas particles, one gets

$$\alpha(\vartheta) = 4 \frac{h}{d_s} \operatorname{tg} \vartheta \qquad (43)$$

where h is the mean step height and d_s the mean distance between neighbouring steps. For h equal to the lattice constant (5.63 Å for rocksalt) and $\vartheta = 60^{\circ}$ (location of maximum of the weight function in eq. (37)

$$\alpha\,(60^{\circ}) \gtrsim 0.1$$

Thus, remembering the conclusion of section 4, microscopic roughness may set a severe limitation on the reduction of tangential momentum transfer. There are, however, no data available on roughness of metallic surfaces on an atomistic scale. Moreover, microscopic roughness is considered irrelevant to energy transfer in gas-surface scattering.

9.2 Mass Ratios

Momentum and energy transfer in a binary collision between free particles is governed by the mass ratio

$$q = m/M \qquad (44)$$

If M is the mass of a collision partner at rest prior to the collision, the dependence on q is the following:

$$\text{relative momentum transfer} \sim \frac{1}{1+q} \tag{45}$$

$$\text{relative energy transfer} \sim \frac{q}{(1+q)^2} \tag{46}$$

These relations can, to a certain extent, be applied to gas-solid surface scattering. Because of binding forces and lattice dynamical effects, M should then be understood as an effective mass which exceeds the mass of a single surface atom. If there is an attractive potential in front of the surface, trapping occurs in connection with an appropriate loss of energy. Trapping leads to an increased transfer of both energy and momentum. Thus a reduced effective mass of surface complexes may cause an increase in momentum transfer (due to an enhanced energy transfer according to (46) with $m < M$, which leads to more trapping) or a reduction (in view of (45)). Both possibilities can be verified by numerical calculations, depending on the incident energy and the depth of the attractive potential well.

References

|1| M.B. Barbin — On the slip velocity and the friction coefficient of liquid against the wall. Kolloidnyi Zhurnal 35 (1973) 328

|2| S.A. Schaaf, P.L. Chambré — Flow of rarefied gases. In: Fundamentals of Gas Dynamics (H.W. Emmons editor), volume III. Princeton University Press, 1958

|3| M. Seidl — This volume

|4| V. Lehmann — Zusammenhang zwischen Gas-Oberflächen-Wechselwirkung und den Randbedingungen der Gasdynamik. Symposium über Gas-Oberflächen-Wechselwirkung, Meersburg, Germany, 3.-5. May 1972. Symposium Proceedings edited by Dornier System GmbH, Friedrichshafen

|5| M. Hollstein, W. Neumann, M. Seidl — Messungen zur Gas-Oberflächen-Wechselwirkung mit einer UHV-Molekularstrahlanlage und Gasreibungsapparaturen. Ibid. See also M. Seidl, this volume

|6| A. Walz — Strömungs- und Temperaturgrenzschichten. Verlag G. Braun, Karlsruhe 1966, p. 18

[7]	H.J. Lugt S. Ohring	Laminar flow behaviour under slip-boundary conditions Forthcoming in Phys.Fluids, 1975
[8]	W.J.C. Müller	Parametric representation of beam accommodation coefficients In: Rarefied Gas Dynamics. Proceedings of the ninth international Symposium 1974 Göttingen (M. Becker, M. Fiebig editors) DFVLR-Press, Porz-Wahn, Germany, 1974
[9]	S.K.Loyalka	The slip problem for a simple gas Z. Naturforsch. 26a (1971) 964
[10]	T. Klinc I. Kuščer	Slip coefficients for general gas-surface interaction Phys. Fluids 15 (1972) 1018
[11]	L.S. De Wainer	On a shadow decoration technique. Thin Solid Films 21 (1974) S. 31

Measurements of Gas Surface Interaction on Well-defined Solid Surfaces

M. Seidl and E. Steinheil
Dornier System GmbH
799 Friedrichshafen, Germany

ABSTRACT

Methods for the preparation of well-defined and reproducible single crystal and engineering grade solid surfaces controlled by modern surface analysis techniques as well as measurements of the interaction of gases with these surfaces are described. AES, SIMS, LEED, electron microscopy and molecular beam techniques are used for surface analysis and for the measurements of the interaction between gases and solid surfaces. Measurements of tangential momentum accommodation coefficient (TAC) were made by the method of rotating cylinders and a newly developed microbalance technique. It was found that the TAC depends mainly on roughness, surface contamination, and bulk composition. Rough and contaminated surfaces yielded TAC-values of about 0.8 to 1.0. In contrast,a smooth, clean, single-crystal surface of gold showed values of TAC's below 0.1, the lowest values measured to date. This way a perceptible reduction of drag in rarefied gas environment is possible.

Introduction

The aim of these investigations is to determine the limits and possibilities for reducing friction between solid surfaces and gases by special surface preparation. For this task, we first had to prepare well-defined and reproducible surfaces. Five years ago this was impossible because there were no surface analysis

methods for determining the physical and chemical structure of surfaces in the monolayer region. Now, due to the development of ultra high vacuum surface preparation techniques as well as of modern diagnostic methods such as Auger Electron Spectroscopy (AES), Secondary Ion Mass Spectroscopy (SIMS), and Low Energy Electron Diffraction (LEED), these investigations can be carried out successfully.

Surface preparation and analysis

With AES (1) one can determine the elementary chemical compositions in the uppermost monolayers. Often it is even possible to get quantitative information. SIMS (2) yields additional information about chemical compounds and about elements for which AES is not very sensitive. Information about the structure of a monocrystal is obtained by the application of LEED (3), (4).

These methods can be combined with suitable preparation techniques such as argon ion bombardment (5), (6) and annealing in ultra high vacuum. In this way it was found that the uppermost monolayer of almost any surface does not consist of the bulk material but of a contamination film. Thus certain surface properties measured in the past without application of these advanced methods do not correspond to properties of the actual bulk materials but to specific contaminants. Therefore we had to find ways for preparing clean surfaces or at least surfaces with a defined contamination.

Generally a surface was initially prepared by grinding mechanically with special sand papers or grinding powders. This method resulted in a certain desired roughness. The state of the resulting surfaces was generally documented by light microscopy, scanning electron microscopy, or by replicas. If a very smooth surface was needed, a suitable method for electropolishing had to be found. The sample was mounted on a manipulator in an ultra

high vacuum chamber where it could be examined with AES and LEED or SIMS. Most often the combination of argon ion bombardment and annealing in certain gas atmospheres or in ultra high vacuum produced a clean surface in several steps.

The following figures represent typical surface structures: Fig. 1a shows an electron microscope replica of a mechanically polished copper surface. The grooves are about 1 µm wide. Fig. 1b shows a replica of the same surface after a short electropolishing. The surface is fairly well smoothed but the grooves are still identifiable. Fig. 1c shows the surface electropolished for a longer time. The grooves have completely vanished. Fig. 1d shows the replica of a copper film which has been epitaxially grown on a rocksalt single crystal.

In Fig. 2 the lower curve documents a typical Auger spectrum of a copper surface after electropolishing and installation in the UHV-chamber. The copper peak in the represented energy range is very small and many contamination peaks such as those of oxygen, carbon, sulfur, and others appear. After the surface was subjected to special cleaning procedures, the contamination peaks vanished and the copper peak was clear (upper curve).

The Auger spectrum of the same copper surface contaminated with about 5 % carbon and 20 % oxygen or compounds of them is shown in Fig. 3. Compounds cannot be identified from an Auger spectrum, but an additional SIMS spectrum (Fig. 4) of the same surface gives the desired information. It does not show any carbides or hydroxides but it does show oxides, carbon and hydrocarbon molecules, and chlorine in a lower concentration. At the moment it is not possible to analyze the SIMS spectra quantitatively because the physical processes are too complicated. However, the capabilities of AES and SIMS complement each other very well.

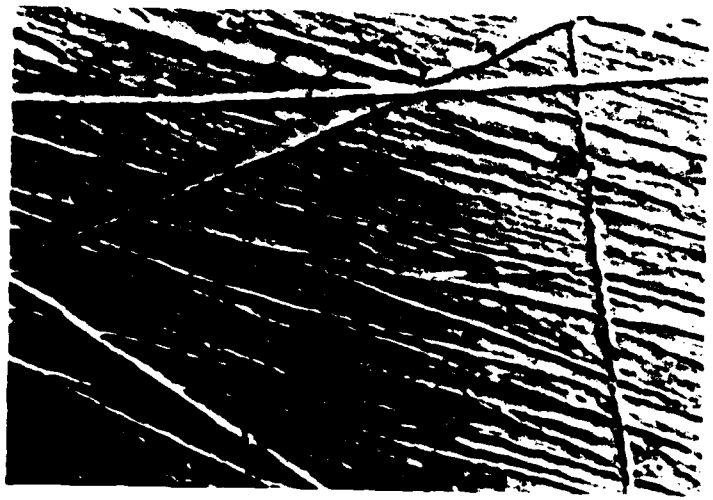

1 a

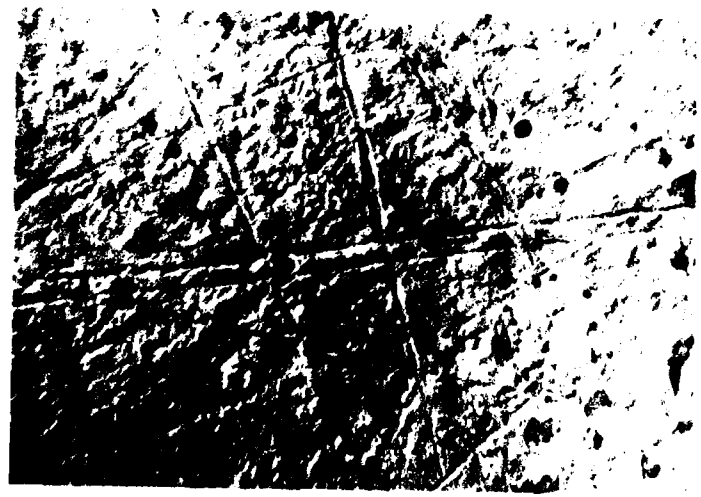

1 b

1 c

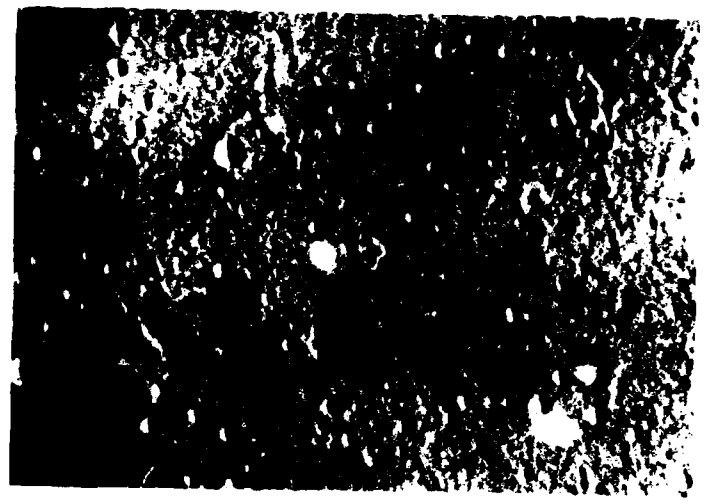

1 d

Fig. 1a - 1d : Electron microscope replicas of copper surfaces

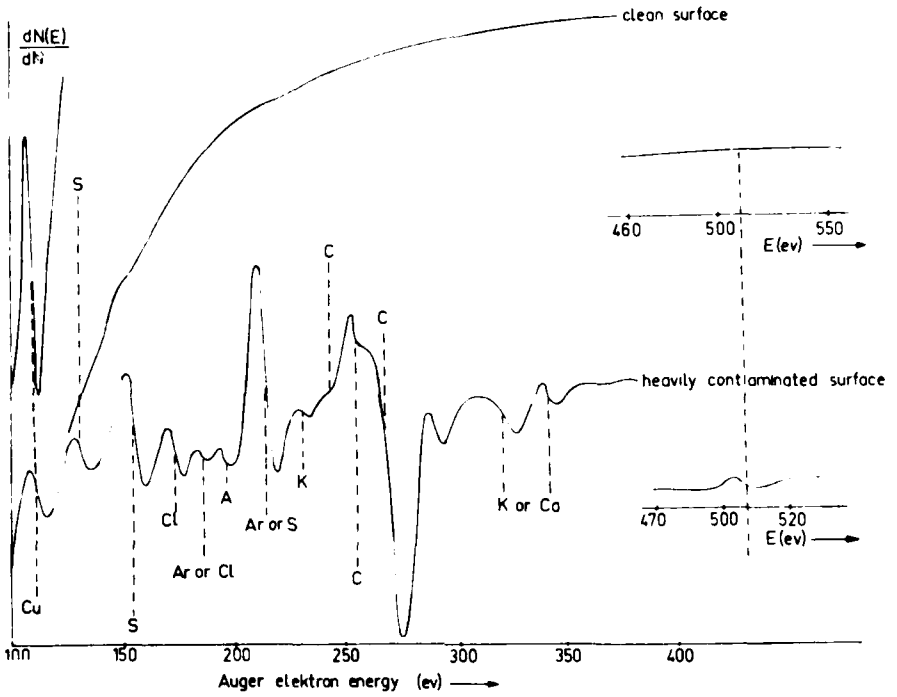

Fig. 2: Auger Spectrum of a Clean and a Contaminated Copper Surface

Figs. 5a - 5c show LEED patterns. The upper picture shows the fundamental lattice of a clean (100) single crystal copper surface. If the surface still contains some adsorbed oxygen, additional spots appear dependent on the oxygen dose, the temperature, and the structure of the surface (Figs. 5b and 5c).

Measurements of gas solid surface interactions by different methods

The SIMS, AES and LEED methods can be used to study the interaction of gases with certain solid surfaces. Adsorption or desorption of gases is revealed by SIMS and Auger spectra as well

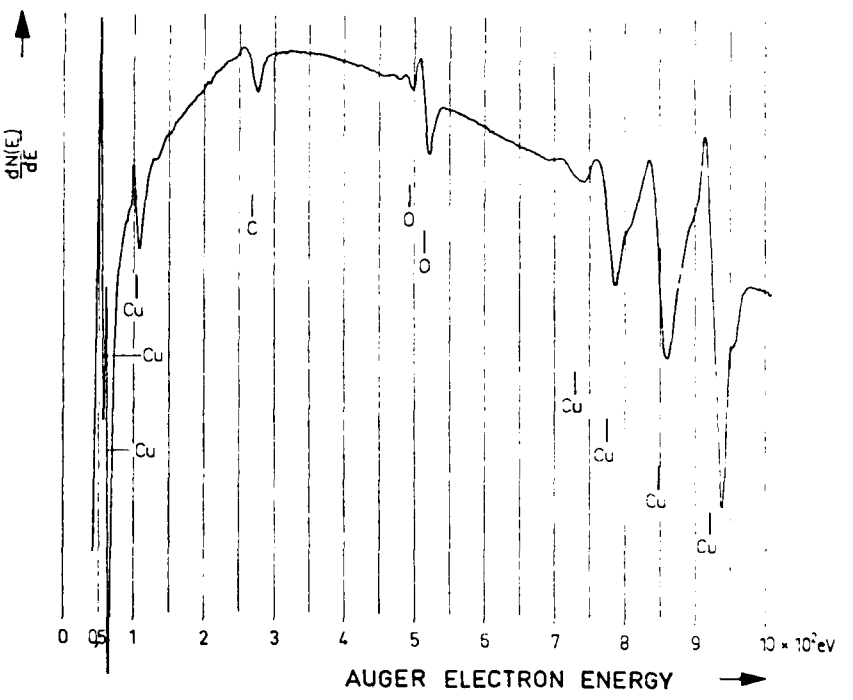

Fig. 3: Auger Spectrum of a Copper Surface Contaminated Only with Carbon and Oxygen

as by LEED patterns. Microbalances, ellipsometry, or spectrophotometers can yield additional information about these interactions if needed.

Using these methods Dornier System found that a surface becomes more inert if it is smoother or if it is doped with such materials as carbons, certain hydrocarbons, or argon. Although this work gives no information about the friction between gases and solid surfaces, it does indicate the importance of maintaining clean or defined surfaces.

To get information about the possibilities of reducing friction, the impact of gas particles on well-defined surfaces

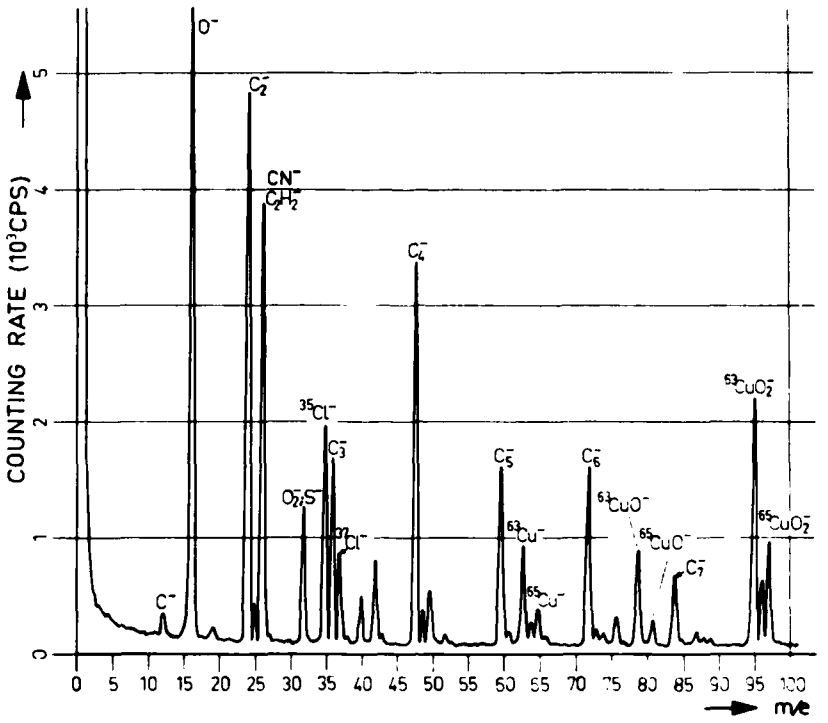

Fig. 4: SIMS Spectrum of a Copper Surface, Identical to that Represented in Figure 3

must be studied and the slip or momentum accommodation coefficients must be measured. To do this a molecular beam scattering apparatus was planned and set up (Fig. 6).

In the two chambers on the right a monoenergetic molecular or atomic beam is produced by a nozzle and skimmers (7). In the scattering chamber the beam impinges on the sample surface, which has been prepared by argon ion bombardment, annealing, and the help of AES and LEED. The scattered molecules, atoms, or ions are analyzed by mass spectrometer and retarding field analyzer for their angle and energy distribution. These investigations showed that an atomic impact is closer to specular reflection the smoother the surface is and the fewer adsorbed gases or

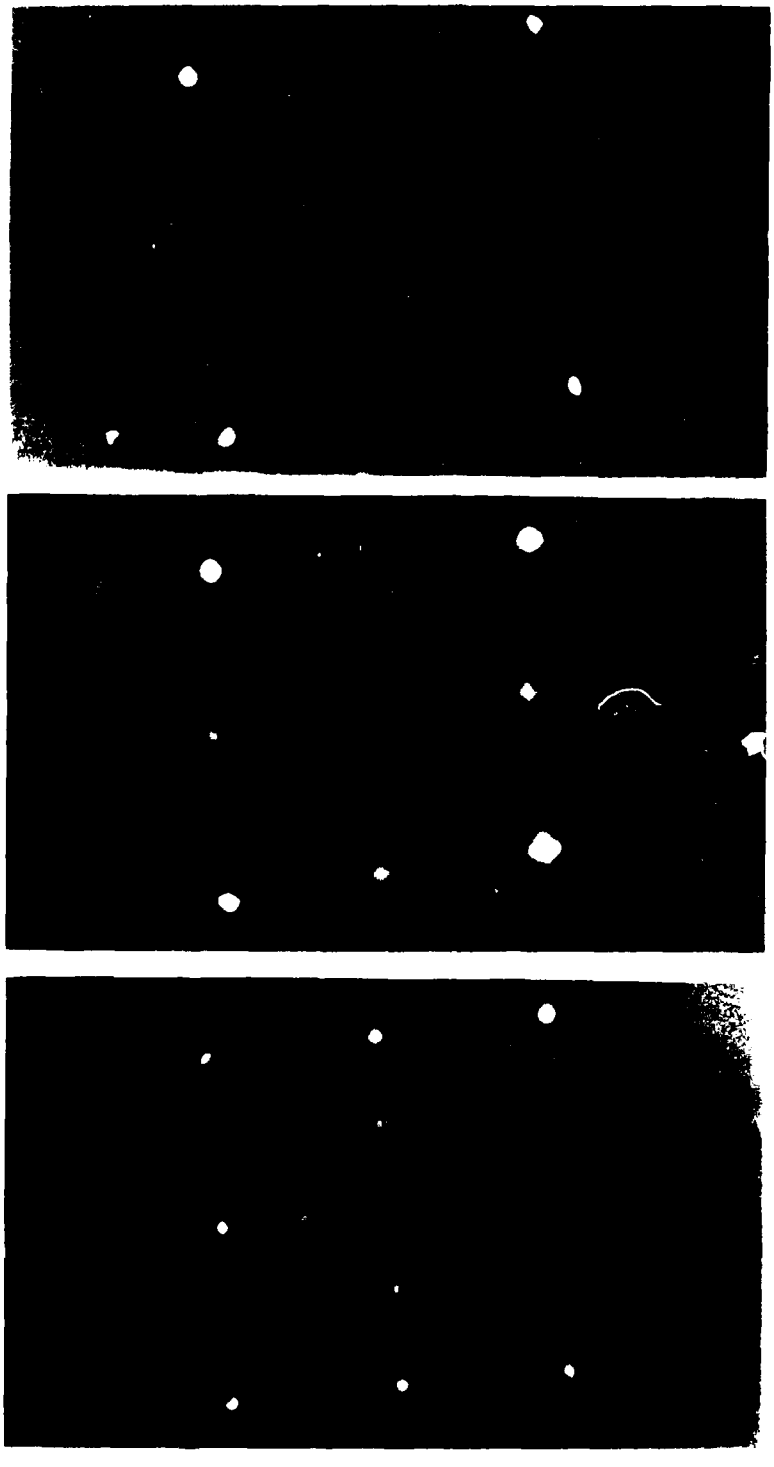

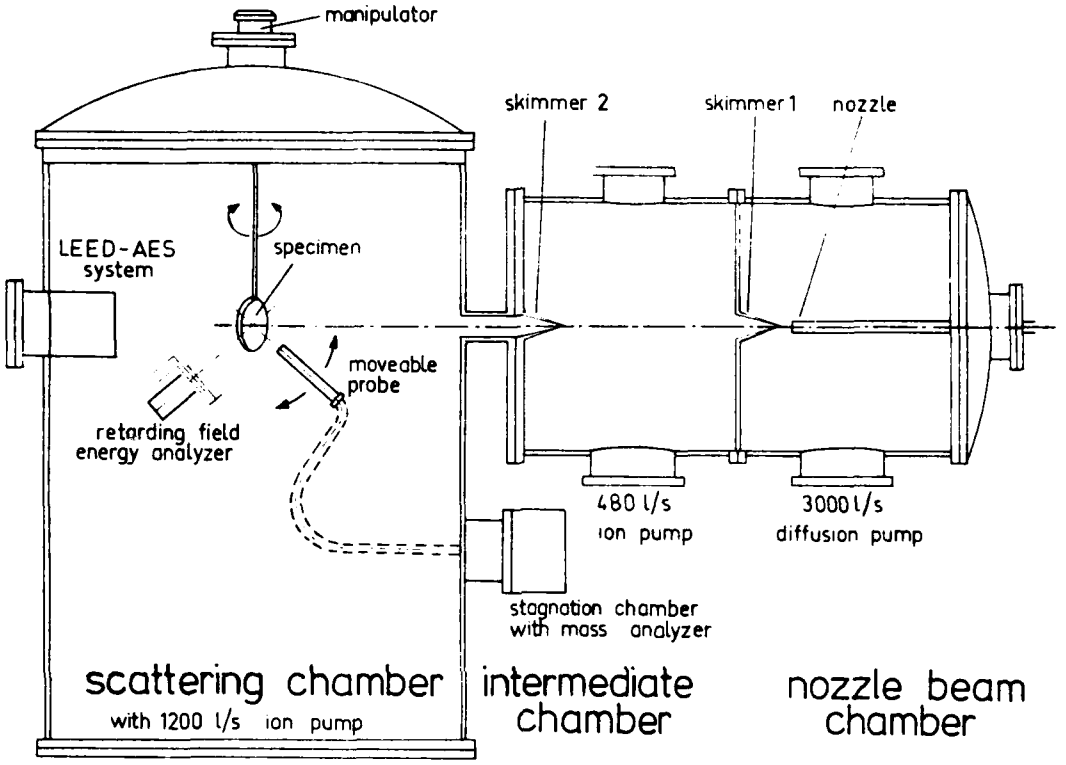

Fig. 6: Molecular Beam Scattering Apparatus

contaminants it contains. Such measurements help to describe the gas/solid surface interactions theoretically (see paper by Dr. Bärwinkel), but one question still remained:

How do the measured effects influence the tangential momentum accommodation coefficient (TAC) and, in this way, friction?

Measurement of tangential momentum accommodation coefficients (TAC)

To answer this question,the tangential momentum accommodation coefficient had to be measured quantitatively. Initially the method of rotating cylinders (Fig. 7) was chosen.

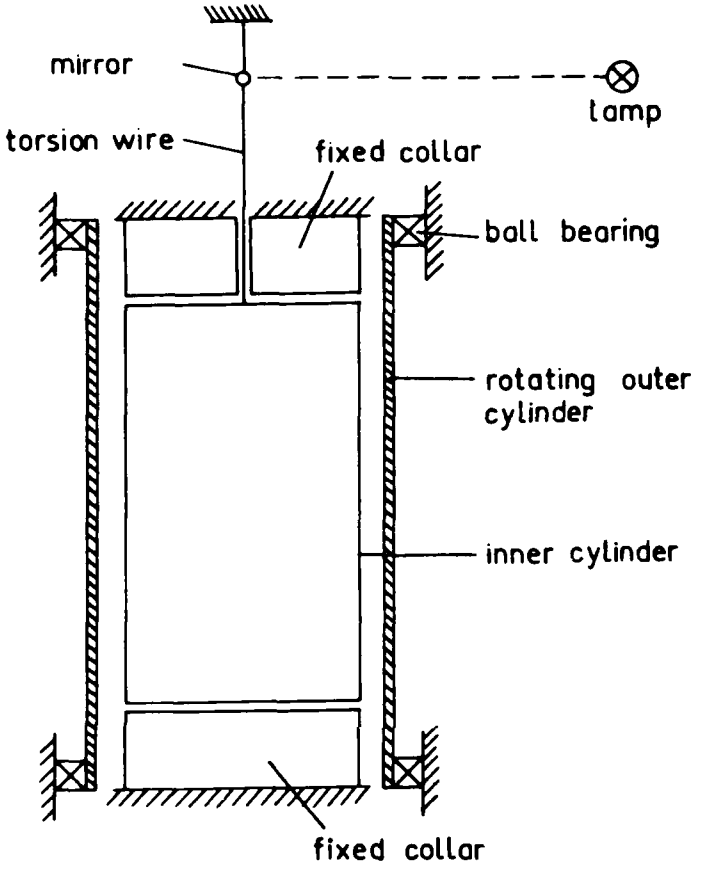

Fig. 7: The Method of Rotating Cylinders

The apparatus consists of an outer cylinder driven by a motor and an inner cylinder fixed to a torsion wire. The inner cylinder is rotated along with the outer one by the impacts of gas particles. A lamp and a mirror fixed to the wire were used to measure deflections. From these deflections, we were able to calculate the tangential momentum accommodation coefficients (8).

In this way values between 0.7 and 0.9 at pressures of about 10^{-3} to 1 torr were measured. The reproducibility of these maesurements was not very good, however, because we had no chance to prepare well-defined and reproducible cylinder surfaces and no occasion to analyze the surface by suitable methods such as AES, SIMS, or LEED.

Fig. 8 shows an apparatus set up at Dornier System which combines measurements of momentum transfer from a monoenergetic molecular beam onto solid surfaces with modern methods of surface analysis and preparation in a single UHV-chamber. The specimen is so mounted on the beam microbalance that it is rotatable and that the angle of incidence between a molecular beam produced by a nozzle beam arrangement and the normal of the plane surface can be varied. In addition, the entire microbalance can be rotated to allow measurements at different angles of incidence between molecular beam and beam of balance, making it possible to separate normal and tangential moment transfer. The rotation of the microbalances also permits use of the equipment for surface cleaning and preparation (such as by argon ion bombardment and radiation heating) as well as for modern surface analysis instruments (such as AES and LEED) which are mounted within the same vacuum chamber.

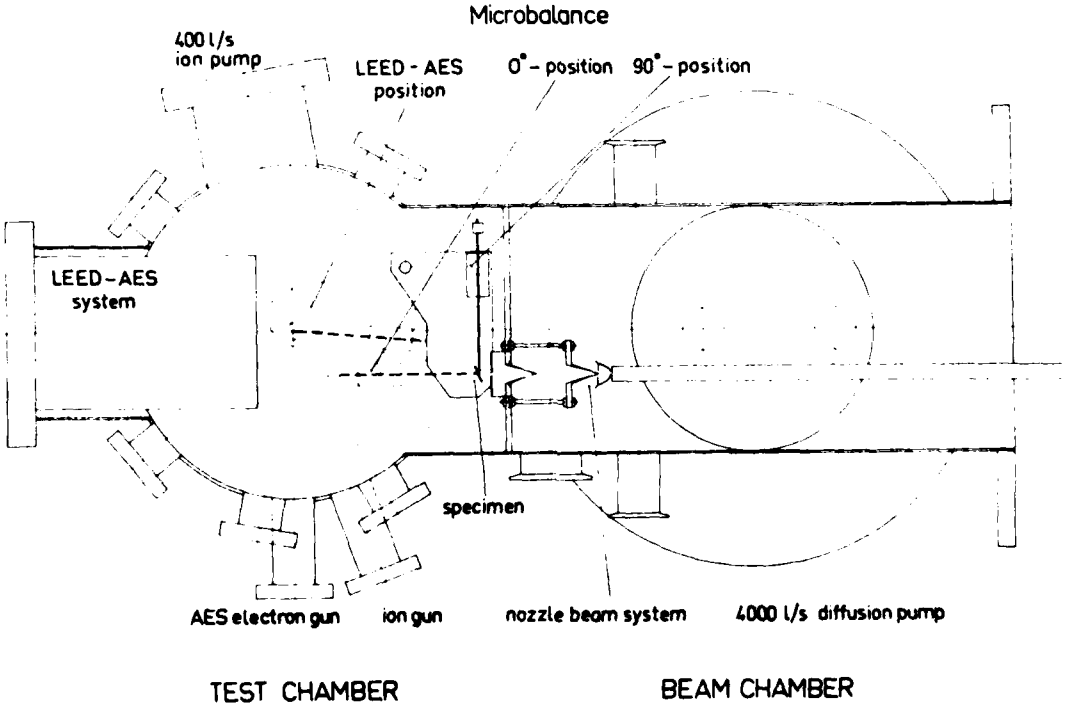

Fig. 8: Microbalance Technique for the Measurement of TAC

So far the momentum transfer from a 0.05 eV Helium beam to various single crystal metal surfaces as well as to polycrystalline (engineering) materials has been measured. Results indicate that momentum accommodation coefficients strongly depend on the material and the surface state, and that the TAC can be greatly reduced in the lower pressure range by reducing roughness and by avoiding adsorption and contamination.

Fig. 9 shows the TAC of Cu(100) plotted against the angle of incidence for various states of the surface. Curve 1 pertains to a surface treated with a grinding paper which resulted in grooves of 5 μm. Curve 2 pertains to the same surface after electropolishing. This surface smoothing results in a reduction of TAC from about 1 to about 0.7 at a medium angle of incidence.

After gas and contamination coverages had been partially removed both surfaces had a reduced TAC (curves 3 and 4).

Fig. 10 shows TAC's in the system Gold(111)-Helium. The single-crystal surface was mechanically and electrolytically polished until a very smooth surface was obtained (structure similiar to that shown in Fig. 1c). This surface contaminated with carbon, hydrocarbon, and oxygen yielded TAC's close to 1.0. After several cleaning procedures consisting of argon ion bombardment and vacuum annealing, the surface was almost completely cleaned and the TAC was reduced below 0.1. This is the lowest value of TAC measured to date.

In Fig. 11 some data for engineering grade surfaces are shown. TAC values between 1.0 and 0.7 were obtained without any special surface prepraration. By some cleaning procedures the values for the polycrystalline copper surface could be reduced below 0.5 while the TAC for tungsten, glass, and sapphire did not change very much, probably because of the bad vacuum annealing behavior after argon ion bombardment. The aging of shellac (for nearly four days) had no noticeable influence on the TAC, either.

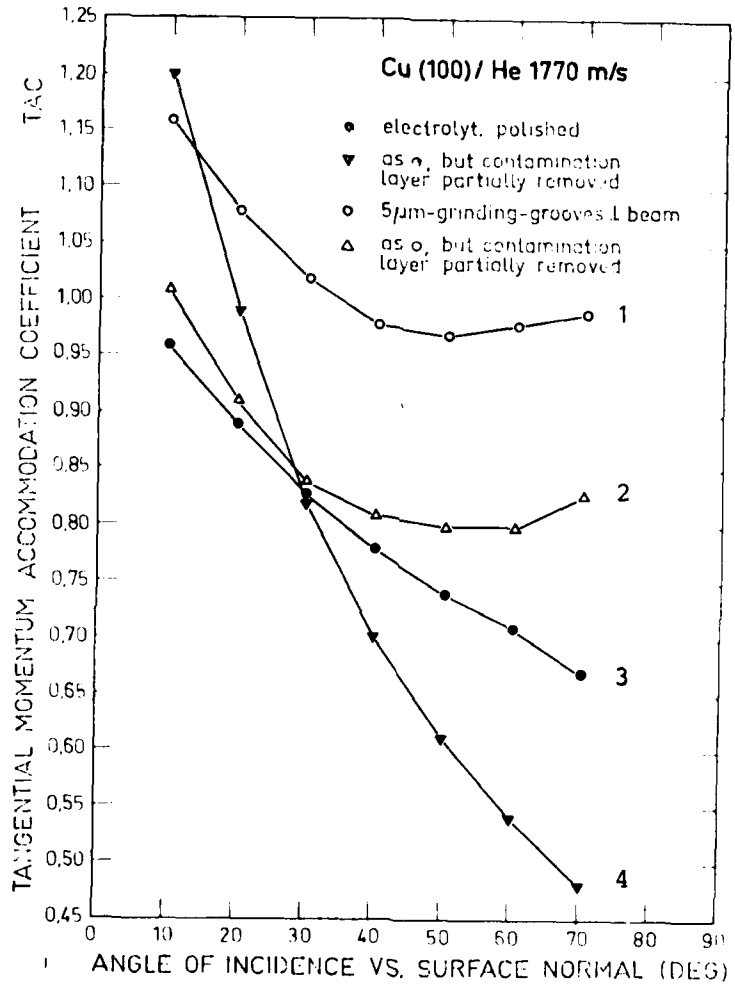

Fig. 9: TAC Measurements in the System Cu(100)-Helium

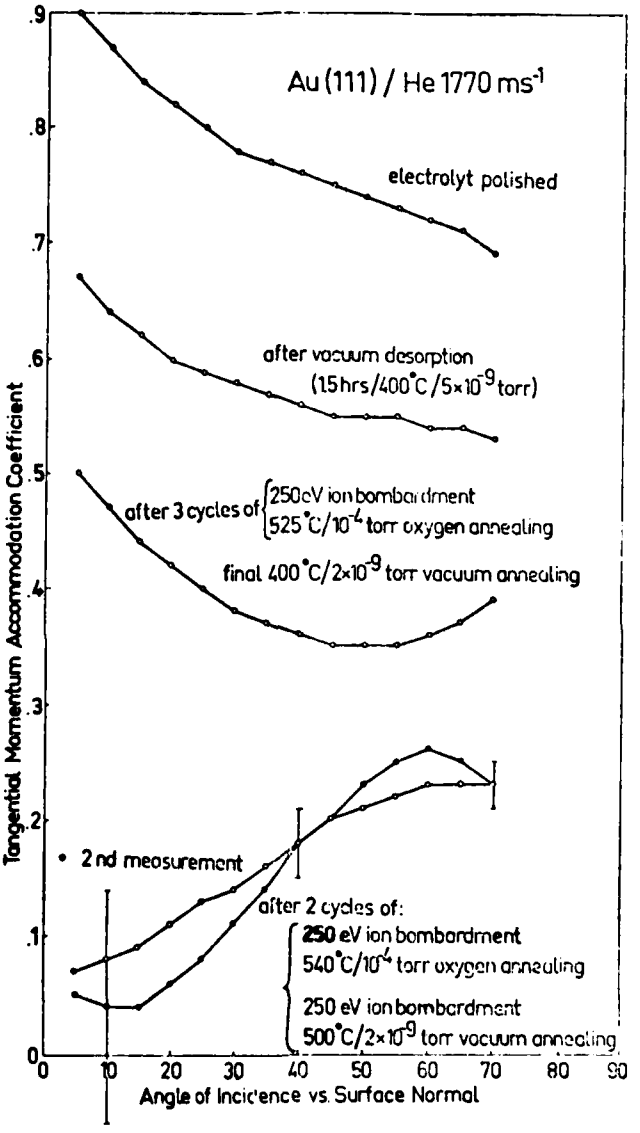

Fig. 10: TAC Measurements in the System Gold (111)-Helium

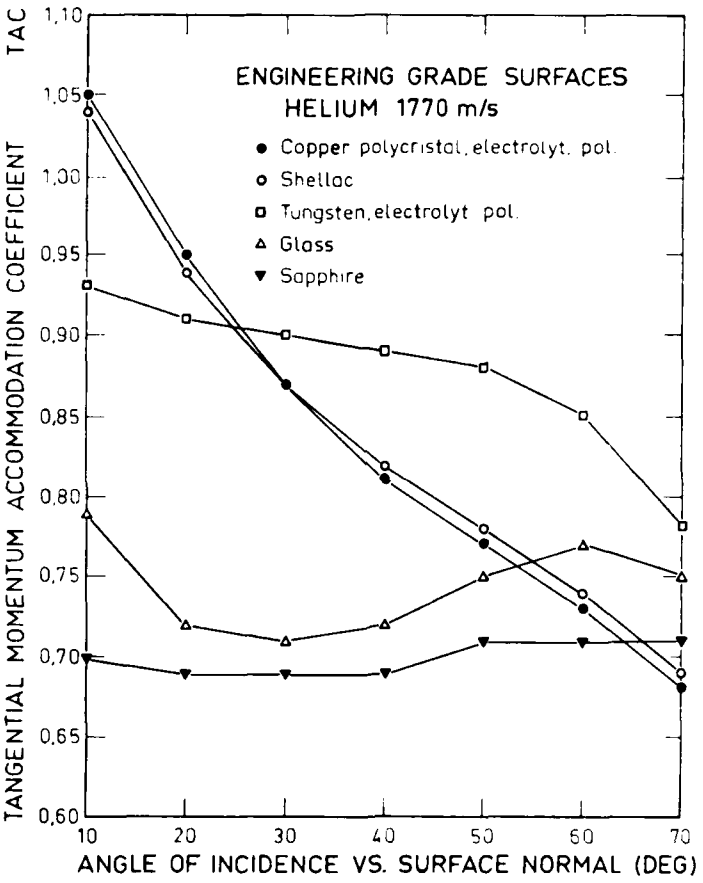

Fig. 11: TAC Measurements of Engineering Grade Surfaces

All these investigations demonstrate the great influence of the surface state on the TAC and thus on drag, but the measurements also showed another effect which could not be explained definitely until now. This is the dependence of the TAC on the angle of incidence, as shown in all the measurements. Fig. 12 shows measurements in the system He-Cu(100). An electrochemically polished copper surface was partially cleaned. The original curve (before cleaning) and the resulting one (after cleaning) cross each other. The explanation could lie in the effect of back-scattering by atomic roughness, as indicated by the little scheme above the definition of the TAC. At a certain angle of incidence the particles can be reflected in the opposite direction. The term p_{tr} in the definition then changes its sign and the TAC may increase above one (Fig. 12).

Discussion

When a single-crystal surface of gold was specially prepared, TAC values below 0.1 were reached. These are the lowest measured values known to date and, according to the estimation of K. Bärwinkel (in his article) could mean a perceptible reduction of drag. For a technical application there are two problems at the moment.

1. The values are measured in a vacuum. The problem is to maintain both a clean surface (without adsorbed gas layers) and low TAC values at higher pressures. Polycrystalline gold does not show any adsorption of oxygen or nitrogen at the Auger spectra up to 10^{-4} torr. This is the pressure limit for Auger spectroscopy. Nor was adsorption seen in the spectra after interaction of this surface with air at atmospheric pressure and subsequent evacuation. However, it is possible that an adsorbed layer built up at atmospheric pressure desorbs again during the evacuation. These possible effects must be studied with microbalances.

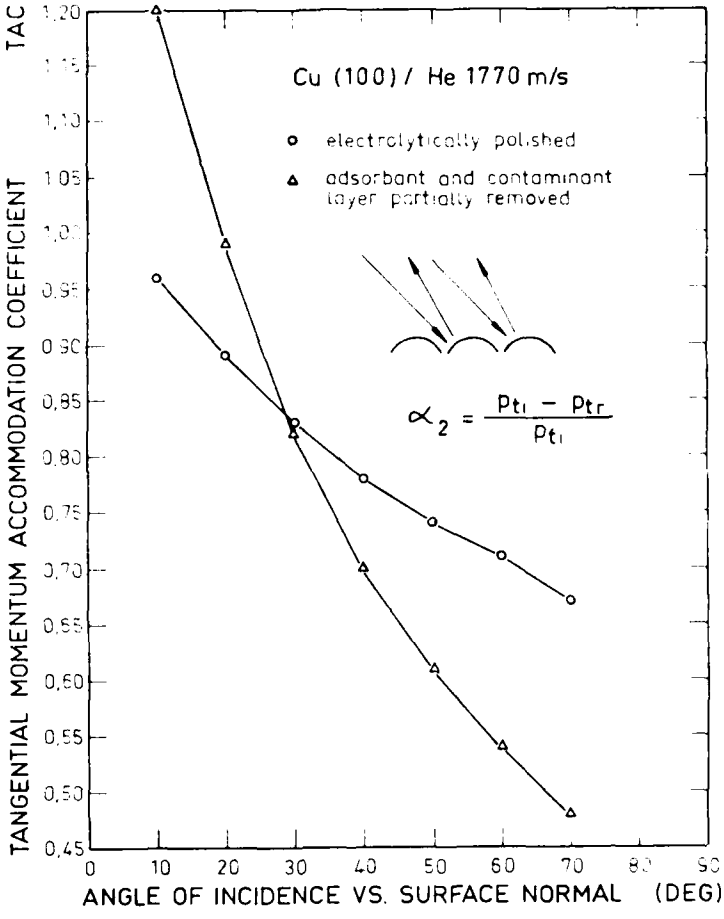

Fig. 12: TAC Measurement of the System Copper(100)-Helium and Scheme for the Explanation of the Dependence on Angle

2. The lowest values were measured on a single crystal surface. The question is whether these values are possible at technical surfaces, too. It was found that polycrystalline gold shows an adsorption behavior similar to that of single crystal surfaces with respect to oxygen and nitrogen but the TAC has not been measured yet.

At lower pressures, microroughness, and at higher pressures, adsorption layers are the limiting parameters for a further reduction of TAC and therefore of drag.

In contrast the energy accommodation coefficient is not dependent on roughness. Reduction of heat transfer is also a very interesting field of investigation because there are many corresponding technical materials problems. A desirable goal for the future will be the determination of the limits for the reduction of the energy accommodation coefficient by special surface selection and preparation as is being done for the TAC.

References

(1) D.F. Stein, R.E. Weber, and P.W. Palmberg; Journ. of Metals, February 1971.

(2) W.K. Huber, H. Selhofer, and A. Benninghoven; Journ. of Vacuum Science and Technology, Vol. 9, No. 1, 482 (1971).

(3) Gang W. Simmons; Dissertation presented to the graduate Faculty of the University of Virginia, April 21, 1967.

(4) E.J. Scheibner, L.H. Germer, and C.D. Hartmann; Review of Scientific Instruments, Vol.31, No. 2, 112 (1959).

(5) H.E. Farnsworth, R.E. Schlier, T.H. George, and R.M.Burger; Journ. Appl. Phys. 26, 252 (1955).

(6) H.E. Farnsworth, R.E. Schlier, T.H. George, and R.M.Burger; Journ. Appl. Phys. 29, 1150 (1958).

(7) U. Bossel; Dissertation, University of California, Berkeley, USA, Report No. AS-68-6,

(8) R.A. Millikan; Physical Review, Vol. 21, No. 3, 217 (March 1923).

Atomic Beam Scattering from Clean Crystal Surfaces

D. R. Frankl

Department of Physics

The Pennsylvania State University

University Park, Pennsylvania 16802

ABSTRACT

One of the basic problems in surface physics has been the determination of the crystallography of surface layers of atoms. The primary tool used so far has been low energy electron diffraction, but interpretation is difficult owing to penetration of the electrons into the crystal. The present paper deals with the scattering of atomic and molecular beams. The basic motivation is that penetration should be drastically reduced by the large size and low energy of the neutral incident particles.

In our apparatus, surfaces for study are prepared by cleaving single-crystal samples in situ in the ultra-high vacuum scattering chamber. We have studied helium scattering from two semiconductors (Si and Ge) and several alkali halides, while various metal surfaces have been studied in other laboratories. Metals generally give strong specular reflection (of light gases) but no diffraction. The semiconductors were found to give nearly diffuse scattering. The insulators, however, gave pronounced diffraction, especially when the surfaces were clean. The results and interpretations will be discussed.

INTRODUCTION

There is much important information to be gleaned from the study of atomic (and molecular) beam scattering from solids. In addition to the information on gas dynamics (i.e., momentum and energy accommodation) which is of primary interest in the present meeting, one may learn about the interaction forces,[1] about the phonon spectra of the solid[2] about mechanism of catalysis and surface reactions,[3] and (hopefully) about surface structure on the atomic scale. The latter question is most commonly attacked by the use of LEED (low energy electron diffraction).[4] However, despite the vast wealth of data obtained, the detailed structural interpretation is only very recently becoming possible. The reason for the difficulty is that even the lowest energy electrons penetrate some few layers into the target, so that multiple-scattering calculations are required. Another method available for structure studies is the FIM (field-ion microscope).[5] However, here there are also some difficulties, mainly that the range of materials is very limited and that the observation is made in the presence of very strong electric fields. Thus there is a definite need for still further methods. Atomic beam scattering has several promising features for this purpose: the particles should be very nonpenetrating and it is very broadly applicable.

DESCRIPTION OF APPARATUS

A schematic overall view of the apparatus is given in Fig. 1. The beam is a so-called "nozzle beam," formed by expanding a gas through a nozzle from a fairly high pressure into vacuum.[6] The beam is roughly defined by a "skimmer" (thin-walled conical aperture) then passed through a chopper, a

velocity selector, a buffer vacuum stage and the final collimator (a pinhole, 0.5 mm diam.) into the scattering chamber. The latter is pumped, by a titanium sublimation pump in parallel with a turbomolecular pump backed by a small oil diffusion pump, to a base pressure typically in the low 10^{-10} Torr range. The surface for investigation is prepared by cleaving a single crystal sample in situ. The sample can then be rotated about a fixed axis to vary the angle of incidence and about the surface normal to vary the azimuth. The detector, a quadrupole mass analyser, can be swung in planes parallel to the plane of incidence and translated perpendicular to it.

CHARACTERISTICS OF THE BEAM

Most of our work has been done with ^{4}He cooled to about 80 K by means of a liquid nitrogen jacket around the nozzle tube (see Fig. 1). With a 0.04 mm nozzle, fairly high pressures can be run without flooding the exhaust pump. Some resulting velocity distributions are shown in Fig. 2. It is seen that a half-width of about 3% is obtained at the highest source pressure. The wavelength is about 1 Å.

In Table I, the parameters of this particular beam are compared with those of a typical LEED beam.[4] It is seen that the intensity and coherence properties are more or less the same. The electron beam does, of course, present great practical advantages in formation, handling, modulation, and detection. Thus it is clear that atomic beams will never replace LEED as a practical wide-usage method. However, as we shall show, there is reason to believe that it will become a valuable companion method.

GENERAL RESULTS

1. Metals

Scattering of various gases from metals has been widely studied in other laboratories (though not yet in our apparatus). The surfaces are, of course, not prepared by cleavage, but are cleaned in various ways. The general results follow a definite pattern[7] which is typified by Fig. 3: the lighter gases are reflected in a fairly specular manner while the heavier ones are scattered more diffusely. In particular, with only very few exceptions, metal surfaces do not show diffraction. The reason is believed to be that the free electrons are readily able to smooth out the periodic structure of the interaction potential.

2. Semiconductors

The first materials studied in our apparatus were the elemental semiconductors, silicon and germanium.[9] Here there was neither diffraction or specular reflection, just a broad and quite diffuse scattering distribution. An example is shown in Fig. 4. Similar results had been obtained on silicon[10] and diamond[11] surfaces that were presumably somewhat contaminated. We found that contamination due to aging for one day in the vacuum (2×10^{-9} Torr) was sufficient to make the scattering become almost completely diffuse. However, even on the cleanest surfaces (i.e., those run within an hour after cleaving), there was only a small degree of directionality.

The reason for the generally diffuse nature of the scattering probably lies in the open structure of the diamond cubic lattice, in which both silicon and germanium crystallize. A photograph of a hald-sphere model, shown in

Fig. 5, illustrates the large open channels in which the incident atoms might readily get trapped.

3. Ionic crystals

This class of materials has been the workhorse of the field for over four decades. Starting with the pioneering work of Stern's group,[12] strong reflection and diffraction peaks were observed, and have been repeatedly studied ever since.

Most of the previous studies were made on surfaces prepared by cleaving the crystals in the room air before mounting them in the apparatus. Such heavily contaminated surfaces gave only diffuse scattering. The diffraction could be seen only after heating to drive off adsorbed water. Even then, it was conjectured that the surfaces were still covered with an epitaxial water layer, and optical (ellipsometric)measurements[13] strongly confirmed this, at least in the case of LiF.

One set of measurements[14] was made on in-situ-cleaved surfaces, but the vacuum was only 10^{-8} Torr and the likelihood is that the surfaces got covered before the measurements were made. In any case, the results were generally similar to the others. However, in our measurements, after cleaving in 10^{-9} Torr or better, the results were strikingly different. Before describing them, we shall briefly review the basic ideas of diffraction theory.

REVIEW OF DIFFRACTION PRINCIPLES

For diffraction from a 3-dimensional lattice, the basic relations are the "Laue equations"[15]

$$\vec{k}' = \vec{k} + \vec{G}^{(3)} \tag{1}$$

$$E' = E \tag{2a}$$

or

$$\frac{h^2}{2m} k'^2 = \frac{h^2}{2m} k^2 \quad . \tag{2b}$$

Here E and $\vec{k}$ are the incident energy and wavevector, respectively, E' and $\vec{k}'$ are the corresponding quantities of the outgoing particle, and $\vec{G}^{(3)}$ is any one of the (3-dimensional) reciprocal lattice vectors. The well-known geometrical solution of this pair of equations is given by the "Ewald sphere" construction; reciprocal lattice points intersected by the sphere give the allowed $\vec{k}'$'s.

For two dimensions, the conditions are somewhat different. If we resolve $\vec{k}$ into its parallel and perpendicular components

$$\vec{k} = \vec{K} + k_z \hat{z} \quad , \tag{3}$$

then the Laue equations become

$$\vec{K}' = \vec{K} + \vec{G}^{(2)} \tag{4}$$

$$E' = E \tag{4a}$$

or

$$E(K') + E_z' = \frac{h^2}{2m} (K^2 + k_z^2) \quad . \tag{4b}$$

Here E_z' is the part of the final-state energy of the particle associated with its motion perpendicular to the surface plane. There are two cases to be considered: E_z' may be either positive (particle reflected from the surface) or negative (particle trapped in the one-dimensional potential well at the surface).

Case A: $E'_z > 0$. The final state is a free state of the particle. Hence

$$E'_z = \frac{h^2}{2m} k'^2_z \quad , \tag{5a}$$

$$E(K') = \frac{h^2}{2m} K^2 \quad , \tag{5b}$$

so the energy balance equation is again just Eq. (2b). But since Eq. (4) is less restrictive than Eq. (1), more solutions are possible. The analog of the Ewald sphere construction is shown in Fig. 6. All reciprocal lattice points lying <u>within</u> the given circle give allowed $\vec{k}'$'s.

Case B: $E'_z < 0$. The final state is now a particle moving in two dimensions (parallel to the surface) but trapped in the third. Equation (4b) may be written

$$\varepsilon(\vec{K}') = K^2 + k_z^2 + |\varepsilon'_z| \quad , \tag{6}$$

where

$$\varepsilon = \left(\frac{2m}{h^2}\right) E \quad . \tag{7}$$

For discrete trapping states (i.e., discrete values of ε'_z), Eq. (6) leads to additional solutions lying <u>outside</u> the "Ewald circle." The loci of these solutions in the K-plane depend on the form of the $\varepsilon(\vec{K}')$ relationship.

Case B1: If the relation is free-particle-like, with an effective mass equal to the true mass, then

$$\varepsilon(\vec{K}') = K'^2 \tag{8}$$

and Eq. (6) is simply

$$\left(\vec{K} + \vec{G}^{(2)}\right)^2 = \varepsilon + |\varepsilon_z'| \quad , \tag{9}$$

which is a circle centered at $-\vec{G}^{(2)}$ with radius $\sqrt{\varepsilon+|\varepsilon_z|}$. Thus, the experimental K values give both $\vec{G}^{(2)}$ and ε_z for the transition.

The transitions are illustrated in Fig. 7a. They obviously lead to an extraction of intensity from any allowed reflections, including the specular one. This was first observed by Frisch and Stern[16] and was given the name "selective adsorption." The theory just given is simply a rewording of that of Lennard-Jones and Devonshire.[17,18]

Case B2: In the final state, the particle is moving in a two-dimensional periodic potential. Thus, the general relation of ε to $\vec{K}'$ is not Eq. (8) but

$$\varepsilon(\vec{K}') = \vec{K}' \cdot \left(\frac{m}{m^*}\right) \cdot \vec{K}' \tag{10}$$

where $(1/m^*)$ represents the reciprocal-effective-mass tensor. The situation is illustrated in Fig. 7b. It is seen that the same transitions may occur, but that the loci of their $\vec{K}$ values are not necessarily circles. In principle, from the loci at several different incident energies not only the ε_z and $\vec{G}^{(2)}$ values but also the $\varepsilon(\vec{K}')$ relationship in each bound state could be determined. The latter would, of course, give much insight into the shape of the periodic potential, i.e., into the "surface structure" of the material.

EXPERIMENTAL RESULTS ON IONIC CRYSTALS

As stated above, some of the ionic crystals, especially lithium fluoride, were extensively studied in the past. Both diffraction and selective adsorption were observed on surfaces "cleaned" by heating. Some of the important recent work includes:

1. Comparative studies of the scattering of several gases.[19-22]
2. Measurement of diffracted intensities over a wide range of angles.[23]
3. Measurement of velocity distributions in the diffracted bames.[24]
4. Observation of inelastic effects due to phonon absorption or emission.[2]
5. Diffraction and selective adsorption of monatomic H and O.[25-27]

Our work on the ionic crystals has been concentrated mainly on the selective adsorption effect. This was done for two reasons: (1) the initial apparatus did not provide the angular precision needed for a really careful diffraction study (though this has since been remedied), and (2) whereas the diffraction from LiF was more or less the same as from the "heat-cleaned" surfaces studied in the past, the selective adsorption was strikingly different. This can be seen by comparing the results[28] shown in Fig. 8 with typical previous ones such as Fig. 5 of Reference 20. The in-situ-cleaved surfaces give sharper and deeper adsorption lines, with much more detail and "fine structure." The major lines obey Eq. (9) and there is evidence for five different energy levels, three bound states and two positive-energy resonances.

To follow up on these results, it was decided to survey several of the other alkali halides, to ascertain the effects of varying the lattice spacing and ion-size ratio. An idea of the values of these parameters, according to Pauling,[29] is given in Fig. 9. Four of them have been studied so far,[30] and we conclude with a brief summary of the results.

The next smallest lattice after LiF is NaF. Figure 10 shows a sampling of selective adsorption scans and Fig. 11 a K-plane plot of the minima. Most of the points can still be fitted to circles, so it looks as if Eq. (9) still holds. However, the energy values (ε_z) deduced unfortunately show rather little consistency, as is shown in Fig. 12. Therefore, the interpretation seems a bit shaky.

The case of NaCl is even worse. Strong adsorptions do certainly occur, as shown in Fig. 13, but there are so many of them that no clear cut fitting of circles can be done. Finally, KF, which has nearly equal ionic radii and might therefore be expected to display some degree of simplicity, is the worst of all. The data are shown in Fig. 14, but little headway has been made in fitting.

CONCLUSIONS

It seems evident that the results to date bring both bad and good news. The bad news is that things are complex: little information of a simple directly interpretable nature seems to be forthcoming. The good news, though, is that the information is there, in abundance and great detail. The situation is somewhat comparable to that in LEED a decade ago, viz., an almost embarassing wealth of experimental data. Thus, there seems a good likelihood that atomic beam scattering will some day take its place as a partner of LEED as a powerful tool for surface structure analysis.

ACKNOWLEDGMENTS

The support of the U. S. Office of Naval Research in this work is gratefully acknowledged. Thanks are also due to the author's students, Dr. Douglas E. Houston and Mr. Jeffrey A. Meyers for their share (the major part) of the work, and to Professor William A. Steele for many helpful discussions.

REFERENCES

1. F. O. Goodman, Surf. Sci. 26, 327 (1971).
2. B. R. Williams, J. Chem. Phys. 55, 1315 (1971); ibid, 3220 (1971).
3. S. L. Bernasek, W. J. Sickhaus, and G. A. Somorjai, Phys. Rev. Letters 30, 1202 (1973).
4. M. B. Webb and M. G. Lagally, Solid State Physics 28, 301 (1973).
5. E. W. Müller and T. T. Tsong, "Field Ion Microscopy - Principles and Applications," American Elsevier Publishing Co., New York (1969).
6. H. Pauly and J. P. Toennies, Capt. 3.1 of "Methods of Experimental Physics, Vol. 7, Part A," B. Bederson and W. L. Fite, eds., Academic Press, New York (1968).
7. W. A. Steele,"The Interaction of Gases with Solid Surfaces," Pergamon Press (to be published).
8. H. Saltsburg and J. N. Smith, Jr., J. Chem. Phys. 45, 2175 (1966).
9. D. E. Houston and D. R. Frankl, J. Chem. Phys. 60, 3268 (1974).
10. N. A. Meshcheryakov, Fiz. Tekh. Poluprovodn. 3, 1262 (1969) [Sov. Phys. Semicond. 3, 1057 (1970)].
11. W. H. Weinberg, Thesis, University of California, Berkeley (1971, unpublished), Appendix E.
12. I. Estermann and O. Stern, ZS f Physik 61, 95 (1930).
13. W. Bayh and H. Pflug, Z. Angew. Physik 25, 358 (1968).
14. J. C. Crews, "Fundamentals of Gas-Surface Interactions," H. Saltsburg, J. N. Smith, Jr., and M. Rogers, eds., Academic Press, New York (1967).
15. C. Kittel, "Introduction to Solid State Physics, 3rd Edition," Wiley, New York (1966), Chapter 2.
16. R. Frisch and O. Stern, ZS für Physik 74, 430 (1933).

17. J. E. Lennard-Jones and A. F. Devonshire, Nature (London) 137, 1969 (1936).

18. A. F. Devonshire, Proc. Roy. Soc., Ser A, 156, 37 (1936).

19. J. N. Smith, Jr., D. R. O'Keefe, H. Saltsburg, and R. L. Palmer, J. Chem. Phys. 50, 4667 (1969).

20. D. R. O'Keefe, J. N. Smith, Jr., R. L. Palmer, and H. Saltsburg, J. Chem. Phys. 52, 4447 (1970).

21. D. R. O'Keefe, J. N. Smith, Jr., R. L. Palmer, and H. Saltsburg, Surf. Sci. 20, 27 (1970).

22. D. R. O'Keefe, R. L. Palmer, and J. N. Smith, Jr., J. Chem. Phys. 55, 4572 (1971).

23. G. Boato, P. Cantini, M. J. Cardillo, and R. Tatarek, Paper presented at Symposium on Surface Science, Cannes (1973, unpublished).

24. S. S. Fisher, M. N. Bishara, A. R. Kulthan, and J. E. Scott, Jr., "Rarefied Gas Dynamics - 6th Symposium," L. Trilling and H. Y. Wachman, eds., Academic Press, New York (1969).

25. H. Hoinkes, H. Nahr, and H. Wilsch, Surf. Sci. 30, 363 (1972).

26. H. Hoinkes, H. Nahr, and H. Wilsch, J. Chem. Phys. 58, 3931 (1973).

27. H. Hoinkes, H. Nahr, and H. Wilsch, Surf. Sci. 33, 516 (1972).

28. D. E. Houston and D. R. Frankl, Phys. Rev. Letters 31, 298 (1973); erratum, ibid 968 (1973).

29. L. Pauling, "Nature of the Chemical Bond, 2nd Edition," Cornell Univ. Press (1948), p 353.

30. J. A. Meyers, D. E. Houston, and D. R. Frankl, Japanese J. Appl. Phys. (to be published).

Table I

COMPARISON OF PARTICLE BEAMS

	Electron (typical)	Atomic (PSU System)
Beam current (particles/sec)	10^{3}	10^{11}
Angular spread (rad)	10^{-2}	5×10^{-4}
Flux (particles/sterad-sec)	10^{17}	10^{19}
Velocity (cm/sec)	10^{8}	10^{5}
Particle density (cm^{-3})	10^{7}	10^{8}
Equivalent pressure at 300K (Torr)	---	1×10^{-9}
Energy resolution $\Delta E/E$	10^{-2}-10^{-3}	$\gtrsim 6\times10^{-2}$
Coherence length $\Delta Z = \frac{2\lambda E}{\Delta E}$	$\sim10^{3}$ Å	30 Å
Coherence width $\Delta x = \frac{\lambda}{2\beta_s}$	$\sim10^{3}$ Å	5×10^{3} Å
Coherence volume $(\Delta x)^2(\Delta Z)(cm^3)$	$\sim10^{-15}$	$\sim10^{-15}$
Degeneracy (particles/coh vol)	10^{-8}	10^{-7}
Intensity modulation	Mech or Elec	Mech
Deflection	Elec or mag	----
Detection efficiency	~1	$\sim10^{-4}$
Background reduction	Energy	Time of flight

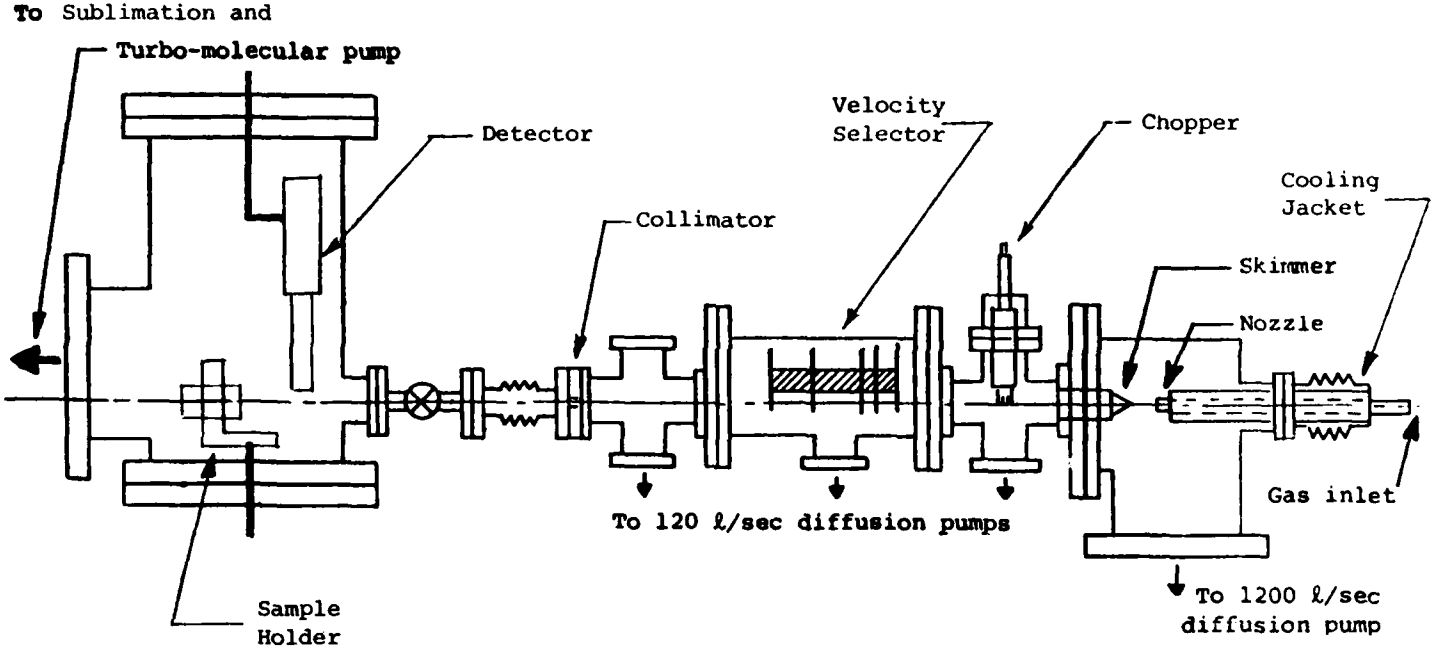

Figure 1. Schematic diagram of molecular beam source and scattering chamber.

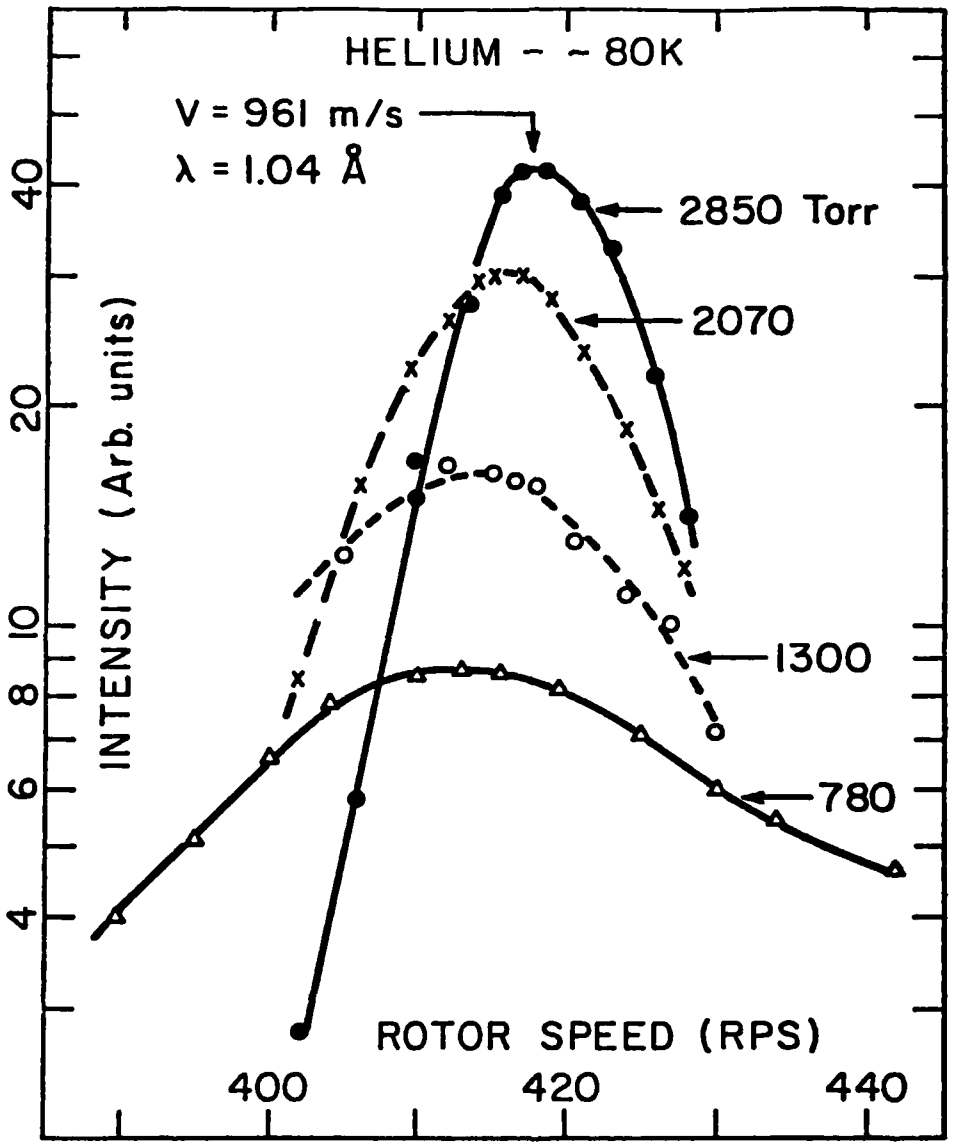

Figure 2. Velocity distributions in ^{4}He beams expanded from various pressures at 80K.

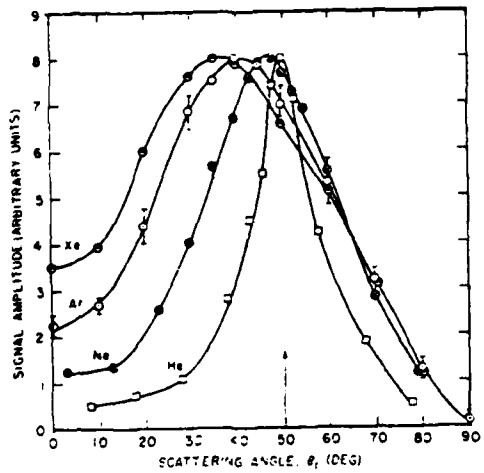

Figure 3. Typical angular distributions in the scattering of rare gases from metals. Data for silver, after Saltsburg and Smith, reference 8.

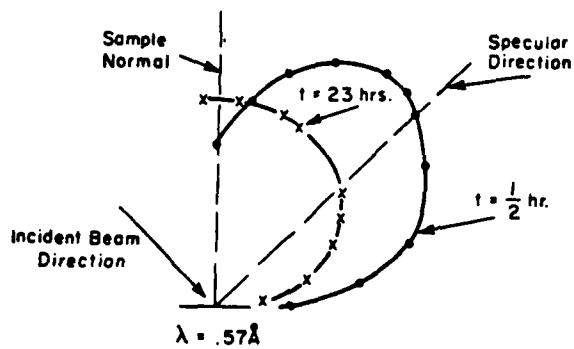

Figure 4. Typical angular distributions in the scattering of rare gases from clean elemental semiconductors. Data for ^{4}He on silicon, after Houston and Frankl, reference 9.

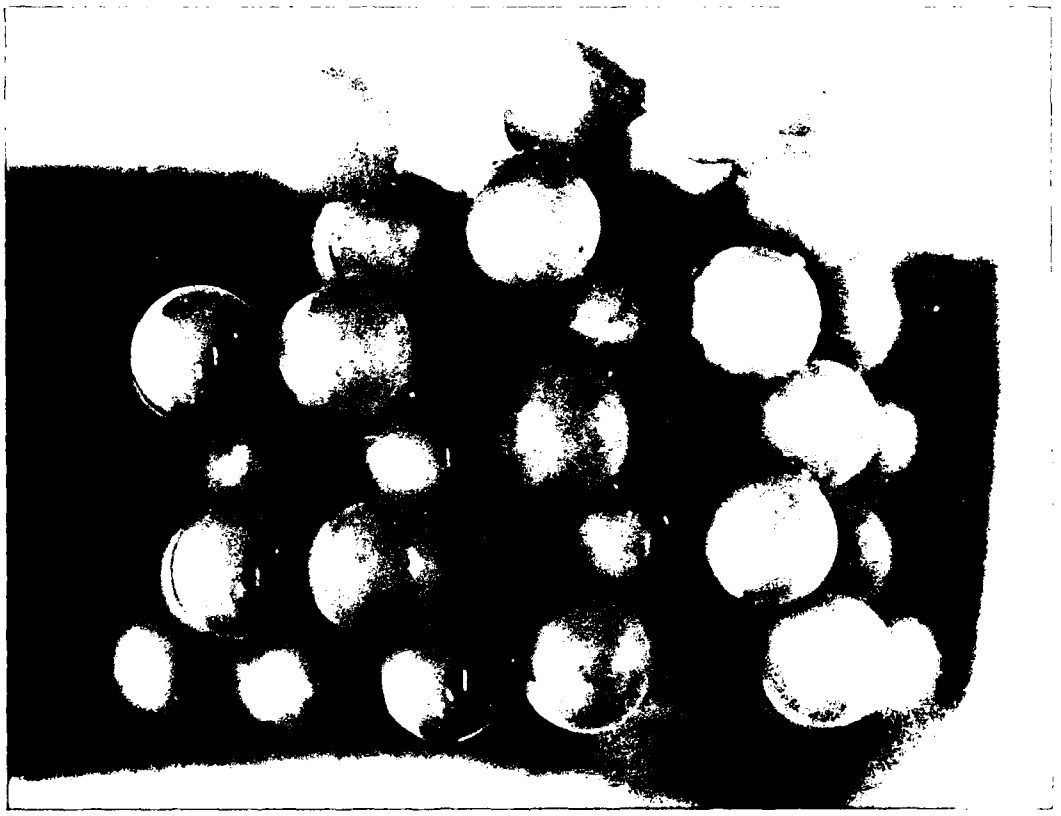

Figure 5. Model of the diamond-cubic lattice, showing the large holes in the (111) face (the cleavage face).

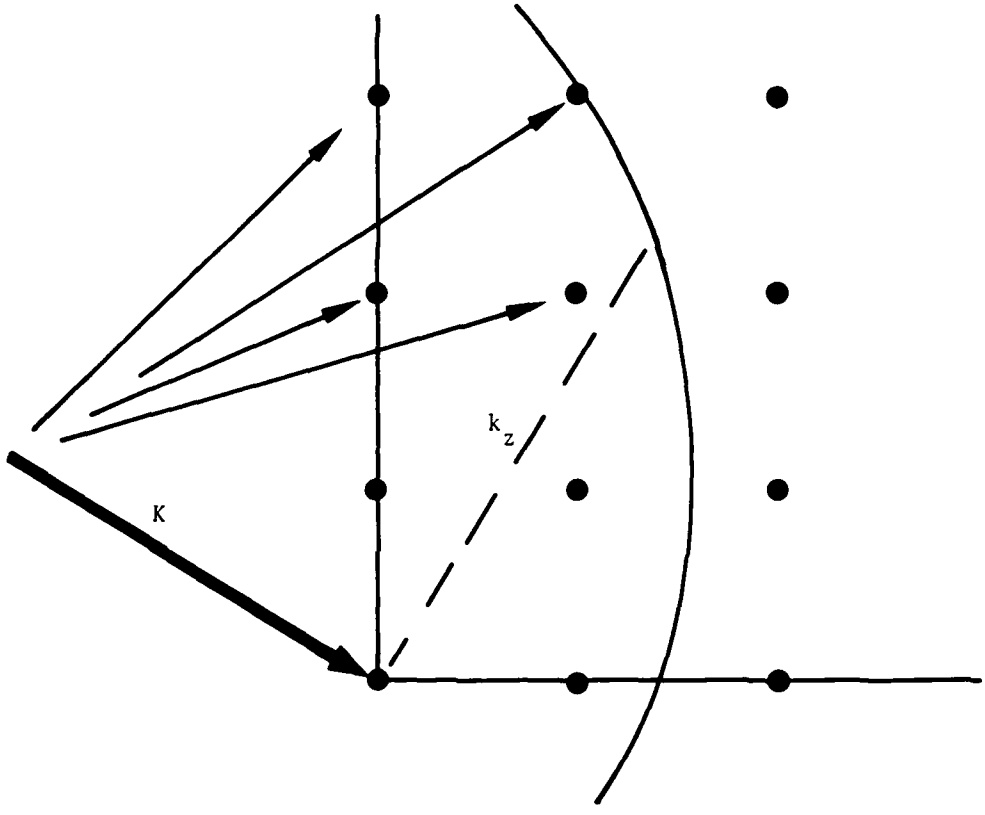

Figure 6. Two-dimensional analog of the Ewald sphere construction. The light arrows show some of the allowed $\vec{K}'$ vectors.

Figure 7. Transitions involved in selective adsorption in a single trapping band. (a) Figure for the case that the trapped particle is free in two dimensions. The solid arrows are several possible $\vec{K}$ vectors and the dashed lines are the corresponding $\vec{K}'$ vectors. (b) Figure for the case that the trapped particle has a tensor effective mass in the two-dimensional periodic potential.

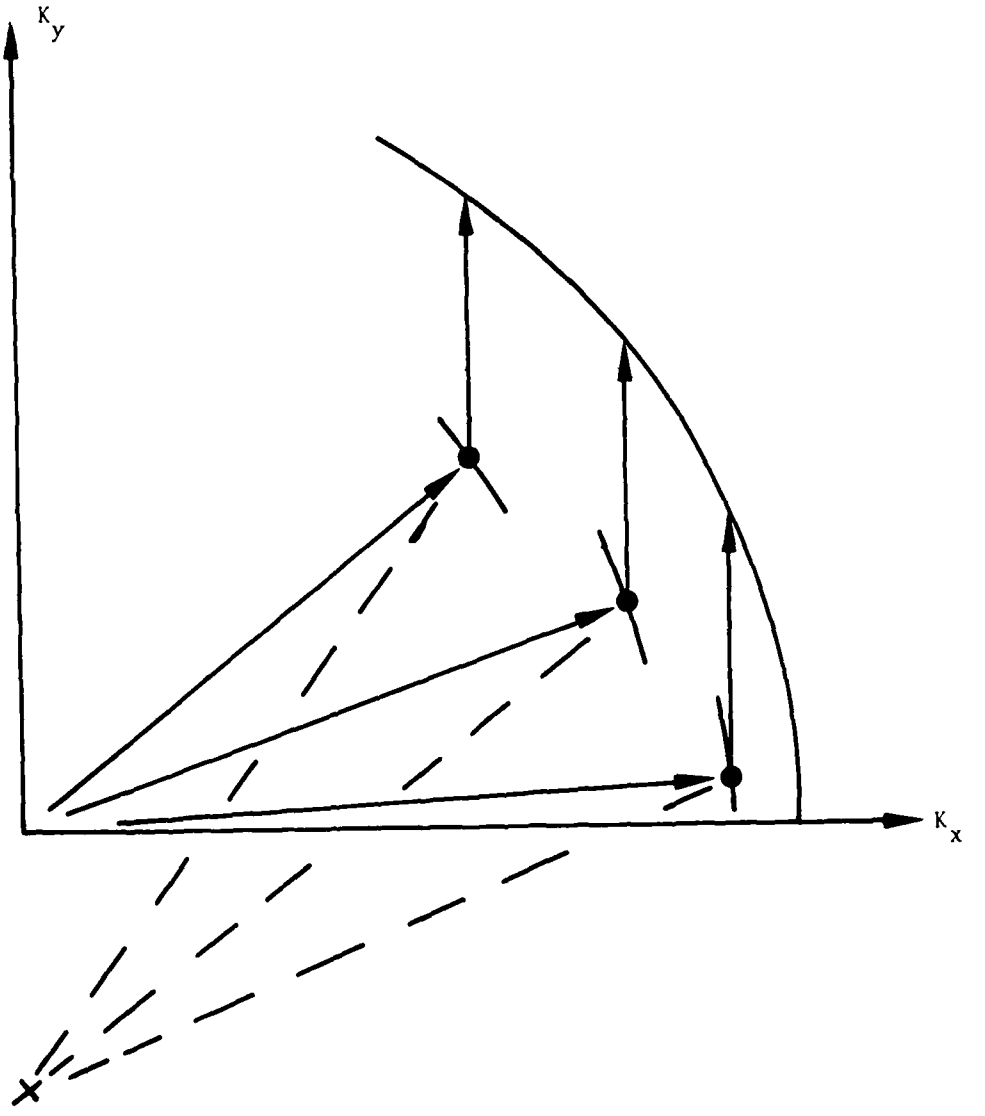

Figure 7a

Figure 7 (Continued)

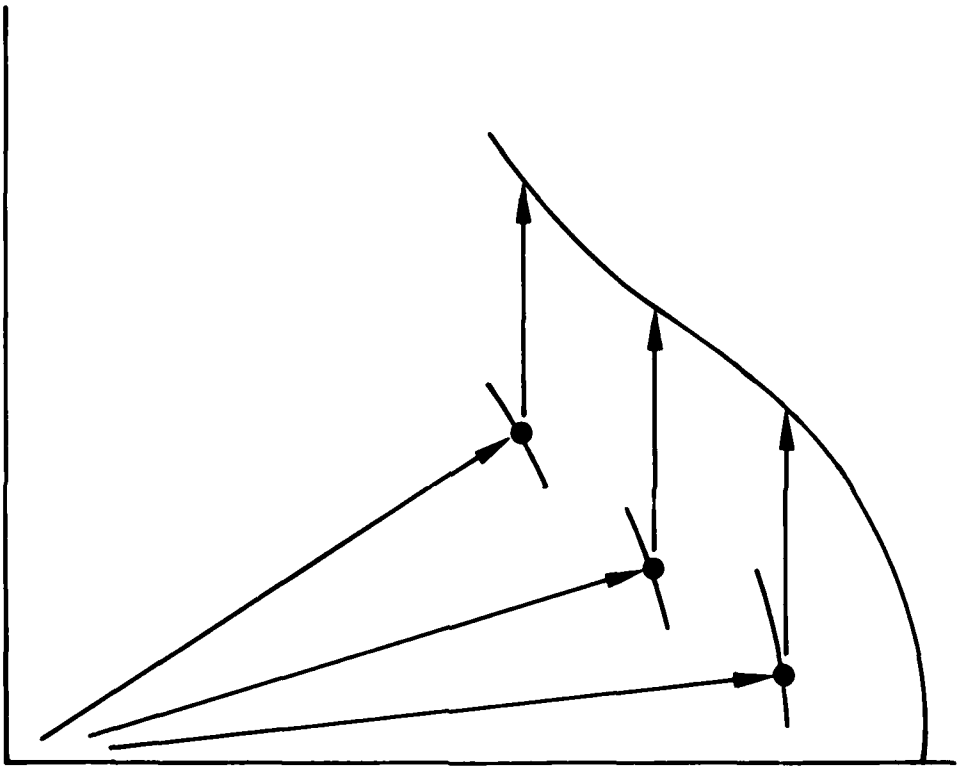

Figure 7b

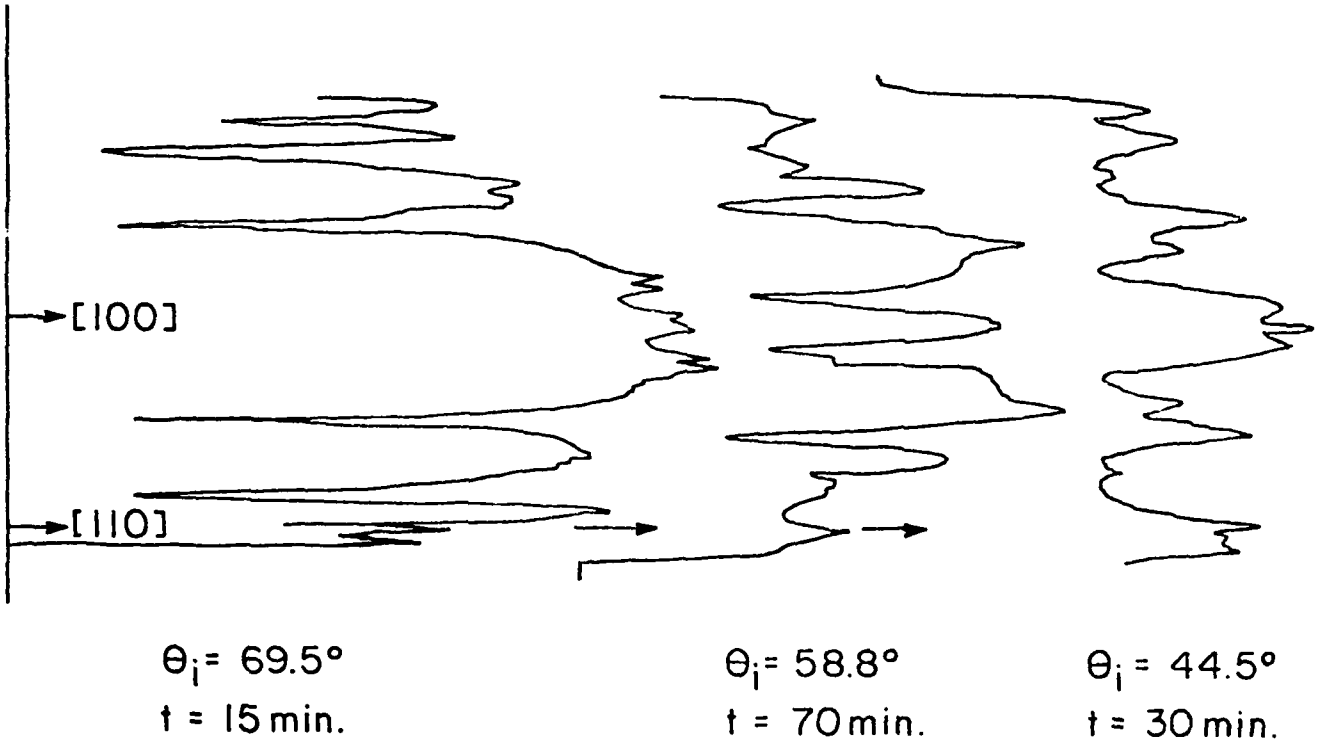

Figure 8. Selective adsorption data for ^{4}He on clean LiF. Each trace gives the specular reflection intensity as function of azimuthal angle for fixed incidence angle. After Houston and Frankl, ref. 28.

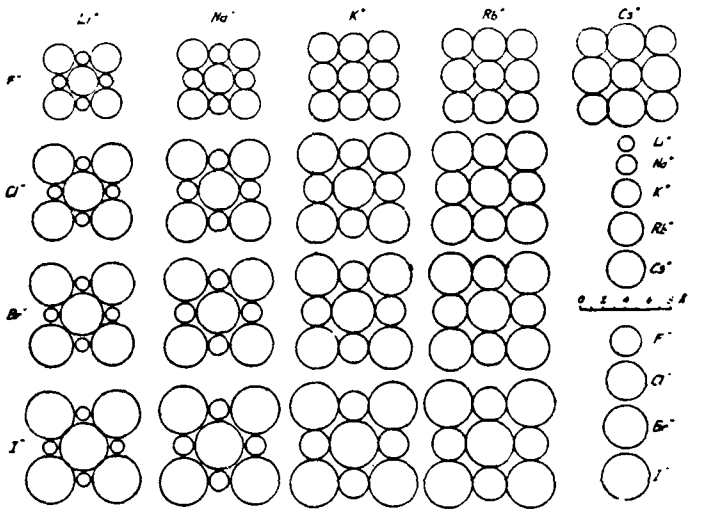

Figure 9. Surface lattices of the various alkali halides.
After Pauling, reference 29.

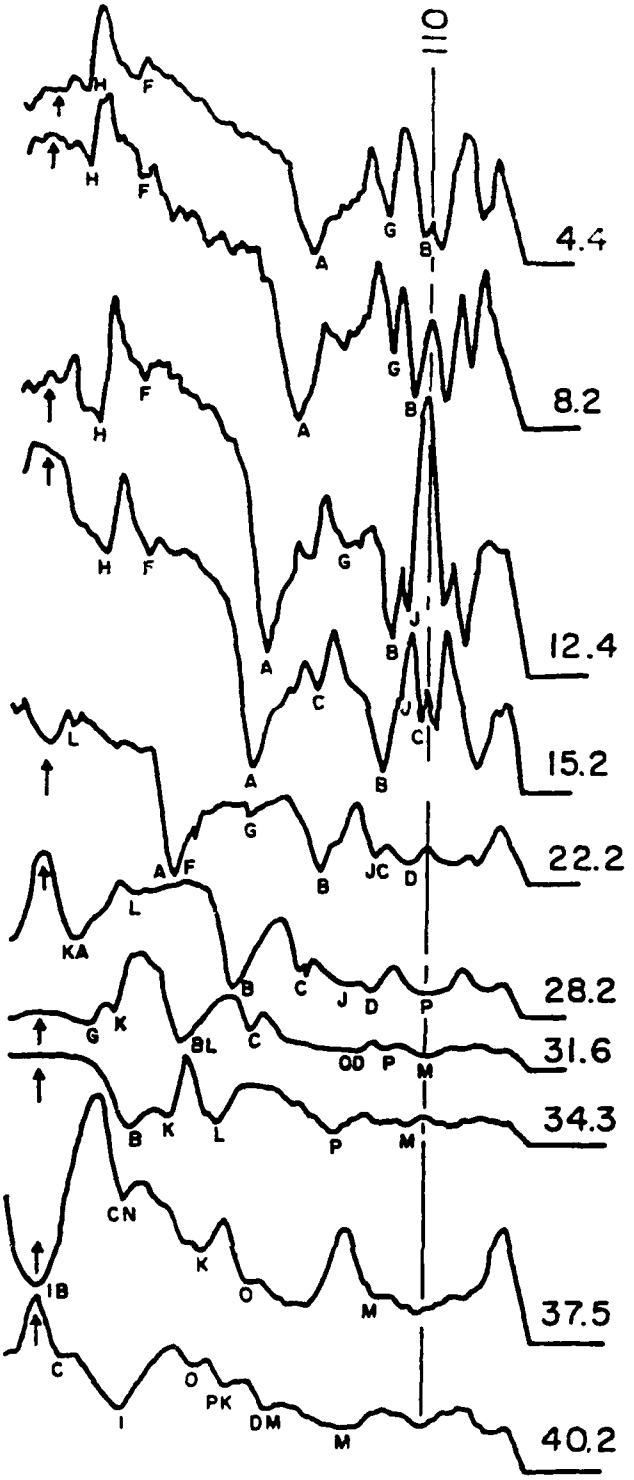

Figure 10. Selective adsorption data for ^4He on clean NaF. After Meyers et al., reference 30.

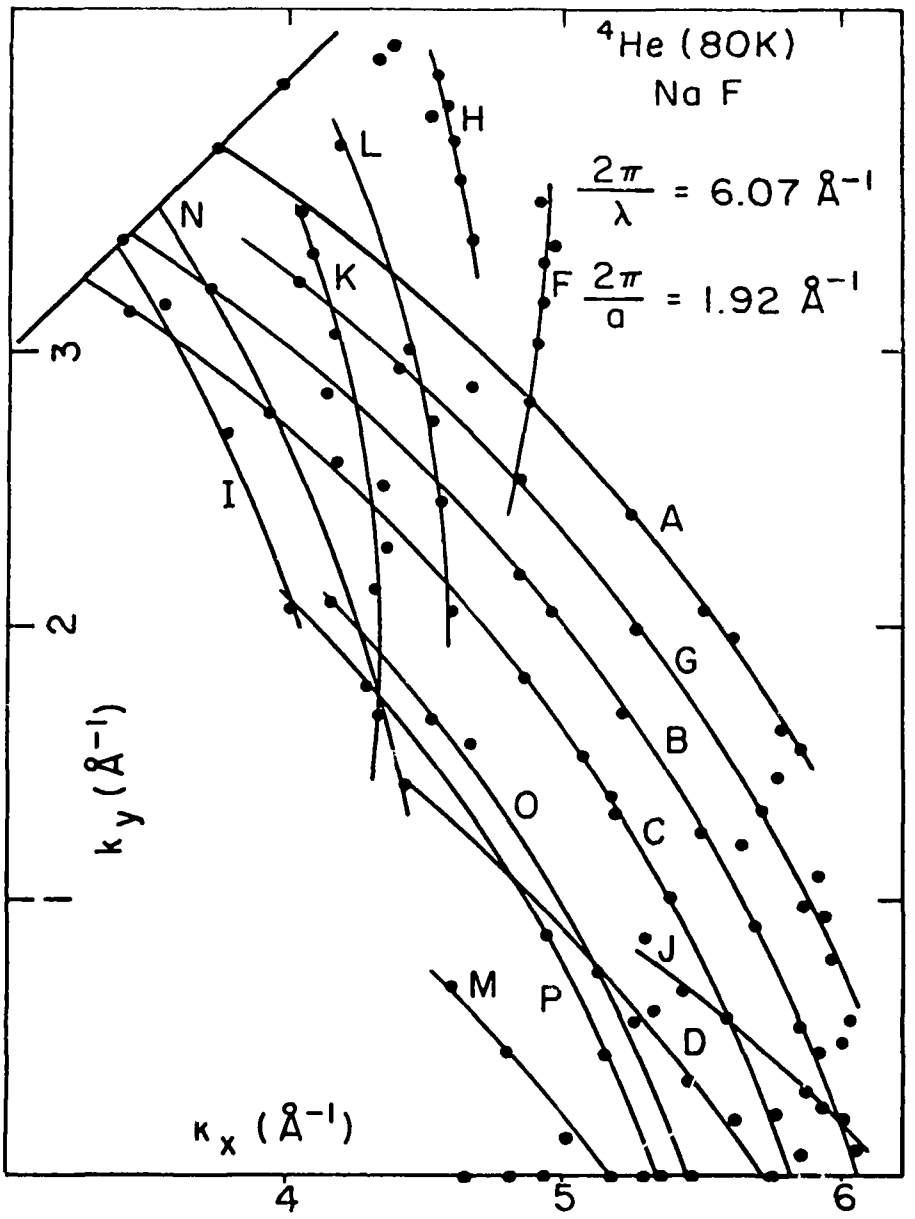

Figure 11. $\vec{K}$-vectors for selective adsorption of ^{4}He on NaF. Curves are circles centered at reciprocal lattice points in accordance with Eq. (9). After Meyers et al., reference 30.

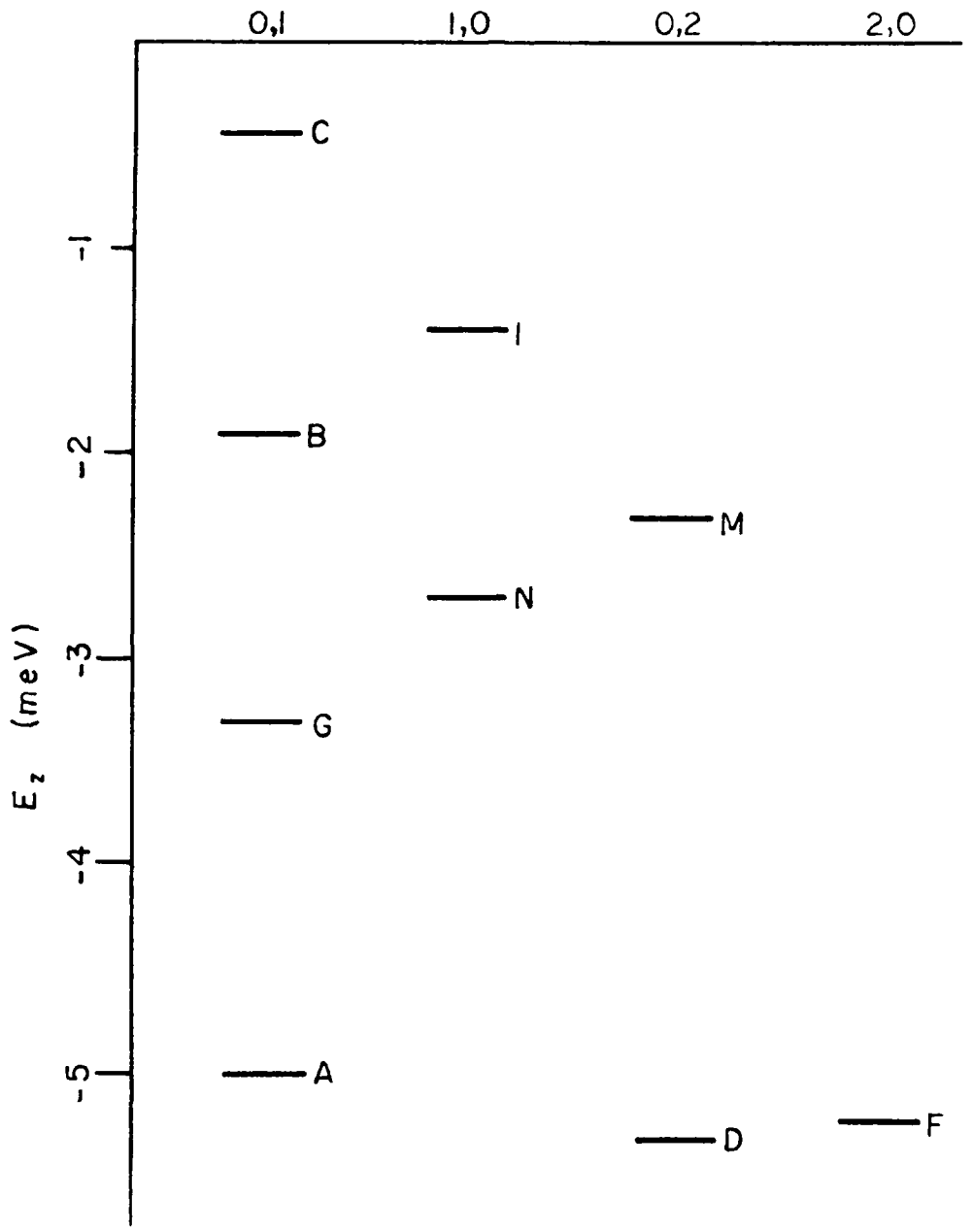

Figure 12. Energies and $\vec{G}$-vectors corresponding to the fitted circles of Fig. 11.

AD-A130 508 PROCEEDINGS OF THE SYMPOSIUM ON FLUID-SOLID SURFACE INTRACTIONS (2ND) HEL..(U) DAVID W TAYLOR NAVAL SHIP RESEARCH AND DEVELOPMENT CENTER BET.. H J LUGT

2/2

UNCLASSIFIED 29 NOV 74 F/G 5/2 NL

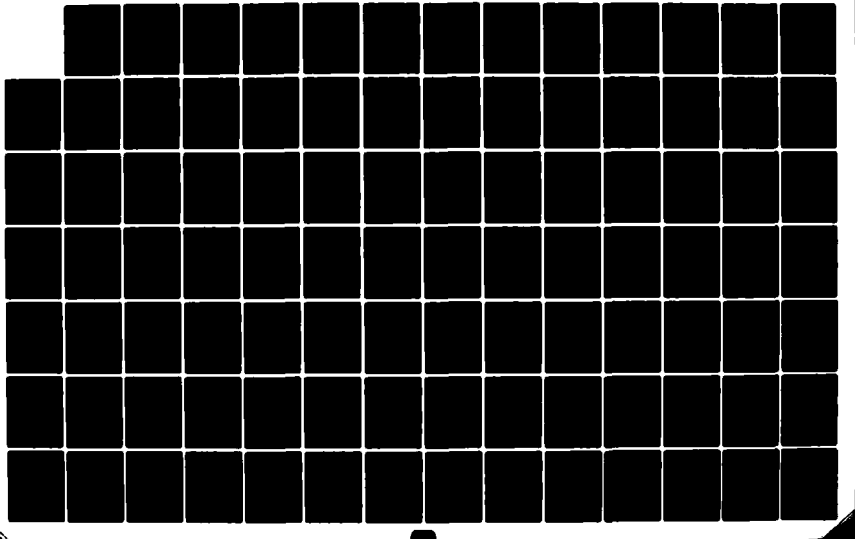

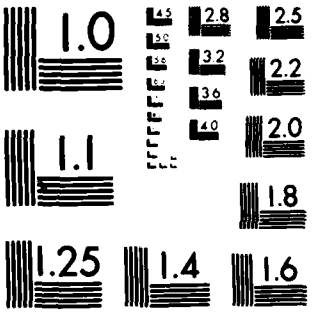

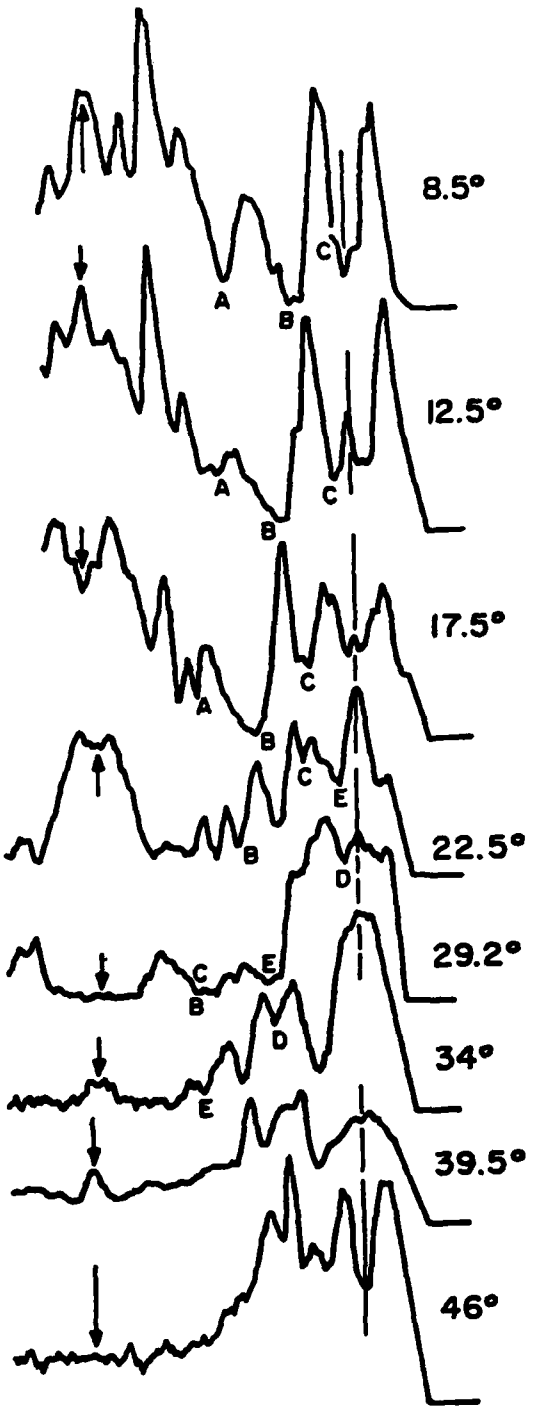

Figure 13. Selective adsorption data for ^{4}He on NaCℓ. After Meyers et al., reference 30.

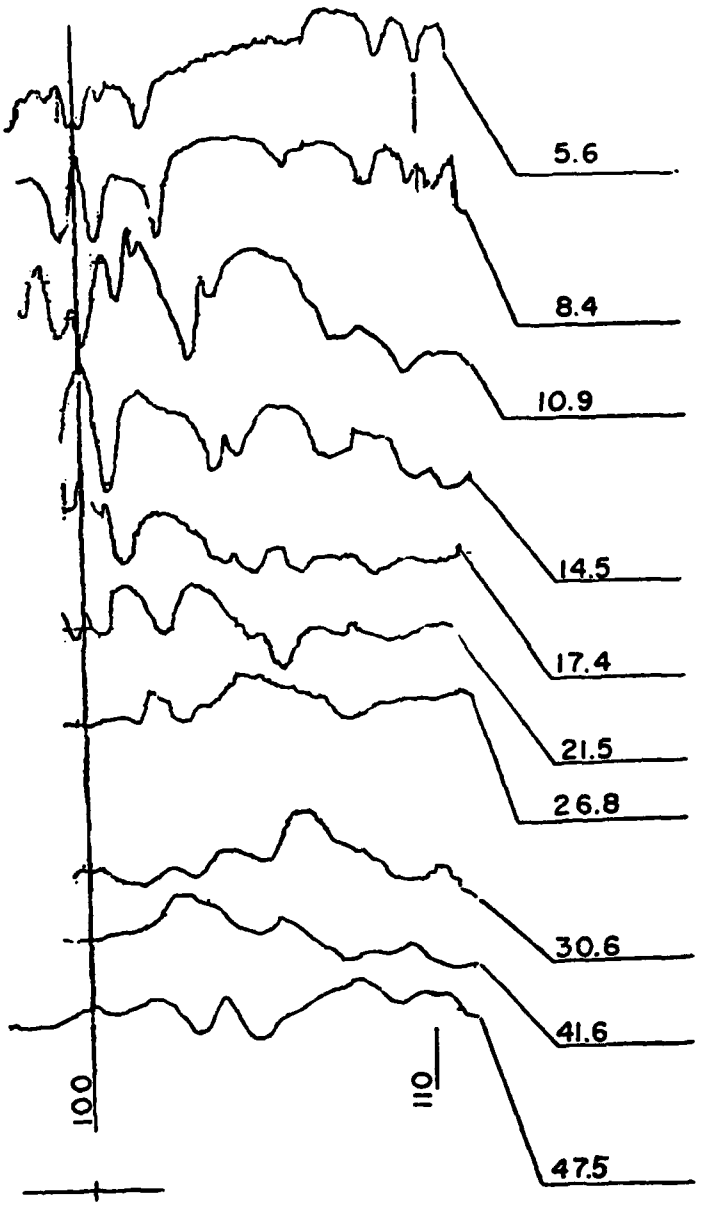

Figure 14. Selective adsorption data for ^4He on KF. After Meyers et al., reference 30.

INVESTIGATIONS ON FLUID-SURFACE INTERACTIONS AT THE DFVLR-INSTITUTE "DYNAMIK VERDÜNNTER GASE" AT GÖTTINGEN

Ulf Bossel and Hubert Legge

Deutsche Forschungs- und Versuchsanstalt
für Luft- und Raumfahrt
AVA - Göttingen
D-3400 Göttingen, Bunsenstraße 10
Fed.Rep.Germany

This paper is a report on past, current and planned activities at the Göttingen Institute of the DFVLR which deal with phenomena of fluid-surface interplay. The domain between the classical macroscopic boundary layer treatment of the continuum and the microscopic description of the elementary particle interactions with solid surfaces are the target of our investigations.

This point is illustrated in Figure 1. Let the drag force be representative for the overall aerodynamic effects caused by a large number of interactions between gas molecules and the solid surfaces of the vehicle. For a non-vanishing ratio of the surface temperature to the stagnation temperature of the flow the drag force is composed of the three contributions:

... a component due to the surface frictional forces, i.e., the exchange of tangential momentum between the gas flow and the body,
... a normal force component, commonly called the pressure force, due to the exchange of normal momentum during the surface interaction and
... a component which has its origin in the acceleration, or deceleration of particles on surfaces whose temperature

is not in equilibrium with that of the incoming gas flow. Internal degrees of freedom must be considered in this temperature dependent phenomenon.

The overall drag force is thus not only dependent on the respective body geometry, but is also affected by the body temperature and the accommodation parameters.

It is certainly of interest to note that, if the coefficient for the accommodation of tangential momentum is smaller than unity, then the frictional contribution is also less than the value indicated in Fig. 1. But since the accommodation coefficient for normal momentum is then - as a rule of experience - also less than one, the pressure contribution to the compound drag force is increased beyond the value given. The overall drag force may thus not be significantly effected by changes in the accommodation pattern.

Figure 1 thus suggests to us the ingredients for additional work in the field. One should have

... a sensitive balance system for the recording of minute forces and force difference,
... a flow generating system providing flow fields of desired properties for wind tunnel type experiments, and
... a system for preparation and diagnosis of the body surfaces exposed to the flow.

The first of those ingredients is available at the DFVLR. We have, for some time now, operated a microbalance system of high sensitivity. The installation of the balance in one of our low density wind tunnels is schematically illustrated in Figure 2. Results of experimental observations on spheres, Figure 3, flat plates and cones can be found in a number of reports issued at this institute (1,2,3,4).

The second author of this paper is presently investigating the effects of wall to stagnation temperature ratios on the drag coefficient as previously discussed. It seems that his results closely follow the predictions, but it is too early to give a comprehensive report on work in progress. A detailed publication will appear within the next 12 months.

The data given so far were recorded by exposing the model to a free jet flow field which bears with it the difficulties of relaxing and diverging gas motions. We feel that a molecular beam would be of advantage for future studies since some of the difficulties can be avoided in both experiment and data analysis. We therefore put a considerable amount of work into further developing the nozzle beam technique schematized in Figure 4. First of all, the beam analysis was modified to take into account the diverging nature of streamlines near the skimmer and the temperature anisotropy in the downstream end of a free jet from which nozzle beams are extracted.

The principal results of this analysis which is decribed in detail elsewhere (5,6,7) are presented in the following figures. The are briefly:

... in a diverging flow the beam density approaches an upper limit when the skimmer diameter is increased (Figure 5),
... the beam density profile behind the skimmer is very sensible to the perpendicular temperature $T_\perp$ at the point of beam formation (Figure 6)
... the beam density profile is very sensitive to the departures of the expansion from the ideal isentropic laws (Figure 7). In fact, a polytropic exponent of $\gamma_{eff} = 1.52$ appears to provide an excellent fit of the experimental data with the forgoing analysis for Nitrogen, Figure 8.

We further studied in some detail the phenomena leading to a

degradation of the molecular beam as schematically illustrated in Figure 9. As a function of the background pressure surrounding the beam, Figure 10, and the density levels within the beam itself, Figure 11, there seems to be a deflection of particles out of the beam center into the evacuated surrounding of the flow. The conclusion that molecular beams are not at all "free molecular flow fields" can be inferred from some reports issued at this institute (8,9) .

Recently we have begun with time-of-flight measurements of nozzle beams to complete the scenario of diagnostic devices needed for a complete experimental verification of the presented beam analysis, or for the empirical description of the properties of rarefied flows which are utilized in future experiments on the fluid-solid surface interactions under realistically simulated conditions.

This addition to our flow diagnostic equipment together with a recently purchased ultra-high vacuum chamber for surface preparation and analysis will enable us to conduct the experiments specified at the beginning of this paper.

R E F E R E N C E S

(1) Legge, H.
Koppenwallner, G.
Sphere Drag Measurements in a Free Jet and a Hypersonic Low Density Tunnel
Internal Report, AVA 70 A 37 (1970)
(7th RGD-Symposium, Pisa, Italy)

(2) Legge, H.
Widerstandsmessungen an parallel angeströmten Platten und senkrecht angeströmten Scheiben in Überschallfreistrahlen großer Verdünnung
DLR-FB 73-17 (Research Report), (1973)

(3) Legge, H.
Drag Measurements of Cones at Zero Angle of Attack in Near Free Molecular Flow
DLR-FB 72-64 (Research Report), (1972)

(4) Legge, H.
A Study of Background Molecule Scattering in Free Jet Expansions Through Flat Plate Drag Measurements. *Rarefied Gas Dynamics*, 9th Symposium (M. Becker and M. Fiebig, Eds.), Vol.2 pp.D. 3-1 to D. 3-10, DFVLR-Press, Porz-Wahn, (1974)

(5) Bossel, U.
David, R.
Faubel, M.
Winkelmann, K.
Free Jet Temperature Extraction from Molecular Beam Profiles Rarefied Gas Dynamics, 8th Symposium (K. Karamcheti, Ed.), Academic Press, New York, (1974)

(6) Bossel, U.
Skimming of Molecular Beam from Diverging Non-Equilibrium Gas Jets DLR-FB 74-28 (Research Report), (1974)

(7) Bossel, U.
Dettleff, G.
Experimental Study of the Molecular Beam Destruction by Beam-Beam and Beam-Background Scattering DLR-FB 73-116 (Research Report), (1973)

(8) Dettleff, G.
Experimentelle Untersuchungen über das Verhalten eines Düsen-Molekularstrahls bei Variation seiner Intensität und des Druckniveaus des ihn umgebenden Untergrundgases IB 252-74 H 04 (Internal Report), (1974)

(9) Dettleff, G.
Bossel, U.
Nozzle Beam Profile Measurements Verify Assumption and Results of Recent Beam Intensity Analysis Rarefied Gas Dynamics, 9th Symposium, (M. Becker and M. Fiebig, Eds.) Vol. 2 pp. C. 12-1 to C. 12-6. DFVLR-Press, Porz-Wahn, (F.R. Germany), (1974)

(10) Hamel, B.B.
Willis, D.R.
Kinetic Theory of Sources Flow Expansions with Application to the Free Jet Phys. Fluids Vol. 9, No.5, pp. 829-841, (1966)

(11) Ashkenas, H.
Sherman, F.S.
The Structure and Utilization of *Supersonic Free Jets in Low Density* Wind Tunnels Rarefied Gas Dynamics, 4th Symposium, (de Leeuw, ed.), Academic Press, New York. Vol. 2, pp. 84-105, (1966)

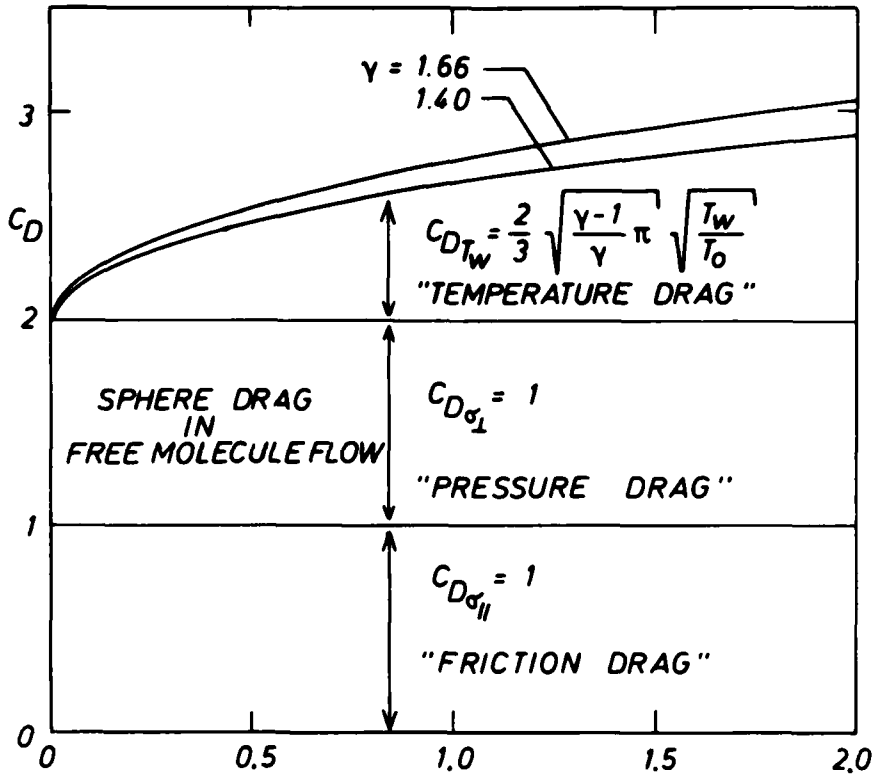

Figure 1

Sphere drag contributions in free molecule flow

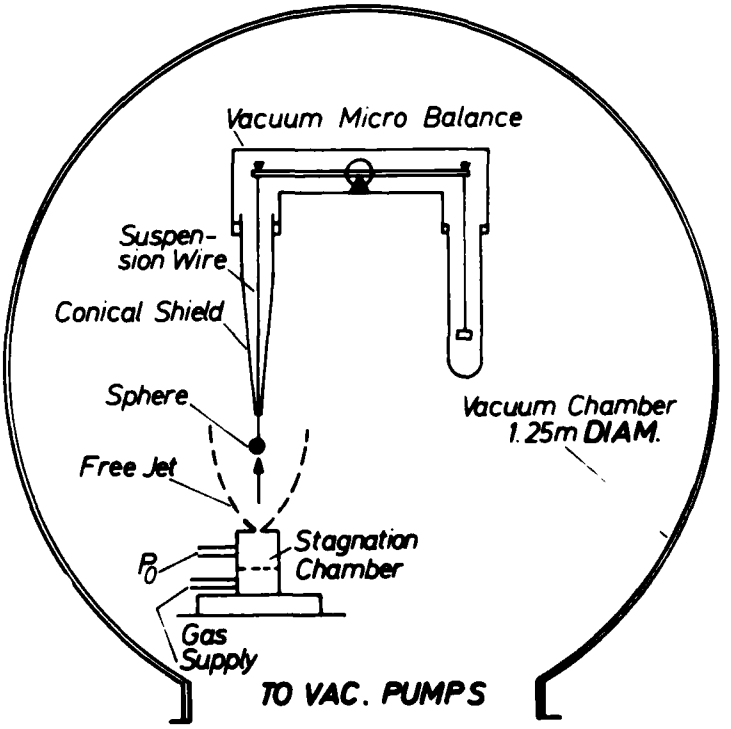

Figure 2

Schematic of micro-balance setup for sphere drag measurements

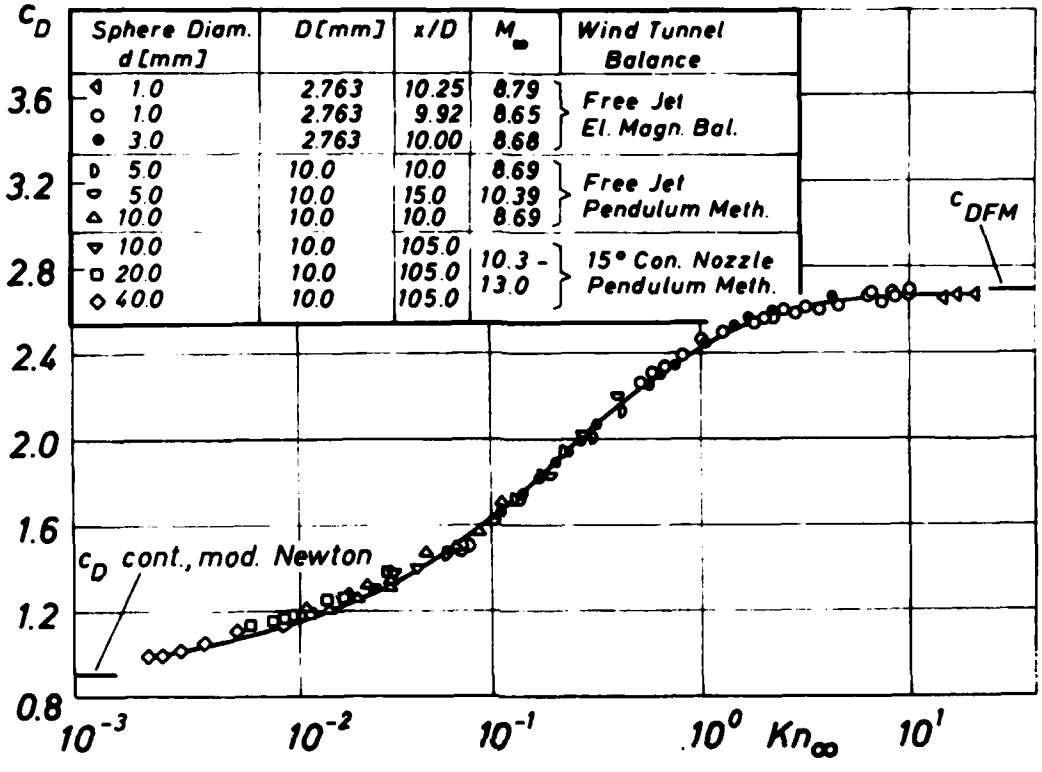

Figure 3: Drag coefficient of spheres in rarefied flows

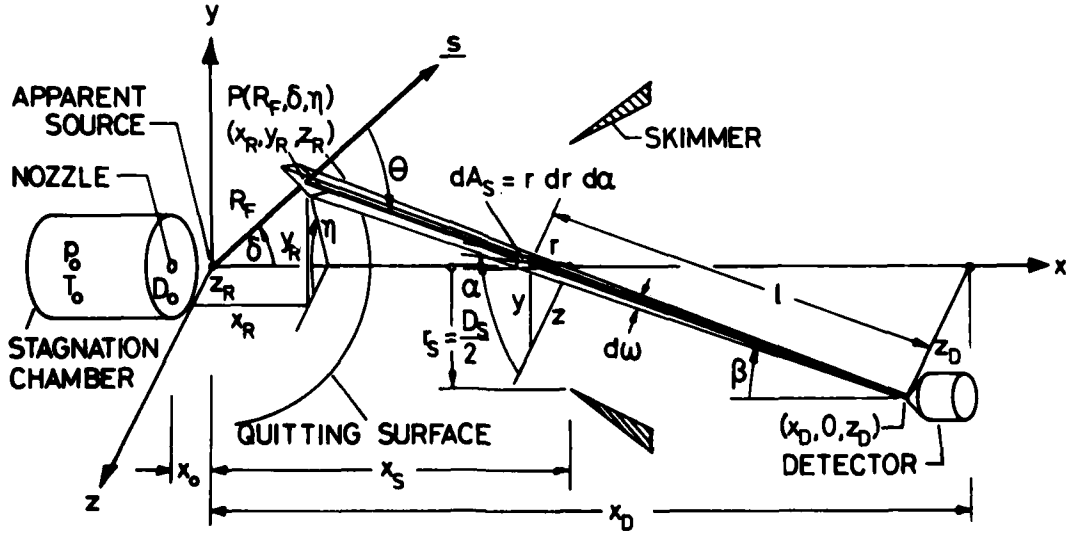

Figure 4: Schematic of nozzle beam formation

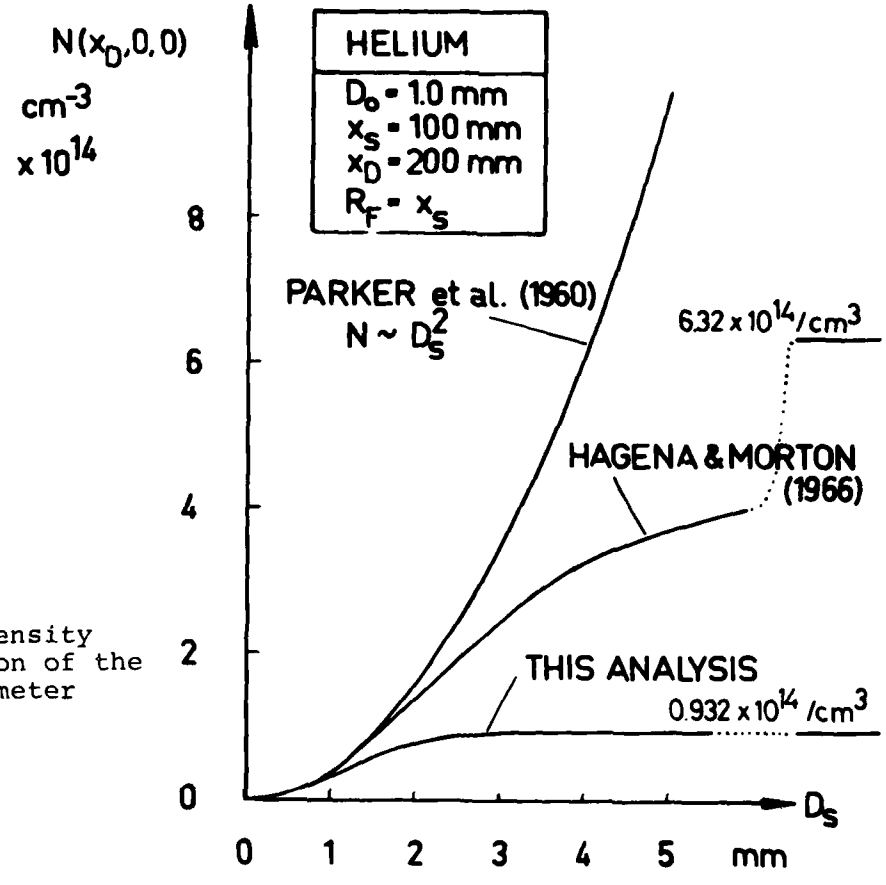

Figure 5

Beam axis density as a function of the skimmer diameter

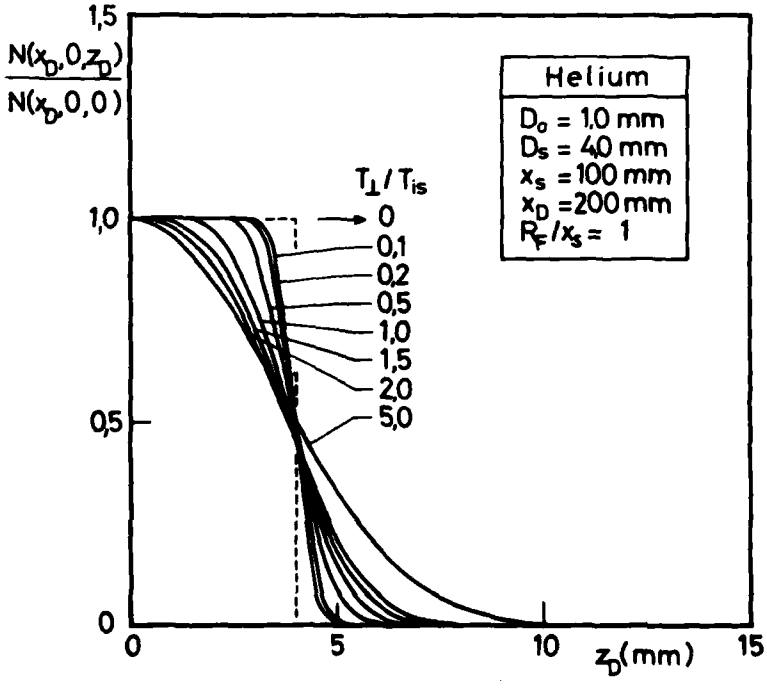

Figure 6

Beam density profiles for various perpendicular temperatures at the quitting surface

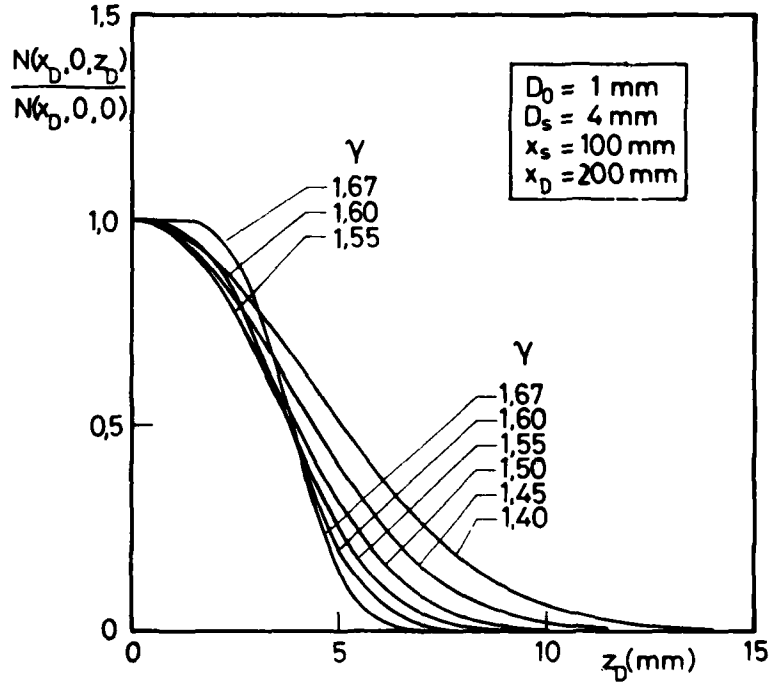

Figure 7

Beam density profiles for different polytropic exponents

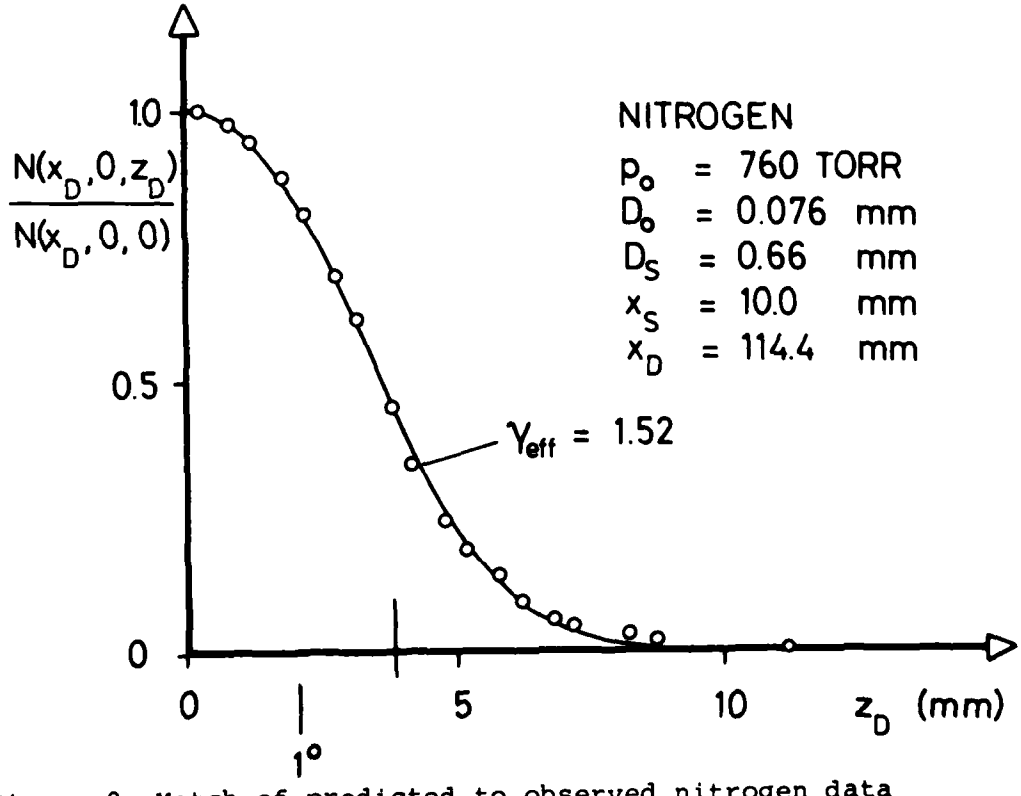

Figure 8: Match of predicted to observed nitrogen data

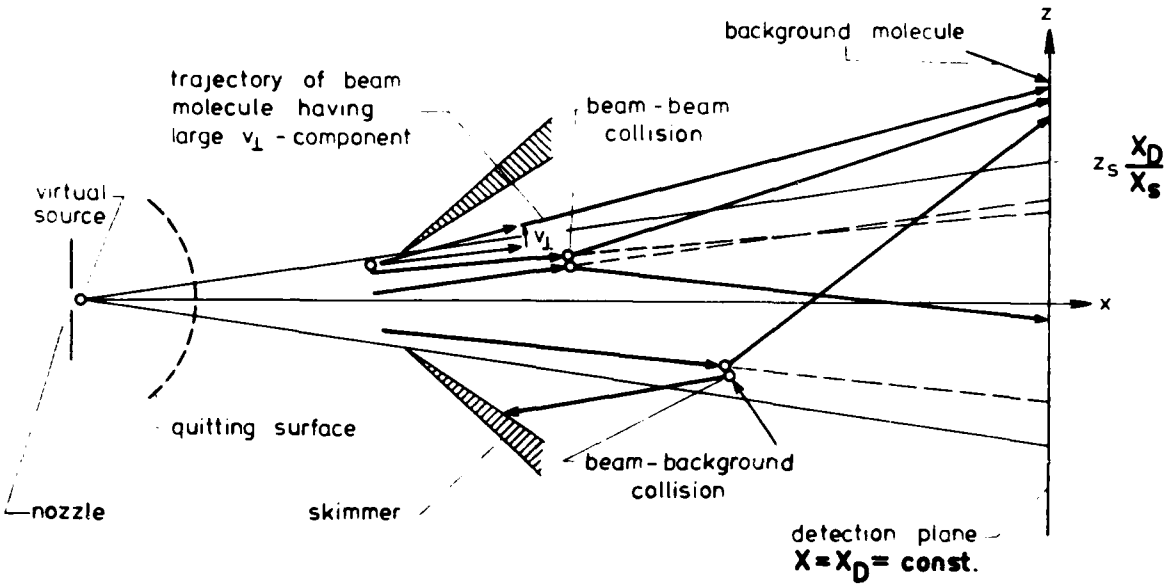

Figure 9: Schematic of beam destruction mechanisms

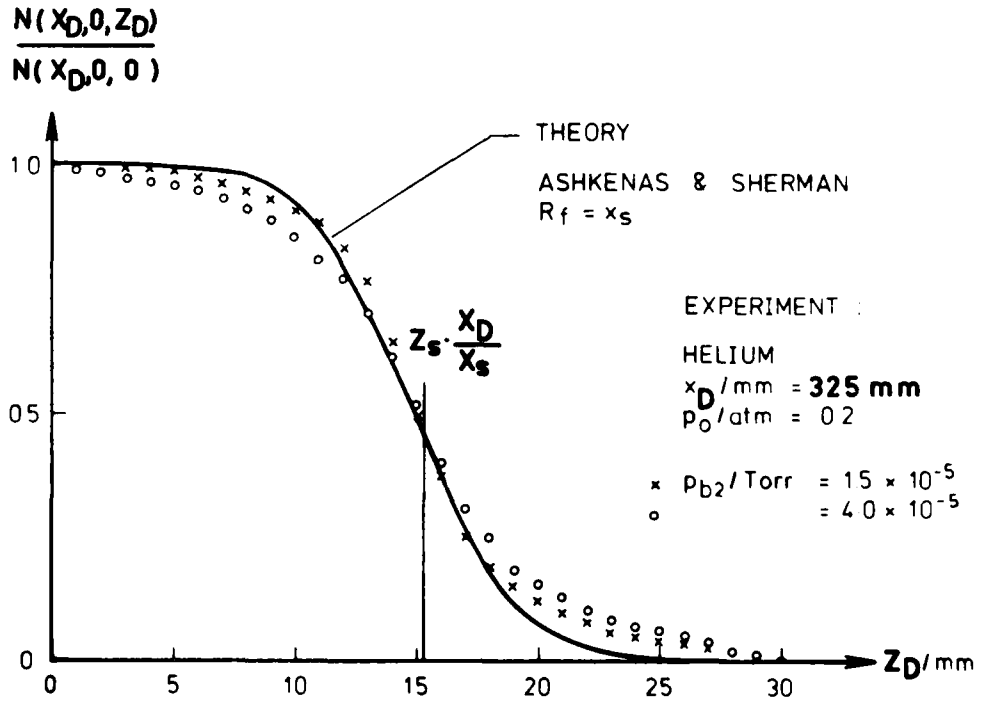

Figure 10: Beam destruction by background interference

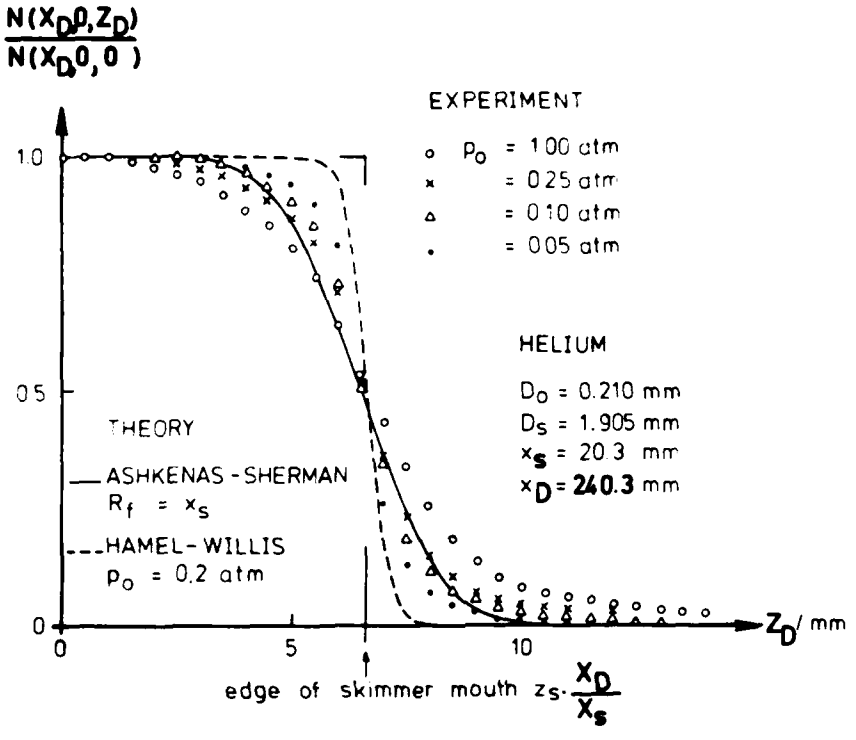

Figure 11: Beam profiles for various stagnation pressures: indication of beam self-destruction by scattering among beam particles

SESSION II

Chairman:

Alfred Walz

Technische Universität Berlin

A Review of Slip Flow in Continuum Physics

H.J. Lugt and J.W. Schot
Naval Ship Research and Development Center
Bethesda, Maryland 20084 U.S.A.

ABSTRACT

In the study of fluid-solid surface interactions the concept of slip of a fluid at a solid wall serves to describe macroscopic effects of certain molecular phenomena. Macroscopic slip may be divided into the following two types:
(1) Real slip, for which molecular interactions cause slip to take place in the bulk fluid, such as in the rarefied gas regime; in flows through minute capillaries and porous media at atmospheric pressures if the dimensions of the pores are comparable to the molecular mean free path of the gas; in certain non-Newtonian fluids; and in mass diffusion theory.
(2) Pseudo slip, which corresponds to the use of fictitious slip conditions to obtain useful models for complicated flow problems, such as those involving suspensions and liquid flows over permeable material and grooved plates. A review of the occurrence of slip flow, its history, its technological importance, and its place in continuum physics is presented along with a collection and discussion of known slip flow solutions of the basic equations of motion.

CONTENTS

1. General Remarks

At the First Symposium on Fluid-Solid Surface Interactions the fluid dynamical implications of perfect slip on incompressible fluids were reported by one of the authors (Lugt, 1973). In contrast to the well-established usage of the nonslip boundary condition for viscous flow problems, it appeared that the perfect slip condition did not apply to realistic flow behavior (Goldstein, 1965, p. 679). However, further investigation of the role of the boundary conditions between a solid surface and an adjacent fluid revealed that a considerable amount of literature exists on various types of slip flow. This literature is growing not only in response to the challenge of understanding flow phenomena in new physical environments, such as in the rarefied atmosphere of outer space, but also in response to man-made

changes in the physical structure of solid surfaces which can alter the interactions between the fluid and the solid. Such changes in the physical or chemical properties of either the solid or the fluid certainly necessitate at least a re-examination of the boundary conditions imposed in mathematical formulations of flow problems. The purpose of this paper is to present a short survey of the literature in an attempt to clarify the significance of slip conditions within the realm of continuum physics. Although the literature cited is by no means complete, it is hoped that this review will provide an introduction to the state-of-the-art of slip flow analysis in continuum theory.

1.1 Occurrence of Slip

Today fluid dynamicists are familiar with the concept that, when a viscous fluid moves relative to a solid-body surface or to a different immiscible fluid, the fluid particles adhere to the solid boundary or to the boundary of the other fluid. Although this condition of "nonslip" at the interface is a valid description of most fluid motions, there are a few areas, however, in which the nonslip condition does not agree with observations or is not a satisfactory model for certain flow phenomena. Instead, a nonzero velocity of the fluid, or "slip", at the boundary must be assumed. The motion of a fluid with such slip behavior is called simply "slip flow". In the limiting case of maximum slippage or "perfect slip" the wall shear stress is zero. Thus, nonslip and perfect slip are the limiting cases of the range of possible amounts of slip that can occur at a solid surface.

Slip occurs for gases when the molecular mean free path is of the order of a characteristic geometrical dimension of the solid. In an analogous way the temperature at the surface exhibits a "jump" behavior under the same conditions. Hence, velocity slip and thermal jump in rarefied gases can occur either in exterior flows, such as hypersonic flow at high altitudes, or interior flows such as those in gas centrifuges. Here one may

distinguish between slip which occurs over the entire surface of the body or container and slip which occurs locally. An example of local slip appears in hypersonic edge flow as shown in Figure 1.

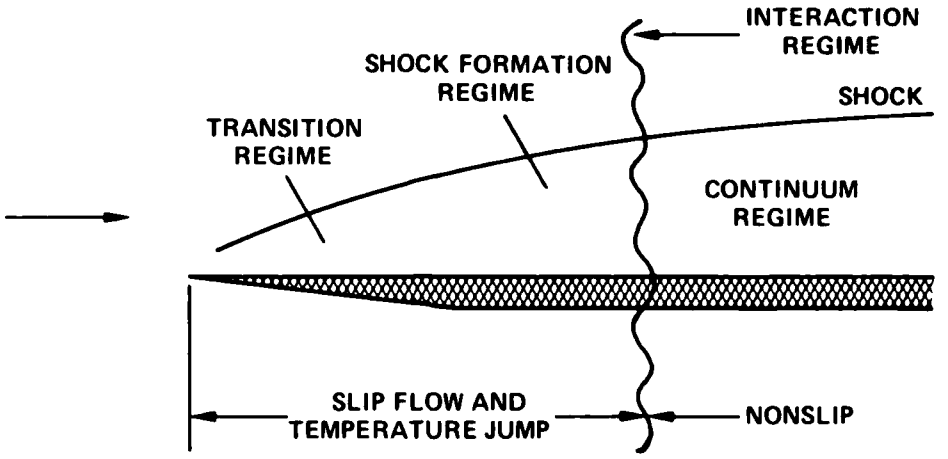

Figure 1: Hypersonic flow past the leading edge of a flat plate.

The above-mentioned condition for slip flow, that is the comparable magnitudes of the mean free path and body geometry, is not restricted to rarefied gases. This condition can also be fulfilled under atmospheric pressure if the characteristic length is minute. For instance, slip occurs in flow through porous media when the pore size is of the order of the mean free path (Carman, 1956, p. 62). Moreover, there is some indication that slip has also been exhibited for liquids flowing through capillaries (Schnell, 1956; Barbin, 1973).

For the description of mass diffusion in liquids, in particular for self-diffusion, a "hydrodynamic" theory has been developed which uses the limiting case of perfect slip to model this molecular phenomenon (Bird, Stewart, & Lightfoot, 1960, p. 514). Experiments have shown that in this theory perfect

slip describes flow phenomena better than nonslip. The concept of slip is also applied in the field of rheology. Certain non-Newtonian fluids, such as solutions of high polymeric substances, exhibit the behavior of slip (Oldroyd, 1956, p. 659).

These examples are representative of real slip flow because the molecular interactions at the boundary cause macroscopic slip to take place for the bulk fluid. However, fictitious slip conditions are also used as simplifying hypotheses in modeling intricate flow problems such as those involving porous walls or grooved plates and fluids with suspensions. Beavers and Joseph (1967) have used this type of pseudo-slip condition in describing the flow of a viscous fluid over a porous wall. Their experiments show that due to the penetration of the moving fluid into the permeable material, a transition region is formed within the wall and a nonzero velocity exists at the boundary, as illustrated in Figure 2a.

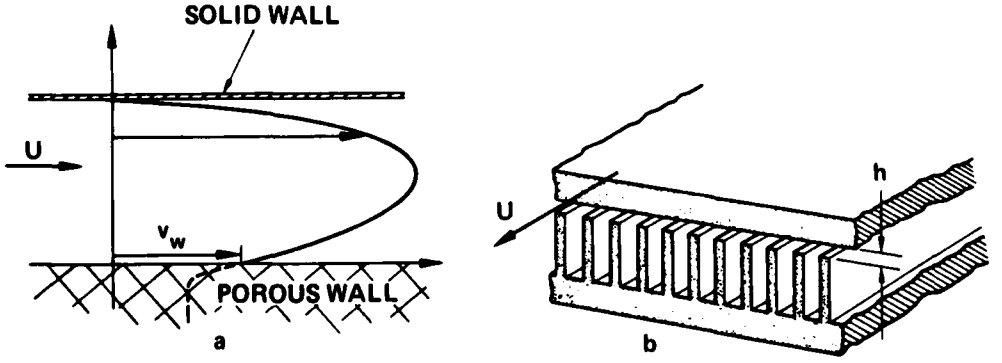

Figure 2. Pseudo slip over porous walls and grooved plates. (Fig. 2a is from Beavers & Joseph, 1967; Fig. 2b is from Taylor, 1971.)

The models for handling boundary conditions for porous materials are also applicable to grooved plates (Taylor,

1971). As shown in Figure 2b, a pseudo-slip condition can be applied to the case of a liquid flowing between a moving solid plate and a fixed, grooved plate, where the motion is parallel to the grooves. Even though the nonslip condition physically prevails at the solid surfaces, the average effect at the surface determined by the tops of the ridges is a slip flow due to the nonzero velocities of the fluid flowing within the grooves.

Another type of pseudo slip occurs whenever the viscous boundary or shear layer is replaced by an infinitely thin vorticity sheet in models based on an ideal fluid. There is then a discontinuity in the values of the velocity components from zero at the wall to a nonzero value in the adjacent inviscid fluid. Similarly, this jump in velocity also occurs at the border of a flowing jet of an inviscid fluid and its surrounding medium.

An even more physically interesting example of pseudo slip arises in the modeling of surface waves of a viscous liquid adjacent to a gas. The boundary condition that the shear stress of the liquid should equal that of the gas at the surface can be approximated quite satisfactorily by setting the surface shear stress to be zero. This is nothing else but the perfect slip condition. Approximations of this condition have been used recently in the numerical calculation of free surface flows (Hirt and Shannon, 1968).

1.2 Brief History of Slip Flow

The historical development of the slip concept reveals the difficulties and controversies which have arisen in the attempt to understand fluid-solid surface interactions. The concepts of fluid resistance and shear stress are intimately connected with these interface phenomena. Yet, in contrast to the idea of resistance, the explicit recognition and formulation of fluid adherence and slip occurred late in the history of science. It is probably safe to say that in earlier times drag

was attributed completely to forces normal to the body surface, or to equivalent concepts prior to Newtonian physics. The work of Aristotle, Buridan's impetus theory, and Leonardo's compressibility arguments must be viewed from that standpoint.

After the time of Newton, who implicitly used the adherence condition for viscous fluids (Nemény i, 1962, p. 73), it was Daniel Bernoulli who in 1738 first asserted that a real fluid could not slip freely over a solid surface (Goldstein, 1965, p. 676). However, the mathematical formulation of fluid dynamics by Euler and d'Alembert was basically inviscid, that is, there was no provision for prescribing the velocity components tangential to the body surface. Characteristically, the first explicit evidence of adherence did not come from a theorist but from the hydraulic engineer, DuBuat (1786). This fact is indicative of the gap which existed between theoretical fluid dynamics and hydraulics, a dichotomy which was to last throughout the 19th century, and which was due to the serious discrepancies between theoretical results based on the concept of an ideal fluid and experimental results obtained for real fluids.

After DuBuat, as recounted by Goldstein (1965, p. 676), three different theories were proposed to explain the physical conditions taking place at the interface between a moving fluid and a solid. One was the assumption of the nonslip condition, i.e., that the velocity of the fluid at a solid surface is the same as the solid itself. Coulomb subscribed to this hypothesis and from his experiments he concluded in 1800 that the nonslip condition was independent of the nature of the solid. In 1818 Girard proposed another theory, namely that a very thin layer of fluid remains completely attached to the wall but that at the outer boundary of this layer the fluid slips over it. He also assumed that the thickness of the layer depends on the curvature of the wall, on the temperature, and on the nature of both the solid and the liquid. The third hypothesis was adopted in 1823 by Navier who deduced from molecular considerations that there

is slipping at a solid boundary, and he derived the slip condition $\beta v = \mu \frac{\partial v}{\partial n}$. (See Section 2.2 for notation.)

In 1851, after considerable vacillation, Stokes decided on the adoption of the nonslip condition, and extensive experimental work followed in the years between 1850-1870 which culminated in the acceptance of the nonslip condition for ordinary gases and liquids, whether the solid surface is wetted or not. By that time the theory of viscous fluid flows at vanishing Reynolds number was well established based on Cauchy's formulation of the shear stress in 1827 and on Stokes' pioneering work in the 1840's. The discrepancy between inviscid flow theory and hydraulics for high Reynolds number flows still persisted even after Stokes' work and Helmholtz's introduction of a discontinuity sheet (1868). This problem was finally resolved by Prandtl in 1904 with his boundary-layer concept which introduced a thin viscous layer between the solid surface and the inviscid outer field, thus forming a transition region extending from the wall, where nonslip holds, to the gliding inviscid boundary. It is worth recalling that Girard's theory had some similarity to Prandtl's boundary layer concept.

The first experimental evidence of the existence of slip was obtained one hundred years ago by Kundt and Warburg (1875) who made an important discovery. They found experimentally that the damping of a vibrating disk decreases at low pressures of the surrounding gas. They correctly interpreted this result as slippage of the gas at the surface of the disk. Maxwell developed a gas kinetic theory for this slip phenomenon in 1879. The temperature condition analogous to slip was suggested by Poisson (Kennard, 1938, p. 311) and experimentally verified by Smoluchowski in 1898.

As already stated, slip occurs if the mean free path of the gas molecules is of the order of a characteristic length associated with the solid. Thus, slip occurs in rarefied gas

flows and in gas motions through capillaries at atmospheric pressure if the tube diameters are comparable with the mean free path. The latter possibility was first recognized by Adzumi (1937).

The first decades of this century produced extensive experimental and theoretical work in the field of internal rarefied gas flow (Kennard 1938, p. 298). Brillouin introduced the use of the Boltzmann equation in 1900 for slip flow calculations (Truesdell, 1952, p. 246). The development of external rarefied gas flow is closely linked with the exploration of high altitudes and outer space. In the thirties two papers on this subject appeared by Zahm (1934) and by Sänger (1938). However, the study which triggered continuous interest in rarefied gases was the work by Tsien (1946). Since then, a flood of papers on slip in rarefied gases appeared. (See Chapter 4.)

Slip flow in rheology was probably first explicitly introduced by M. Reiner (1930) in setting up a constitutive equation relating liquid viscosity with shear stress. However, investigations of non-Newtonian fluids can be traced to much earlier work which included considerations of adherence and slip. (Coleman, Markovitz, & Noll, 1966, p. 88.)

In the last decade two new developments in slip flow have taken place. One is the application of the slip concept to flows over porous or grooved surfaces, a type of flow for which the term "pseudo slip" was coined in Section 1.1. This development apparently started with the paper on the flow of liquid water over a permeable surface by Beavers & Joseph (1967). G.I. Taylor (1971) used grooved plates to model slip flow over such porous material. The second development is the attempt to influence fluid-solid surface interactions by special treatments of the solid surface. This fascinating advancement for man-made slip became possible with the advent of improved techniques in measurement, such as Low Energy Electron Diffraction, Auger spectroscopy, and Nuclear Magnetic Resonance, in obtaining

molecularly clean surfaces, and in vacuum technology. The initial results on this effort have been and are the subject of these two Symposia on Fluid-Solid Surface Interactions.

1.3 Importance in Technology

There are enormous technological advances to be gained from improved understanding and control of fluid-solid surface interactions. Examples of anticipated breakthroughs in military applications, in the chemical industry, and in the manufacture of high-strength, high-performance materials are presented elsewhere in these Proceedings, especially in the paper by Hoff. Slip flow, whether involving real or pseudo conditions, forms a small but important part of the total effort in this new field of interface research and its application in science and industry.

Practical applications of real slip flow arise both in external and internal flow situations. Of these the most significant and best-explored example at present is the application of the slip concept in rarefied gas dynamics. Specific developments are underway or foreseen to determine and improve drag and heat reduction of high-altitude aircraft, space vehicles, re-entry bodies, and rockets (see Hoff's paper). It is in these areas that manufactured slip will probably find its first engineering application. Estimates on how far slip flow can be extended to higher densities, that is to lower altitudes, are given in Bärwinkel's paper in these Proceedings.

The knowledge of internal slip-flow behavior is of value for controlling the meridional flow circulation in ultra-high gas centrifuges (Krause, 1970). Other internal slip-flow applications are foreseen in the better understanding of the borderline region of gas flow and gas diffusion in very fine porous media and capillaries (Carman, 1956). In such materials the slip property of certain non-Newtonian fluids can become crucial, for instance in physiology (organic tissues and membranes) and in lubrication. Polymer solutions, which play an

important role in drag reduction due to their damping effect in turbulent boundary layers, may also have slip characteristics which affect the laminar sublayer (Oldroyd, 1956, p. 659).

The concept of pseudo slip as applied to discontinuities in inviscid fluid motions of course has had its place in fluid dynamics since the days of Helmholtz. Books on shocks, wakes, waves, and cavitation deal to a great extent with this concept.

Pseudo slip in viscous fluids, which is used for liquid or gas flow over porous and grooved surfaces, has recently attracted the attention of engineers in the field of lubrication. Several research papers are cited in Section 3.

2. Basic Concepts

2.1 Continuum versus Molecular Aspects

Although the border between two distinct media or between two different phases of a material is geometrically two-dimensional, in reality the transition from one medium to the other occurs in a thin three-dimensional layer. This transition region is determined and described by the forces of the interacting atoms and molecules. Usually, an intermediate layer of contaminants between fluid and solid exists which is loosely structured or amorphic and which does not behave like a well-defined crystal structure. Hence, any theory on fluid-solid surface interactions must be based ultimately on the concepts and laws of the microscopic or molecular level. The link to the phenomenological or macroscopic level can be achieved either by an integrated process of the microscopic phenomena, as in the kinetic theory of gases through the solution of the Boltzmann equation, or by the continuum-physics approach. In order to exploit the advantages of the continuum theory the question arises: how good a model is the continuum concept? To answer this question the various regimes of fluid flow must be identified.

The flow characteristics of a gas are essentially determined by the ratio of the mean free path λ to a characteristic length of the body L. This ratio is called the Knudsen number

$$Kn = \lambda/L \ . \qquad (1)$$

According to Schaaf & Chambré (1961) one may distinguish the following flow regimes

Continuum flow	:	$Kn < 0.01$
Slip flow	:	$0.01 < Kn < 0.1$
Transition flow	:	$0.1 < Kn < 3$
Free-molecule flow	:	$3 < Kn$

In the continuum-flow regime, fluid-solid surface interactions are built into the nonslip conditions, that is, velocity and temperature of the gas adjacent to the solid surface must be the same as those of the solid surface. The basic equations of motion are the Navier-Stokes equations. In the slip-flow regime the application of the continuum theory, that is the use of the Navier-Stokes equations, is by no means obvious. However, it is now generally agreed upon (Street, 1959; Sherman, 1969) that the Navier-Stokes equations can be used if bulk slip-boundary conditions are considered. At a distance of the order of λ from the wall, in the so-called Knudsen layer, the continuum approach does not hold. However, by introducing extrapolated values for the slip velocity and the wall temperature from inside the flow field, the continuum theory can be used in the entire flow field. See Figure 3. A relation between these fictitious and the real quantities at the wall must be obtained with molecular theories. Details can be found in Bärwinkel's article and in the survey paper by Müller (1974).

Unfortunately, there is much less known about liquid-solid surface interactions than about gas-surface interactions. A theory for describing molecular random behavior is fundamentally different from and apparently easier to formulate

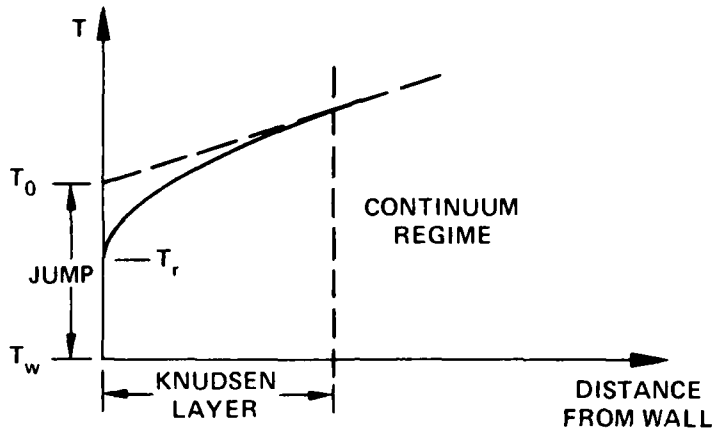

Figure 3: Definition of the extrapolated gas temperature T_0 at the wall, the "microscopic" gas temperature T_r at the wall, and the wall temperature T_W of the solid.

than that encompassing the ordered structure of liquids (Hughel, 1965). For a number of years the technique of Nuclear Magnetic Resonance has been used to study substances absorbed on solid surfaces. In particular, the mobility of water molecules held on a surface has been investigated to obtain information on wettability (Clifford & Lecchini, 1967). However, a satisfactory theory which bridges the molecular and macroscopic approaches does not yet seem to exist.

In order to describe the bulk phenomena of liquid-surface interactions the laws of continuum physics are used with a provision for slip in the form of an empirically obtained slip coefficient. In this way the flow of water through capillaries with hydrophobic and hydrophilic surfaces was investigated by Barbin (1973). Slip for non-Newtonion fluids was incorporated into constitutive equations by Oldroyd (1956, p. 659). It is anticipated that continued research into the molecular structure of liquids at solid surfaces will open the way for other applications of slip flow in continuum physics.

2.2 Notation and Definitions

Fluid motion in continuum physics is described by the conservation laws of mass, momentum, and energy. In addition, constitutive equations which describe the properties of matter (such as the equation of state for a gas) must be given. Conservation laws and constitutive equations specify the relationships among the velocity vector $\vec{v}$, the pressure p, the density ρ, the temperature T, and the coefficients of matter like the dynamic viscosity μ, the kinematic viscosity ν, and the thermal conductivity k, etc. By assuming linearity between the stress and deformation tensor one arrives at the Navier-Stokes equations. A further quantity of physical and numerical importance is the vorticity vector defined by $\vec{\omega} = \text{curl } \vec{v}$. For the following discussions it is convenient to write the shear stress and the vorticity of a two-dimensional flow in intrinsic coordinates (n,s) (Milne-Thomson, 1968, p. 648) as follows

$$\tau/\mu = -\frac{\partial v}{\partial n} - \kappa v \ , \tag{2}$$

$$\omega = -\frac{\partial v}{\partial n} + \kappa v \ , \tag{3}$$

where v is the velocity component in the s-direction, κ the curvature of the lines of n = const. See Figure 4.

If one writes the basic equations in dimensionless form, a set of flow parameters occurs. The most important ones for the discussion of flow behavior under slip are

$$Re = UL/\nu, \quad \text{Reynolds number,} \tag{4}$$

$$Ma = U/c \ , \quad \text{Mach number.} \tag{5}$$

Here, U is a characteristic velocity scale, L a characteristic length scale, and c is the velocity of sound. These two parameters can be related to the Knudsen number in the extreme cases of high and low Reynolds numbers (Tsien, 1946).

$$\text{For } Re \gg 1: \quad Kn \sim Ma/\sqrt{Re} \ , \tag{6}$$

$$\text{for } Re \ll 1: \quad Kn \sim Ma/Re \ . \tag{7}$$

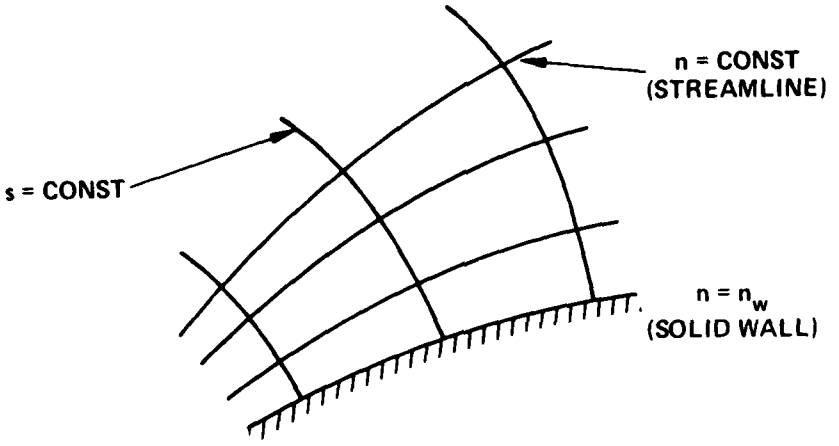

Figure 4: Intrinsic coordinates.

Incompressible fluids are of special interest mathematically since the Navier-Stokes equations are then not coupled with the energy equation.

2.3 The Boundary Conditions at a Solid Surface

Suitable boundary conditions for the basic equations of motion must be prescribed to specify the physical problem. Here, the boundary conditions at the solid surface are of main interest. In addition to the kinematical condition that the velocity component of the fluid normal to the surface is equal to that of the body, the tangential components of the velocity and the temperature are specified by

$$\beta(\vec{v}_W - \vec{v}_B) = \vec{j}\,\tau_W \qquad \text{Slip condition,} \qquad (8)$$

$$\gamma(T_0 - T_W) = q_W \qquad \text{Temperature-jump condition (Tsien, 1946).} \qquad (9)$$

Here β is the slip coefficient, γ the temperature-jump coefficient, $\vec{v}_W$ the velocity vector tangential to the wall, $\vec{v}_B$ the velocity vector of the moving body tangential to the wall, τ_W the component of the wall-shear stress in the direction of

$\vec{v}_W - \vec{v}_B$ with $\vec{j}$ the unit vector, T_0 the temperature defined in Figure 3; T_W is the wall temperature of the solid, and q_W the heat transfer at the wall, where $q_W = k(\partial T/\partial n)_W$. In most cases the reference frame of the flow is fixed to the body so that $\vec{v}_B \equiv 0$. In equation (8) the creep velocity is neglected (Kennard, 1938, p. 327). For the limiting case of nonslip, $\beta = \infty$ in equation (8); for the other limiting case of perfect slip, $\beta = 0$ and hence $\tau_W \equiv 0$.

It is important to point out that the physics contained in equations (8) and (9) lies outside the realm of continuum theory. This information must be provided either by experiments or by a molecular theory (see Section 2.1). It may also be mentioned that through equation (8) the fluid flow is influenced by the solid surface (via β) but not vice versa. Furthermore, equation (8) was derived from molecular theories by Navier and later by other investigators (see Müller, 1974) for plane walls only. Indications are that this equation can be verified for curved surfaces as well (Lehmann & Müller, 1974).

Many flow characteristics like separation, instability, force and moment coefficients are described by the surface vorticity and the surface vorticity flux. The generation of vorticity and vorticity flux at the surface depends greatly on the boundary condition (8). Here, it is pointed out that according to equations (2) and (3) τ_W/μ is not equal to ω_W. In the limiting case of perfect slip, $\tau_W \equiv 0$ but $\omega_W = 2\kappa v$. This means that in general perfect-slip flow cannot be equated with potential flow (see Section 3.6). For flat surfaces with $k = 0$ the surface vorticity vanishes under perfect slip. However, this does not mean that the flux $(\partial\omega/\partial n)_W$, which contributes to drag, lift, and torque, also vanishes (Lugt, 1973).

3. Laminar Incompressible Flows

3.1 Closed-form Solutions of the Navier-Stokes Equations

Closed-form solutions of the Navier-Stokes equations are rare and limited to simple flow configurations (Schlichting, 1968, p. 76). These solutions can easily be modified to include slip effects. Some examples are given to demonstrate the influence of slippage.

The steady flow through a straight pipe of circular cross-section is described by the Hagen-Poiseuille solution. If p_1-p_2 denotes the pressure drop along the pipe length $z_2-z_1 = L$, the mean velocity $\bar{v}_z = \frac{4}{\pi d^2} \int_0^{d/2} v_z \, 2\pi r dr$ is

$$\bar{v}_z = \frac{p_1-p_2}{L} \left(\frac{d^2}{32\mu} + \frac{d}{4\beta}\right) , \tag{10}$$

where d is the diameter of the pipe (Lamb, 1945, p. 586). Here cylindrical coordinates (r,ϕ,z) are used and v_r, v_ϕ, v_z are the corresponding velocity components. For nonslip, $\beta = \infty$, the well-known solution, usually found in textbooks, is retrieved. Near perfect slip, $\beta = 0$, the pressure loss approaches zero in a linear manner:

$$p_1-p_2 \propto \beta \quad \text{for} \quad \beta \simeq 0. \tag{11}$$

In a similar way slippage can be included in the plane Hagen-Poiseuille flows and in the plane and axisymmetric Couette flows. These solutions (with slip) have been used recently to study flows over porous walls (Beavers & Joseph, 1967; Beavers, Sparrow, & Magnuson, 1970). As an example the constant flow between two rotating concentric cylinders with the inner and outer radius r_i and r_0 and with the constant angular velocities Ω_i and Ω_0 is given. If slip is permitted at the inner cylinder (Krause, 1970) the boundary condition (8) yields

$$r=r_i: \quad \beta(v_\phi - \Omega_i r_i) = \mu\left(\frac{\partial v_\phi}{\partial r} - \frac{v_\phi}{r}\right) . \tag{12}$$

With the nonslip-boundary condition at the outer cylinder

$$r=r_0: \quad v_\phi = r_0\Omega_0 \tag{13}$$

the velocity is:

$$v_\phi = \left[\frac{(\Omega_i-\Omega_0)r_i^2}{1-\frac{r_i^2}{r_0^2}+\frac{\mu}{\beta}\frac{2}{r_i}}\right]\frac{1}{r} + \left[\Omega_0 - \frac{(\Omega_i-\Omega_0)r_i^2}{r_0^2-r_i^2+\frac{2\mu r_0^2}{\beta r_i}}\right] r \ . \tag{14}$$

If the outer cylinder or both cylinders slip, similar expressions can be derived. For perfect slip, $\beta=0$, the fluid rotates like a solid body, and the torque on the cylinder is zero. It may be pointed out that near $\beta=0$ the torque depends linearly on β.

For the stagnation-point flow a similarity solution of the Navier-Stokes equations exists (Schlichting, 1968, p.91). In the axisymmetric case the assumptions

$$v_r = r\sqrt{a\nu}\ \phi'(\xi), \quad v_z = -2\sqrt{a\nu}\ \phi(\xi) \tag{15}$$

with $\xi = \sqrt{a/\nu}\ z$ lead to the ordinary differential equation

$$\phi''' + 2\phi\phi'' - \phi'^2 + 1 = 0 \tag{16}$$

with the boundary conditions

$$\begin{aligned} &\xi=0: \quad \phi = 0, \quad \beta^*\phi' = \phi'' \ , \\ &\xi=\infty: \quad \phi' = 1, \end{aligned} \tag{17}$$

where a is a constant and $\beta^* = \frac{\beta}{\mu}\left(\frac{\nu}{a}\right)^{1/2}$ the dimensionless slip coefficient. For nonslip the solution is given in Schlichting (1968, p. 91); for perfect slip the solution coincides with the potential-flow result

$$v_r = ar, \quad v_z = -2az \ . \tag{18}$$

For $\beta^*=10$ Lin & Schaaf (1951) obtained the solution which is displayed together with the nonslip and potential-flow solutions

in Figure 5.

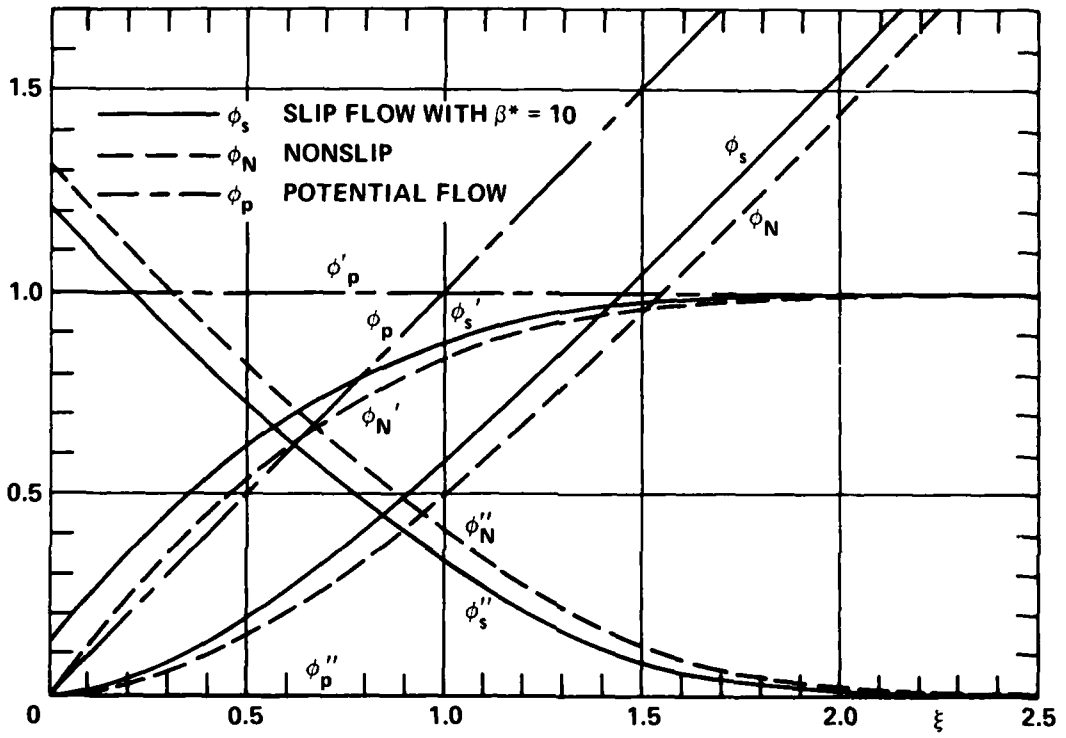

Figure 5: Axisymmetric stagnation-point flow. Nonslip, potential flow, and slip with $\beta^*=10$ are considered.

An unsteady flow solution of the Navier-Stokes equations exists for the Rayleigh problem, that is for the impulsive start of an infinite flat plate with a constant velocity parallel to itself. In this case the equations of motion degenerate to the heat transfer equation

$$\frac{\partial v_x}{\partial t} = \nu \frac{\partial^2 v_x}{\partial y^2} , \qquad (19)$$

where t is the time, and x,y are Cartesian coordinates parallel to and normal to the plate, respectively. The solution is discussed in Section 4.1 in connection with the physical meaning of slip flow at the singularity t=0 when the shear stress is infinite under nonslip.

It can be argued that other singularities which occur in solutions of the Navier-Stokes equations are instances in which the continuum concept breaks down. For example, flows past wedges under nonslip cause an infinite shear stress (and an infinite pressure) at the tip (Lugt & Schwiderski, 1965). Here, slip flow should probably be considered also.

3.2 Stokes and Oseen Flows

If viscous forces dominate over inertial forces, that is when Re < 1, the approximations by Stokes and Oseen permit closed-form solutions of the equations of motion. The classical example is that of a steady flow past a sphere. The solution is due to Basset, and the drag D is

$$D = 6\pi\mu r_0 U \frac{\beta r_0 + 2\mu}{\beta r_0 + 3\mu}, \qquad (20)$$

where r_0 is the radius of the sphere and U the constant main flow velocity (Happel & Brenner, 1965, p. 126). It is interesting to observe that for the sphere the two limiting cases of nonslip and perfect slip cause drag values which differ only by a factor of 2/3. This is in contrast to the examples of planar and pipe flows presented in Section 3.1 in which perfect slip resulted in flows without dissipation. Obviously, the value of $\partial\omega/\partial n$ at the surface vanishes in these cases, whereas in the case of the sphere motion the vorticity flux is nonzero, even under perfect slip. An examination of the pressure and the friction part of the drag reveals that under perfect slip the pressure drag is even larger than under nonslip. If one introduces the drag coefficient C_D defined by $D/(\rho/2)U^2\pi$ with $C_D = C_{DP} + C_{DF}$, the

contributions due to pressure and friction, respectively, then for

$$\begin{aligned} \text{nonslip:} \quad & C_{DP}Re=8, \; C_{DF}Re=16 \\ \text{perfect slip:} \quad & C_{DP}Re=16, \; C_{DF}Re=0 \; . \end{aligned} \tag{21}$$

The larger C_{DP}-value is due to the contribution of the surface velocity. There is even a case known in the literature where the drag is larger for perfect slip than for nonslip (Lugt, 1973). For disc-like bodies (oblate spheroids) of 5% thickness the drag coefficients are

$$\begin{aligned} \text{nonslip:} \quad & C_{DP}Re=18.891, \; C_{DF}Re=1.504 \\ \text{perfect slip:} \quad & C_{DP}Re \simeq 28 \quad , \; C_{DF}Re=0 \; . \end{aligned} \tag{22}$$

For prolate spheroids and slightly deformed spheres where $\varepsilon << 1$ is the deviation from the unit radius, Hu (1973) determined the torque under perfect slip. The torque $\overline{T}$ for the sphere under *nonslip* is

$$\overline{T} = -8 \pi \mu r_0^3 \Omega \; , \tag{23}$$

whereas under perfect slip $\overline{T} = 0$. For the spheroid under perfect slip, the torque is

$$\overline{T} = -\frac{32}{25} \pi \mu \, r_0^3 \, \Omega \varepsilon^2 + O(\varepsilon^3) \; . \tag{24}$$

The limiting cases of nonslip and perfect slip for flows past bodies at $Re < 1$ have become of interest in the studies of molecular diffusion (Bird, Stewart, & Lightfoot, 1966; Zwanzig & Bixon, 1970; Hu, 1973).

For steady two-dimensional flows around bodies with $Re < 1$ the Oseen-approximation has been used to overcome the Stokes paradox. Tsien (1946) and Atassi & Shen (1968) studied the slip flow around a circular cylinder. Their result

$$C_D Re = 4\pi/(\ln \frac{4}{Re} - 1.28 + \frac{\mu}{\beta r_0}) \tag{25}$$

does not appear to be correct since it gives $C_D Re=0$ for perfect slip. The analysis of the sphere case and of the elliptic cylinders discussed in Section 3.4 reveals that the vorticity flux must produce a nonzero drag, even under perfect slip.

Recently Hocking (1973) studied the flow between two solid surfaces approaching each other, for instance the motion of a sphere close to a wall or the motion between two spheres. In order to obtain contact in a finite time under a finite force Hocking had to introduce slip.

The pseudo slip achieved with porous or grooved surfaces was studied by Richardson (1971) for grooves and by Prakash and Vij (1974) for porous journal bearings. Sparrow, Beavers, & Hwang (1972) showed that the response time and the load-carrying capacity of squeeze films are diminished by slip of porous surfaces.

The slow-motion inlet flow in a pipe was studied by Abarbanel (1968). However, the author did not use the boundary condition (8) but the relation v_W = const.

For the finite-flat plate problem Laurmann (1958) linearized the Navier-Stokes equations through a perturbation technique in 1/Kn and found a closed-form solution.

Solutions for time-dependent flows under the restriction of Re < 1 have been constructed to study oscillating viscometers (Macwood, 1938 a and b; Shah, 1971). For given values of the logarithmic decrement and the oscillation period the viscosity μ and the slip coefficient β can be determined.

3.3 Boundary-layer Flows

For high Reynolds-number flows the boundary-layer approximations can be made in many flow problems. The classical problem is the flow past a semi-infinite flat plate which is described by Blasius' similarity solution (Schlichting, 1968, p. 126). The assumption

$$v_x = U\phi'(\xi),\ v_y = (\nu U/2x)^{1/2}(\xi\phi' - \phi),\ \xi = (U/2\nu x)^{1/2}y \qquad (26)$$

leads to the ordinary differential equation

$$\phi''' + \phi\phi'' = 0. \qquad (27)$$

For nonslip the boundary conditions are

$$\xi = 0:\ \phi = \phi' = 0,\ \xi = \infty:\ \phi' = 1\ . \qquad (28)$$

However, the slip condition (8) is not compatible with the similarity assumption (26). This is in contrast to the similarity solution of (16) and (17) for which the slip condition can be incorporated. Clauser (1956) has presented Blasius' velocity profiles with a slip velocity to study turbulent flow. However, these solutions were found by using v_W = const and not by equation (8). Lin & Schaaf (1951) assumed a perturbation of the Blasius solution ψ_N (for nonslip) to include slip in the form

$$\psi = \psi_N + \frac{\mu}{\beta}\frac{\partial \psi_N}{\partial n} + \cdots\ ,\quad \mu/\beta << 1\ , \qquad (29)$$

where ψ is the stream function. The boundary-layer displacement thickness decreases with slip, but no change in the friction coefficient is observed. Similar results were obtained by duP. Donaldson (1949) with a simple integral method. It was shown that the effect of slip on the drag coefficient requires a non-zero pressure gradient along the surface. This result was also obtained by Glauert (1957) in the context of presenting a more general theorem on surface conditions for the boundary-layer equations. He found the general relation

$$\tau_W = \tau_{WN} + \frac{\mu}{\beta}\frac{\partial p}{\partial s}\ , \qquad (30)$$

where τ_W is the wall-shear stress along s under slip, and τ_{WN} the corresponding value for nonslip. For two-dimensional flow Nonweiler had already obtained this result in 1952. This result is also verified for the solution of boundary-layer flow over a wedge which satisfies the Falkner-Skan equation (Schaaf &

Chambré, 1961). With a perturbation of the form (29) one arrives at a local friction coefficient $C_F = \frac{2}{\rho U^2}\tau$ given by

$$C_F = C_{FN}\left(1 - \frac{1}{\beta}\,\frac{\mu\theta}{\pi-\theta}\,\frac{\sqrt{Re}}{\phi''(0)}\,\frac{1}{x} + \cdots\right), \tag{31}$$

where C_{FN} is the coefficient for the nonslip case, θ the semi-vertex angle, and ϕ'' the second derivative with respect to $\xi = \sqrt{\frac{U}{\nu x}}\,y$ of the Falkner-Skan function.

Another boundary-layer flow problem, which is under investigation for slip, is the entrance flow in a parallel-plate channel or in a circular pipe (Sparrow, Lundren, & Lin, 1962; Hanks, 1963; Quarmby, 1968; Chen, 1971). Slip increases the length of the entrance region, that is, the region before the flow is fully developed.

3.4 Numerical Solutions of the Navier-Stokes Equations

For flows with moderate Re-values solutions of the Navier-Stokes equations must be constructed numerically. Recently, three papers (Lugt, 1972; Lugt, 1973; Lugt & Ohring, 1975) were published which describe the flow behavior of suddenly accelerated and constantly moving bodies under slip. A few of the results are cited in the following paragraphs.

In Figures 6 and 7 the velocity profiles and the drag coefficients C_D and C_{DP} are displayed for the steady flow past a thin elliptic cylinder of 10% thickness under zero angle of attack for $Re = Ud/\nu = 200$, where d is the chord of the ellipse and U the constant speed of the fluid far away from the body. The velocity profiles are shown for the surface point at the middle of the ellipse. The drag curves are almost linear near $\beta^* = 0$.

The situation is different for blunt bodies. One would expect from Stokes' and Basset's solutions given in Section 3.2, that the deviation between the two extremes of nonslip and perfect slip should not be large. This statement

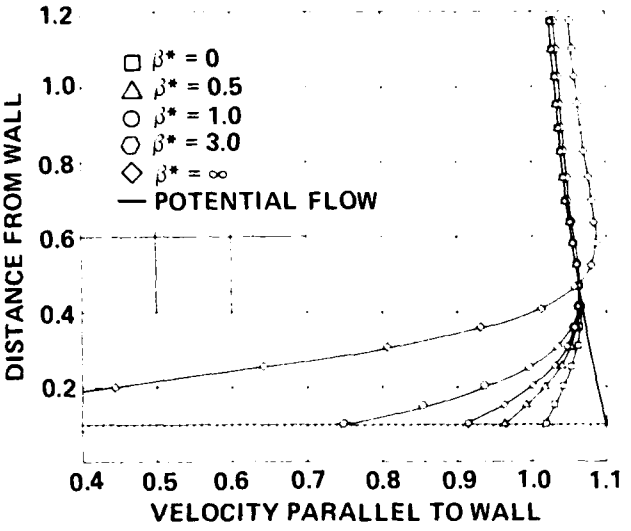

Figure 6: Velocity profiles at the middle of the surface for flows past an elliptic cylinder of 10% thickness and at zero angle of attack. Re = 200, $\beta^* = \beta(d/2\mu) = 0$; 0.5; 1; 3; ∞; and potential flow.

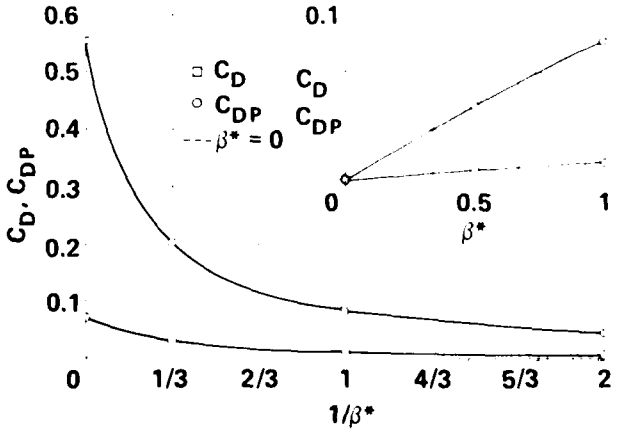

Figure 7: Drag coefficient versus $1/\beta^*$ for the case explained in Figure 6.

is in general true except for certain cases in which the body curvature is relatively small, and hence the vorticity generation under perfect slip is reduced. For instance, at Re = 10 for circular cylinders flow separation occurs under nonslip but not under perfect slip. The drag coefficient is reduced from C_D= 5.69 for nonslip to C_D = 2.34 for perfect slip. The situation changes for a thin elliptic cylinder perpendicular to the flow. Now, under both nonslip and perfect slip the vorticity production at the tips is high, flow separation occurs in both cases, and the flow fields are quite similar. The drag coefficients at Re = 10 are C_D = 6.00 for nonslip and C_D = 5.73 for perfect slip.

For thin elliptic cylinders under nonzero angles of attack, the sudden start of airfoil-type bodies has been studied. Under both nonslip and perfect slip the Kutta condition (extended to viscous fluids) is established, a starting vortex is generated and shed, and lift is created. The further development of the flow to a Kármán-vortex street is demonstrated in Figure 8. Notice the close similarity of the flow patterns for nonslip and perfect slip! The force and moment coefficients are of the same order of magnitude (Lugt, 1972).

3.5 Heat Transfer

For incompressible homogeneous fluids the momentum equation can be studied independently from the energy equation. Then, with a given flow field, the energy equation can be solved.

The simplest case for which the temperature-jump condition (9) can be incorporated is Couette flow. With the flow field given between the two plates at y=0 and y=h, where the second plate is moving with constant speed U, the velocity v_x in the x-direction is specified by

$$v_x = U \frac{y + \mu/\beta}{h + \mu/\beta} . \tag{32}$$

Slip is assumed only at the plate y=0. By incorporating the temperature-jump condition (9) at y=0 the heat transfer at that

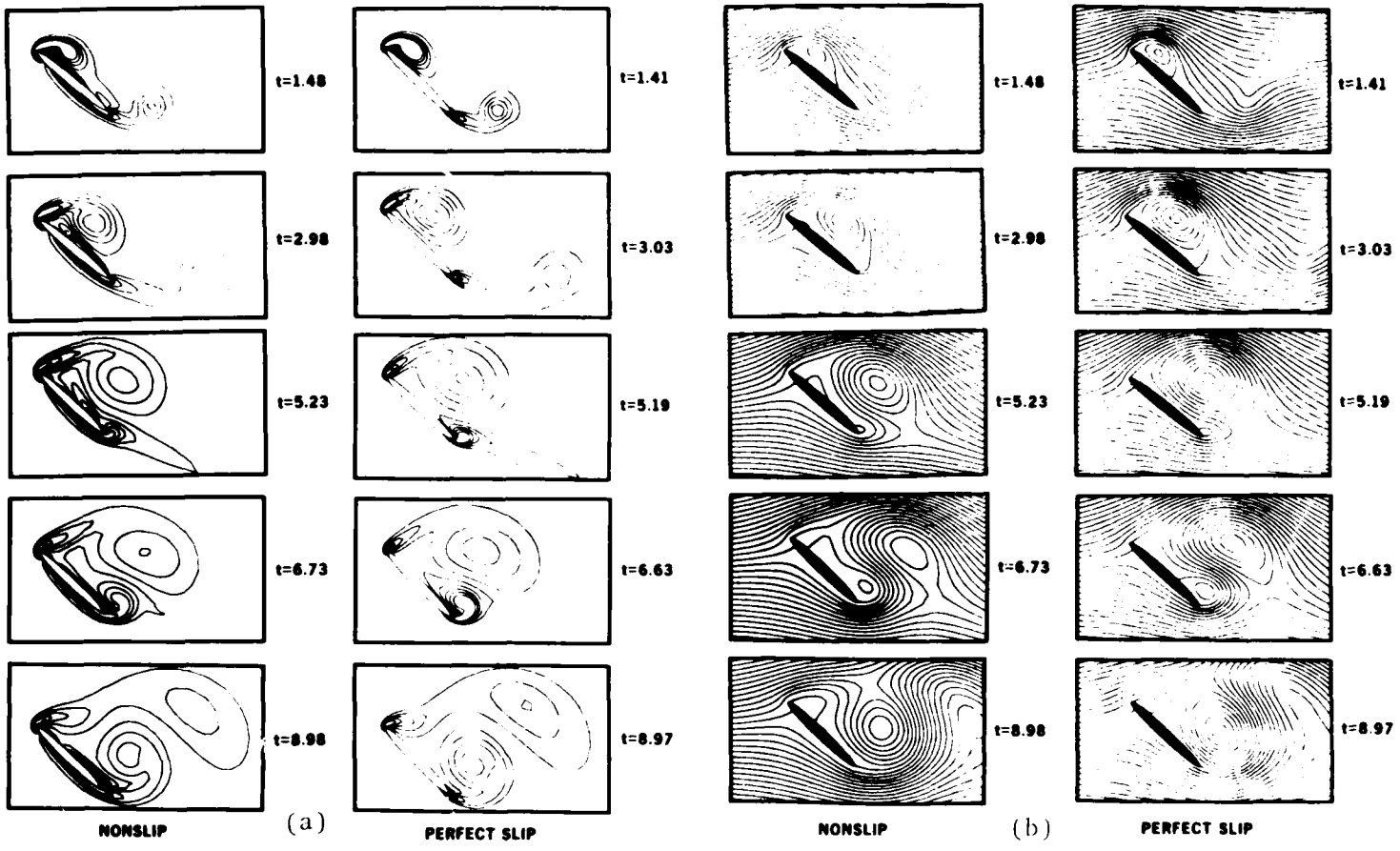

Figure 8: Time sequence of equal-vorticity lines (a) and streamlines (b) for nonslip and perfect slip after the abrupt start of an elliptic cylinder at Re = 200 under an angle of incidence of 45°.

surface is

$$q_0 = k(\partial T/\partial y)_0 = \frac{k\gamma}{h\gamma+k}(T_h - T_W) + \frac{\mu\gamma}{h\gamma+k}\,\frac{h^2}{2}\,\frac{U^2}{(h+\mu/\beta)^2} \quad . \qquad (33)$$

Clearly, the heat transfer is reduced by decreasing both β and γ. For the axisymmetric Couette flow the temperature field is given by Krause (1970).

Rayleigh's problem was investigated by Reddy (1967); the flat-plate flow by Drake & Kane (1950). The cylinder and sphere problems were tackled by Saver & Drake (1953) and by Drake & Backer (1952). However, the basic equations in these cases are severely truncated and linearized.

3.6 Conclusions

The effects of slip and temperature-jump conditions on the flow and temperature fields of incompressible fluids are summarized.

(1) Vorticity is produced at the body surface even under perfect slip. In this limiting case vorticity generation is solely due to the surface curvature.

(2) Drag and heat-transfer reduction depend on the vorticity flux and heat flux at the solid surface. For perfect slip there is no dissipation if the vorticity flux vanishes. The motion approaches potential flow when $\beta \to 0$ in the manner described by equation (11). Examples are: flows in straight pipes, channels, and in rotating circular cylinders. For these cases, the pressure loss and torque approach zero as $\beta \to 0$. On the other hand, if the vorticity flux is large, the effect of slip is small. Examples are: blunt bodies and plates normal to the flow. In these cases the drag and lift values under nonslip and perfect slip are of the same order of magnitude.

(3) Boundary layers become thinner with increasing slippage.

(4) Flow separation can occur even under perfect slip. The

criterion for flow separation under slip is Lighthill's criterion (1963): $\omega_W = 0$, $(\partial\omega/\partial s)_W < 0$.

(5) Slip stabilizes flow (Schaaf & Chambré, 1961).

(6) The establishment of the Kutta condition and the generation of lift occur even under perfect slip. The classical circulation hypothesis is applicable for slip too.

(7) The frequency of vortex shedding is the same for nonslip and perfect slip for an elliptic cylinder at a 45° angle of attack and Re = 200.

4. Laminar Compressible Flows

Exact solutions of the Navier-Stokes equations for compressible fluids under the slip condition are known for Couette flows (Enkenhus, 1962; Shidlovskiy, 1967) and for Poiseuille flows (Erk, 1932; Shidlovskiy, 1968; Sreekanth, 1968). The expression for the pipe flow with constant wall temperature is similar to the incompressible-fluid case (10)

$$(\bar{v}_z\, p)_1 = \frac{p_1^2 - p_2^2}{2L}\left(\frac{d^2}{32\mu} + \frac{d}{4\beta}\right) . \qquad (34)$$

Slip flow of compressible fluids is discussed in the literature essentially in connection with rarefied-gas theory. Here, slip can occur locally depending on the magnitude of the local Knudsen number. Four such cases may be distinguished in the literature:
(1) In a gas centrifuge the density of the gas can become so low at the inner wall of the centrifuge that slip at this wall occurs.
(2) The impulsive start of an infinite flat plate moving parallel to itself (Rayleigh problem) requires in the initial phase a slip condition in order to avoid the infinite shear stress that occurs in the continuum solution under nonslip.
(3) The free molecular flow past a semi-infinite plate is compressed such that after a transition length near the leading

edge the flow can be considered as a continuum with nonslip. In this transition region the slip condition must be applied (Talbot, 1963).

(4) In hypersonic flows, case (3) leads to the formation of a shock wave near the leading edge. Immediately behind the shock wave slip must be considered, called "Shock-Wave Slip" (Probstein & Pan, 1962),

For the solution of flow problems in these four cases perturbation methods and numerical techniques have been used. The perturbation methods lead either to equations which coincide with those for incompressible fluids or they degenerate to boundary-layer type equations.

4.1 Incompressible-Flow Approach

Incompressible-flow solutions as a first approximation to compressible fluids have been used by Krause (1970) to describe case (1). His solution for v_ϕ is equation (14). The Rayleigh problem (2) was tackled by Schaaf (1950) and Reddy (1967).

For the leading-edge case (3), a rough estimate was made by Schaaf & Sherman (1954) who considered the heat-transfer equation (19) by replacing $\partial v_x/\partial t$ with $U\partial v_x/\partial x$.

4.2 Other Approximate Solutions

The Rayleigh problem, case (2), with compressibility effects was studied by Mirels (1952) and Russo & Arnas (1967). They used the von-Mises transformation $(x,y)\rightarrow(x,\psi)$ with $\partial\psi/\partial y = \rho/\rho_\infty$, $\partial\psi/\partial t = -\rho v_y/\rho_\infty$ to obtain the heat-transfer equation

$$\frac{\partial v_x}{\partial t} = c\,\nu_\infty \frac{\partial^2 v_x}{\partial \psi^2} \quad , \tag{35}$$

where $c = \rho\mu/\rho_\infty\mu_\infty$ is assumed to be a constant and the subscript ∞ refers to free-stream values. The leading-edge problem of case (3) is then considered by these authors through the replacement of t by $t = 2.88\ x/U$. More accurate solutions were obtained by

Shidlovskiy (1967) and Chow & Chao (1968) for the flow past a semi-infinite plate. Figure 9 shows the dimensionless slip velocity as a function of the dimensionless distance from the tip.

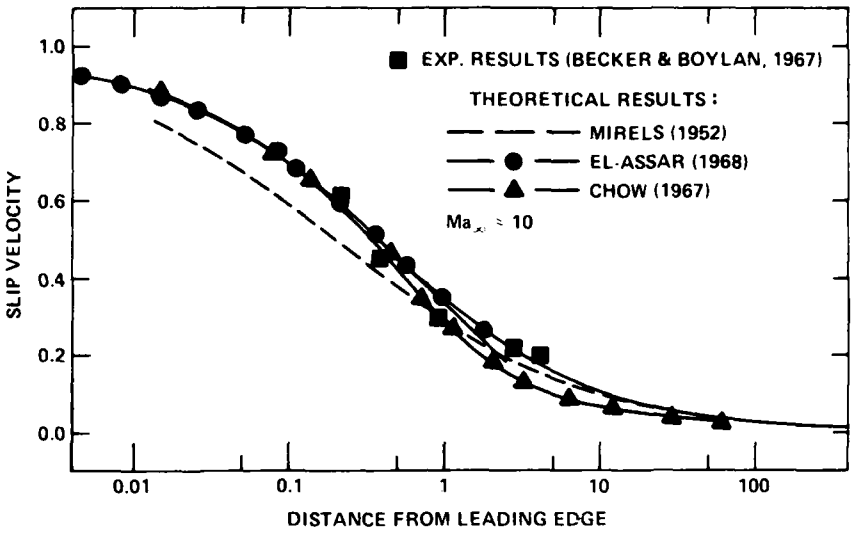

Figure 9: Dimensionless slip velocity near the leading edge in hypersonic flow, plotted against dimensionless distance from the edge (from Chow & Chao, 1968).

Boundary-layer flows past slender bodies of revolution were described by Shen & Solomon (1961), and boundary layer flows near rotating disks by Shidlovskiy (1967).

4.3 Hypersonic Edge Flow

Considerable effort has been expended on the study of hypersonic flows when Ma >> 1. This situation occurs for re-entry bodies and other vehicles operating at high altitudes. In this case the interaction of the boundary layer with the inviscid outer flow must be considered. If the displacement effect of the boundary layer induces only a small perturbation of the outer flow, one speaks of "weak interaction". If the growth of the viscous layer and the state of the outer flow are mutually dependent on each other, the interaction is considered "strong"

(Kasza & Chow, 1973). Slip occurs in the transition region. See Figure 1.

The bulk of the literature on this subject deals with boundary-layer type approaches for the semi-infinite plate and the wedge problem. For the flow past a semi-infinite plate Oguchi (1962) used the Howarth-Dorodnitsyn transformation, Chow (1967) an integral method, Shorenstein & Probstein (1968) and Rudman & Rubin (1968) a boundary-layer type approach, and Hirschel (1972) an implicit finite-difference scheme. Kasza & Chow (1973) applied Meksyn's asymptotic method for integrating the boundary-layer equations. Hirschel (1970) also considered the flow of a dissociated gas. The wedge problem was investigated by Kumar & Jain (1972); flows past slender axisymmetric bodies by Mirels & Ellinwood (1968), and past spinning cones by Lin & Rubin (1974).

Series expansions of the Navier-Stokes equations for solving the flow past a semi-infinite plate were used by Morito Ii & Street (1964) and by Laurmann (1966). Cheng et al. (1968) solved the truncated Navier-Stokes equations with a finite-difference technique. Numerical methods were also applied by Butler (1967) and Cheng & Chen (1973). They showed that the pressure gradient near the leading edge cannot be neglected; this gradient is neglected in the boundary-layer approach.

The effects of slip on compressible fluid flow may be summarized in the following way.

(1) The shock-wave angle is smaller for slip than for nonslip.

(2) The surface pressure near the leading edge is reduced with slip. At the leading edge the surface pressure is finite with slip.

(3) The slip velocity decreases with increasing wedge angle.

5. A Remark on Turbulent Flows

Theoretical studies directly related to slip effects on turbulent flow are not known to the authors. A comment is

appropriate concerning the effect of slip on turbulence.

Viscous effects dominate over inertial effects in the laminar sublayer. Compared to the turbulent boundary layer this region is so small that, in the derivation of the universal velocity distribution law of turbulence, it is only considered in the integration constant (Schlichting, 1968, p. 556). This led Clauser (1956) and Bradshaw (1967) to the idea of using a "pseudo-slip" wall condition (in our terminology) for the turbulent flow.

It may be recalled (Schlichting, 1968, p. 555) that the universal velocity distribution law was derived under the condition that near the wall $\tau = \tau_W$. Then

$$\frac{v}{v_{*_W}} = A \log \frac{y v_{*_W}}{\nu} + B \ , \tag{36}$$

where A and B are integration constants, and $v_{*_W} = (\tau_W/\rho)^{1/2}$ is the friction velocity. The constant B is determined from the properties of the laminar sublayer. It is here where the slip effect enters. Unfortunately, B is determined empirically only (for nonslip), and there seems to be no theoretical evidence relating the properties of the laminar sublayer to B. Qualitatively, the following statement can be made: Slip diminishes the wall-shear stress and, hence, reduces the production of turbulence near the wall.

REFERENCES*

Abarbanel, S., RGD 6 (1968), 839.
Adzumi, H., Bull. Chem. Soc. Japan 12 (1937), 304.
Atassi, H. & Shen, S.F., RGD 6 (1968), 805.
Barbin, M.B., Kolloidnyi Zhurnal 35 (1973), 328.
Beavers, G.S. & Joseph, D.D., Journ. Fluid Mech. 30 (1967), 197.
Beavers, G.S., Sparrow, E.M., & Magnuson, R.A., Journ. Basic Engineering, Trans. ASME 92 (1970), 843.

* The following abbreviation is used: RGD n = Proceedings of the n^{th} International Symposium on Rarefied Gas Dynamics.

Bird, R.B., Stewart, W.E., & Lightfoot, E.N., Transport Phenomena, John Wiley & Sons, Inc., New York, 1966.
Bradshaw, P., National Physical Laboratory, Aero Note 1057, 1967.
Butler, T.D., Physics Fluids 10 (1967), 1205.
Carman, P.C., Flow of Gases through Porous Media, Butterworths Scientific Publications, London, 1956.
Chen, R.Y., Journ. Basic Engineering, Trans. ASME 1971, 324.
Cheng, H.K., Chen, S.Y., Mobby, R., & Huber, C., RGD 6 (1968), 451.
Cheng, S.I. & Chen, J.H., Friction and Heat Transfer Laws in Slip Flows. Princeton University AMS Rep. 1121, August 1973.
Chow, W.L., AIAA Journ. 5 (1967), 1549.
Chow, W.L. & Chao, B.T., RGD 6 (1968), 441.
Clauser, F.H., Advances in Appl. Mech. Vol. IV, 1956, Academic Press, Inc., New York, 1.
Clifford, J. & Lecchini, S.M.A., The State of Liquid Water Near Solid Interfaces, in Wetting, S.C.I. Monograph No. 25, Soc. Chem. Industry, London, 1967.
Coleman, B.D., Markovitz, H., & Noll, W., Viscometric Flows of Non-Newtonian Fluids: Theory & Experiment, Springer-Verlag, N.Y., 1966.
Donaldson, C. duP., NACA RM No. L9C02, May 1949.
Drake, R.M. & Backer, G.H., Trans. Am. Soc. Mech. Engineers 74 (1952), 1241.
Drake, R.M. & Kane, E.D., Univ. Calif. Inst. Eng. Res. Report HE-150-73, October 1950.
DuBuat, P.L.G., Principes d'Hydraulique et de Hydrodynamique, 1, Paris (1786), 92.
Enkenhus, K.R., RGD 3 (1962), II, 132.
Erk, Zeitschrift Phys. 79 (1932), 141.
Glauert, M.B., Journ. Fluid Mech. 2 (1957), 89.
Goldstein, Sydney, Modern Developments in Fluid Dynamics, Vol. II, Dover Publications, N.Y., 1965, 676.
Hanks, R.W., Physics Fluids 6 (1963), 1645.
Happel, J. & Brenner, H., Low Reynolds Number Hydrodynamics, Prentice-Hall, Inc., Englewood Cliffs, N.J., 1965.
Hirschel, E.H., Proc. Twenty-first Intern. Astronautical Congress, North-Holland Pub. Co., Amsterdam, 1971, 158.
Hirschel, E.H., Zeitschrift für Flugwissenschaften 20 (1972), 470.
Hirt, C.W. & Shannon, J.P., J. Computational Physics 2 (1968), 403.
Hocking, L.M., Journ. Engineering Mathematics 7 (1973), 207.
Hu, Chih-Ming, Rotational Stokes Resistance of a Prolate Spheroid in an Incompressible Viscous Fluid under Perfect Slip, PhD-Thesis, University of Maryland, 1973.
Hughel, T.J. (ed.), Liquids: Structure, Properties, Solid Interactions, Elsevier Pub. Co., N.Y., 1965.
Kasza, K.E. & Chow, W.L., Journ. Appl. Mech. Dec. 1973, 857.
Kennard, E.H., Kinetic Theory of Gases. McGraw-Hill Book Co., N.Y., 1938.
Krause, E., Gleitströmungen in eindimensionalen Gaszentrifugen. DFVLR-Kolloquium 1970, Porz-Wahn, 29.

Kumar, A. & Jain, A.C., AIAA Journ. 10 (1972), 1081.
Kundt & Warburg, Ann. Physik, 155 (1875), 337.
Lamb, H., Hydrodynamics. Sixth Ed., Dover Publications, N.Y., 1945.
Laurmann, J.A., RGD 1 (1958), 293.
Laurmann, J.A., RGD 5 (1966), 955.
Lehmann, V. & Mueller, W.J.C., Zeitschrift Naturforsch. 29a (1974), 296.
Lighthill, M.J., in Laminar Boundary Layers, Ed. Rosenhead, L., Oxford Univ. Press, 1963, p. 64.
Lin, T.C. & Rubin, S.G., AIAA Journ. 12 (1974), 975.
Lin, T.C. & Schaaf, S.A., NACA Tech. Note 2568, 1951.
Lugt, H.J., Naval Ship Research and Development Center Rep. 3794, 1972.
Lugt, H.J., Naval Ship Research and Development Center Rep. 4227, 1973.
Lugt, H.J. & Ohring, S., Laminar Flow Behavior Under Slip-Boundary Conditions, Phys. Fluids, Forthcoming in 1975.
Lugt, H.J. & Schwiderski, E.W., Proc. Roy. Soc. A 285 (1965), 382.
Macwood, G.E., Physica 5 (1938a), 374.
Macwood, G.E., Physica 5 (1938b), 763.
Milne-Thomson, L.M., Theoretical Hydrodynamics, The MacMillan Co., N.Y., 1968, 5th ed.
Mirels, H., NACA TN 2609, 1952.
Mirels, H. & Ellinwood, J.W., AIAA Journ. 6 (1968), 2061.
Morito Ii, J. & Street, R.E., RGD 4 (1964), 416.
Müller, W.J.C., Akkommodationseffekte in Hyperschallströmungen. Report from Max-Planck-Institut für Strömungsforschung, Göttingen, Feb. 1974.
Neményi, P.F., Archive for History of Exact Sciences, Ed., Truesdell, C., Vol. 2, No. 1 (1962), 52.
Nonweiler, T., College of Aeronautics, Cranfield, Rep. No. 62, 1952.
Oguchi, H., RGD 3 (1962), II, 181.
Oldroyd, J.G., in Rheology, Vol. 1, Ed., Eirich, Academic Press, N.Y., 1956.
Prakash, J. & Vij, S.K., Journ. Appl. Mech., Trans. ASME, 1974, 348.
Probstein, R.F. & Pan, Y.S., RGD 3 (1962), II, 194.
Quarmby, A., Applied Science Research 19 (1968), 18.
Reddy, K.C., Journ. Appl. Mech., Trans. ASME 1967, 833.
Reiner, M., J. Rheol. 1 (1930), 250.
Richardson, S., Journ. Fluid Mech. 49 (1971), part 2, 327.
Rudman, S. & Rubin, S.G., AIAA Journ. 6 (1968), 1883.
Russo, E.P. & Arnas, O.A., Journ. Appl. Mech., Trans. ASME 1967, 837.
Sänger, E., Gaskinetik sehr hoher Fluggeschwindigkeiten, Deutsche Luftfahrtforschung, Bericht 972, Berlin, 1938.
Sauer, F.M. & Drake, R.M., Journ. Aeron. Sci. 20 (1953), 175.
Schaaf, S.A., Univ. Calif. Inst. Eng. Res. HE-150-66, 1950.

Schaaf, S.A. & Chambré, P.L., Flow of Rarefied Gases, Princeton University Press, 1961.
Schaaf, S.A. & Sherman, F.S., Journ. Aeron. Sci. 21 (1954), 85.
Schlichting, H., Boundary-Layer Theory. McGraw-Hill Book Co., N.Y., 1968, 6th ed.
Schnell, E., Journ. Appl. Phys. 27 (1956), 1149.
Shah, V.L., Journ. Appl. Mech., Trans. ASME, 1971, 659.
Shen, S.F. & Solomon, J.M., Journ. Aero. Sci. 28 (1961), 508.
Sherman, S., in Annual Review of Fluid Mechanics, Vol. 1, Palo Alto, Calif. (1969), 317.
Shidlovskiy, V.P., Introduction to Dynamics of Rarefied Gases. Elsevier, New York, 1967.
Shidlovskiy, V.P., RGD 6 (1968), 215.
Shorenstein, M.L. & Probstein, R.F., AIAA Journ. 6 (1968), 1898.
Smoluchowski, M., Ann. Physik 64 (1898), 101.
Sparrow, E.M., Beavers, G.S., & Hwang, I.T., Journ. Lubrication, Trans. ASME 94 (1972), 260.
Sparrow, E.M., Liu, S.H., & Lundgren, T.S., Physics Fluids 7 (1964), 338.
Sreekanth, A.K., RGD 6 (1968), 667.
Street, R.E., RGD 1 (1958), 276.
Talbot, L., AIAA Journ. 1 (1963), 1169.
Taylor, G.I., J. Fluid Mech. 49 (1971), part 2, 319.
Truesdell, C., J. Rat'l. Mech. & Analysis, 1 (1952), 125.
Tsien, H.S., Journ. Aeron. Sci. 13 (1946), 653.
Zahm, A.F., J. Franklin Institute 217 (1934), 153.
Zwanzig, R. & Bixon, M., Phys. Rev. A2 (1970), 2005.

An Interdisciplinary Approach to the Study of the Drag Reduction Phenomenon

R. Y. Ting, R. C. Little, D. L. Hunston,
O. K. Kim and R. L. Patterson
Naval Research Laboratory
Washington, D. C. 20375

ABSTRACT

It is well-known that the addition of minute quantities of certain high molecular weight polymers can dramatically reduce the production of wall turbulence and therefore the associated frictional drag. By combining expertise in the fields of polymer physics, colloid chemistry, rheology and fluid mechanics, recent work done at the Naval Research Laboratory has made it possible to correlate molecular characteristics and polymer rheology with the turbulent drag reduction effect, thus leading to a better understanding of the phenomenon. Recent experimental results concerned with the effects of polymer type, homology and the solvent environment on drag reduction will be presented. Theoretical analyses examining the effects of viscoelasticity on transient shear and elongational flows will also be discussed to show the relative merits of previously proposed drag reduction mechanisms involving these simple flows.

1. Introduction

The drag-reduction phenomenon has been the subject of intense interest and activity among scientists and engineers for the past decade. This phenomenon is observed when solutions of very small amounts of high-molecular-weight linear polymers are subjected to turbulent pipe flow. The resultant effect is that the pressure gradient required to move the fluid is substantially reduced at a given flow rate. Toms (1) gave the first clear description of this phenomenon in his study of the turbulent flow of poly(methyl meth-

acrylate) in monochlorobenzene. He reported frictional reductions of up to 30% compared with the pure solvent with a 0.2% by weight addition of polymer. Many investigators since then have confirmed this effect in many other combinations of polymer-solvent systems. In spite of the extensive research activity in the past, there is still no agreed interpretation of the mechanism of drag reduction. It is generally accepted, however, that the presence of the polymer may alter the turbulence production near the boundary, turbulent drag reduction being essentially a "wall phenomenon". Recent experimental evidence indicated that for a free jet of dilute polymer solution issuing from a nozzle the mean velocity profile and turbulent intensity are not affected when compared with the solvent case (2,3). The effect of polymer additives on grid turbulence was also found to be negligibly small (4). But in the case of wall turbulence, the velocity profile in a turbulent boundary layer and the turbulent intensity in the wall region are greatly changed by the presence of polymer. Therefore, it is clear that drag reduction represents a very complicated interaction among the polymer molecules, the solvent system and the solid boundary in high Reynolds number flows. The problem is really a composite one which straddles several fields of expertise - fluid mechanics, rheology, polymer physics and perhaps surface chemistry. An interdisciplinary group was therefore established to approach the solution of this problem. Some of the research results obtained by this group have been made the subject of this report.

2. Experimental Technique

Details of the turbulent pipe flow system used have been reported elsewhere (5). The device is basically a metal syringe controlled by a DC motor which drives the test liquid through a 0.62 cm diameter pipe. The flow rate was monitored by a small DC generator coupled to the motor drive. Two pressure taps were placed at approximately 13 and 17 diameters from the upstream end of the flow. The pressure differences between taps was measured by a differential pressure transducer. The outputs from the DC generator and the transducer were recorded continuously. The flow rate and the wall shear stresses were

then calculated by using the calibrated constants of the apparatus. The percent drag reduction was computed by using the following relationship:

$$\text{percent drag reduction} = \left(1 - \frac{f_{polymer}}{f_{water}}\right) \times 100 \qquad (1)$$

where $f_{(\,)}$ is the friction coefficient, defined as the ratio of wall shear stress to the mean dynamic pressure head of turbulent flow, $1/2\ \rho(\bar{u})^2$, where ρ is the density of the fluid and $\bar{u}$ the mean velocity of the solution.

The polymeric materials used included Polyox (polyethylene oxide, Union Carbide Corporation) and polyacrylamide which was synthesized in the laboratory as reported in (6).

3. Effect of Homology and Solvent

The development of even an empirical function to relate drag reduction to relevant solution properties would greatly reduce the amount of time spent in evaluation procedures. Based on literature data (7), it was suggested (8) that the polymer critical concentration - defined as the concentration where random coils begin to touch (9) - might be used to normalize the drag reduction data since the same fraction of critical concentration appeared to produce the same degree of drag reduction irrespective of polymer molecular weight. However, the use of critical concentration as a normalizing factor seems to be limited to capillary tube flows and restricted to the higher molecular weight homologs of a drag reducing family (10).

Virk (11), in developing an empirical correlation between concentration and drag reduction, defined a characteristic intrinsic concentration as

$$[c] = DR_m / \lim_{c \to o} (DR/c) \qquad (2)$$

where DR = percent drag reduction,

c = polymer concentration,

$\lim_{c \to o} (DR/c)$ = intrinsic drag reduction

DR_m = maximum drag reduction for a given rate.

The parameter [c] was found useful in superposing all the experimental data onto a single universal drag reduction curve well represented by

$$\frac{(DR/c)}{\lim_{c \to o} (DR/c)} = \frac{1}{1 + c/[c]} \qquad (3)$$

For experimental use (10), it was found more suitable to simplify Eq. (3) into

$$\frac{DR}{DR_m} = \frac{c}{c + [c]} \qquad (4)$$

Rearrangement of Eq. (4) leads to

$$\frac{c}{DR} = \frac{[c]}{DR_m} + \frac{c}{DR_m} . \qquad (5)$$

Equation (5) indicates that a linear relationship exists between c/DR and c when the concentration dependence of drag reduction obeys Eq. (4). This drag reduction equation has been shown to be applicable to most drag reducing polymers (10,12). As a typical example, Figure 1 presents the concentration dependence of Polyox Coagulant at Reynolds number 9000. A plot of c/DR vs c is linear and shows the validity of Eq. (4). The intercept value at c/DR = 0 yields the intrinsic concentration [c] and this quantity divided by the intercept at c = 0 permits evaluation of DR_m.

It is readily seen from Eq. (4) that $DR/c = DR_m/([c] + c)$. So drag reduction becomes more efficient on a unit concentration basis as the concentration decreases. Henry's law conditions are reached when c/[c] values approach 0.01. This corresponds to a drag reduction of 1%, well inside the error limit of all current drag reduction equipment. The distance between the random coils of the polymers at this level of drag reduction may be estimated by using a relation developed by Paterson (13). For a Polyox compound having a molecular weight of 7×10^6, the random coils, at the 1% drag reduction level, are 20 diameters apart. Only at these intermolecular distances is percent drag reduction a linear function of polymer concentration. When

conditions close to an optimum drag reduction condition are approached, the polymer molecules are only a few diameters apart, or virtually tough. Eq. (4) successfully describes the drag reduction results up to concentrations somewhat below that needed to produce an optimum drag reduction and only accounts for dilute solution behavior. Further increases in concentration bring decreases in drag reduction, hence the equation will fail. The maximum drag reduction, DR_m, to be obtained as $c \to \infty$, is therefore not really a value attainable in the experiment.

The modified universal drag reduction equation, Eq. (4), is in nature an empirical correlation including two adjustable constants [c] and DR_m. However, these parameters, being constants characteristic of a given polymer compound, serve as a measure of the drag reduction effectiveness. The physical significance of these parameters becomes very clear if the limit of Eq. (4) at zero concentration is examined:

$$\lim_{c \to o} \frac{DR}{c} = \lim_{c \to o} \frac{DR_m}{[c] + c} = \frac{DR_m}{[c]} \qquad (5)$$

The parameter $DR_m/[c]$ defines the "effectiveness" of the polymer compounds on a unit concentration basis at infinite dilution. Figure 2 shows the correlation between this drag reduction "index" and the polymer molecular weight for the Polyox and the polyacrylamide family. In such a surprisingly linear plot, the intercept value of molecular weight at $DR_m/[c] = 0$ represents a cutoff point below which no drag reduction takes place. The slope indicates the rate of increasing drag reduction effectiveness with increasing polymer molecular weight.

The solvent effects in general have a great influence on the physico-chemical properties of the polymer molecules and hence are expected to be important in drag reduction. The effect of salt concentration on the drag reduction effectiveness was therefore studied. In cases where DR_m is approximately constant, the reciprocal of the intrinsic concentration alone serves as a simplified measure of the effectiveness. The effect of salt on [c] and the intrinsic viscosity, $[\eta]$ (14), was found to follow equations of the type:

$$\frac{1}{[c]} = \frac{1}{[c]_{H_2O}} \left(1 - \frac{M}{M'}\right) \tag{7}$$

$$[\eta] = [\eta]_{H_2O} \left(1 - \frac{M}{M''}\right) \tag{8}$$

where M' is the molarity at $[c] = \infty$
and M'' is the molarity at $[\eta] = 0$
The M' and M'' constants are, of course, analytical conveniences.
These equations may be combined to express $[c]$ as a function of $[\eta]$ as follows:

$$([\eta] + A_1)\,[c] = A_2 \tag{9}$$

where $A_1 = \dfrac{(M' - M'')\,[\eta]_{H_2O}}{M''}$

and $A_2 = \dfrac{M'}{M''}\,[\eta]_{H_2O}\,[c]_{H_2O}$

It is clear that when $M' = M''$ the relation simply reduces to

$$[\eta]\,[c] = [\eta]_{H_2O}\,[c]_{H_2O} \tag{10}$$

which was approximately true for the low molecular weight polymers. This relation suggests an interesting new avenue in the characterization of drag reducing polymers in various solvent systems; that is,

$$\text{if } [\eta]_\theta [c]_\theta = [\eta][c]$$

$$\text{then } [c] = [c]_\theta \frac{[\eta]_\theta}{[\eta]} = \alpha^{-3}\,[c]_\theta \tag{11}$$

where α is the polymer expansion factor and θ refers to a theta solvent. This would then imply that one need only characterize the drag reduction efficiency of a given polymer under theta solvent conditions. Drag reduction research in other solvent systems might, in principle, merely

be accomplished through use of a viscometer.

4. Viscoelastic Analyses

While the preceding sections provide valuable information regarding the relationship between the molecular structure of a polymer additive and its drag reducing properties, they do not explain how the polymer molecules produce such a dramatic change in flow. Recently, flow visualization experiments (15) have been carried out in dilute solutions of drag reducing polymers. These experiments indicate that the spatially-averaged bursting rate (16) is greatly decreased by the addition of the polymer. This evidence strongly suggests that the turbulence production is decreased by the presence of the polymeric additive through inhibition of the formation of low speed streaks or the attenuation of the bursting. To understand the mechanism of drag reduction, therefore, it is necessary to determine how small amounts of polymer can alter the bursting process. Since the flow patterns associated with bursting are very complex, it cannot be treated quantitatively. One alternative is to examine a number of simple well-defined flows that closely model the types of motion which appear to be associated with the bursting phenomenon. Since drag reduction is characterized by large changes in flow produced by the addition of very small amounts of polymer, the objective in these studies is to seek a simple flow in which the behavior of a very dilute solution is significantly different from that of the solvent.

(1) Models: The solvent is usually assumed to be a Newtonian fluid; that is, the stress tensor is directly related to the strain rate tensor. Schematically, this model can be represented as a dashpot, Figure 3A. The addition of polymer molecules to the solvent not only increases the viscosity but also adds an elastic contribution to the total response. As a result some previous studies have described solution behavior with a Maxwell model since it combines both viscous and elastic behavior, Figure 3B. While this model has the advantage of mathematical simplicity, it does not provide a very good description for polymer solutions because the responses of the solvent and the polymer do not combine as a simple sum. Consequently, a two element

model such as that developed by Oldroyd (17) is needed. The Oldroyd model combines a Newtonian element for the solvent with a Maxwell element for the polymer, Figure 3c. The stress tensor, $\underset{\sim}{\sigma}$, and the strain rate tensor, $\underset{\sim}{d}$, are related by

$$\underset{\sim}{\sigma} + \frac{\eta'}{G} \frac{D\underset{\sim}{\sigma}}{Dt} = (\eta' + \eta_s)\, \underset{\sim}{d} + \frac{\eta'\eta_s}{G} \frac{D\underset{\sim}{d}}{Dt} \qquad (12)$$

where η_s is the solvent viscosity (Newtonian element), η' and G are the viscous and elastic contributions of the polymer molecules (Maxwell element), and D/Dt represents a convected time derivative. The response time of such a system to an applied stress can be characterized by a time constant called the relaxation time $\tau = \eta'/G$. This model provides a good qualitative description of solution behavior and is used in considering the following deformations thought to be important in drag reduction.

(2) Simple Shear Disturbances: One theory that has been proposed to explain drag reduction involves transient or steady-state shear disturbances (18,19). It has been suggested that the propagation velocity for such disturbances in very dilute polymer solutions is substantially less than that in the solvent (20). Since a certain stage of the bursting phenomenon may involve a deformation of this type, a large decrease in the propagation velocity may result in less bursting and thus less turbulent drag.

The propagation of a transient or steady-state shear disturbance is dependent on the behavior of simple sinusoidal shear waves. It is of interest therefore to evaluate the phase velocity and amplitude attenuation coefficient for shear wave propagation as a function of frequency. For illustrative purposes a 100 parts per million by weight (ppmw) solution of a commercial sample (Polyox WSR-301, Union Carbide Corporation) will be used as an example. The weight average molecular weight of this polymer is about 2.4×10^6 while the solution viscosity is 1.21 centipoise. The results of calculations for this solution and water are shown in Figures 4 and 5. These figures clearly indicate that no significant differences between solvent and solution

behavior are predicted, even at the relatively high concentration of 100 ppmw. Therefore, in its present form a mechanism based on the propagation of a shear disturbance is definitely unsatisfactory.

(3) Elongational Flow: A second possible explanation for drag reduction involves elongational flow. The bursting process contains a stage which is characterized by a stretching motion similar to elongational flow. It has been suggested that the addition of small amounts of polymer to a solvent substantially increases its resistance to elongational flow (21). It is proposed, therefore, that the increased resistance to stretching results in less bursting and thus less turbulent drag.

Elongational flow is defined by a strain rate tensor of the following form:

$$\underset{\sim}{d} = \begin{bmatrix} 2\Gamma & 0 & 0 \\ 0 & -\Gamma & 0 \\ 0 & 0 & -\Gamma \end{bmatrix} \qquad (13)$$

where Γ is the stretching rate which is taken to be a constant here. The reduced elongational viscosity, $\bar{\eta}$, is a measure of the resistance to this type of flow compared to the resistance of the solvent to simple shear flow and will be defined as, $\bar{\eta} = (\sigma_{11} - \sigma_{22})/\eta_s\Gamma$.

To examine elongational flow in solvent and solution, Eq. (13) is combined with the appropriate constitutive equation and the correct values for the relevant parameters. Such calculations were made, again using a 100 ppmw solution of WSR-301 as an example. Figure 6 shows a plot of reduced elongational viscosity vs normalized flow time (t/τ) for solution and solvent at several different stretching rates. As seen in this figure, the Oldroyd equation predicts that the solution behavior will be significantly different than the solvent behavior when the flow time and stretching rate exceed certain critical values. Moreover, recent treatments (22) of elongational flow using more sophisticated molecular models have reached the same conclusions.

The experimental evidence for this type of behavior is quite limited but studies such as those by Metzner and Metzner (23) seem to indicate that large values of $\bar{\eta}$ can be obtained at low polymer concentrations. Although a great deal more experimental work is needed before quantitative comparisons with theory are possible, it is clear that elongational flow must be given serious consideration as an explanation for drag reduction. A mechanism based on elongational flow has the advantage that the effects are predicted to be very large; $\bar{\eta}$ for a 1 ppmw Polyox WSR-301 solution may exceed that for water by a factor of 10^3 or more. With effects this large it is not difficult to understand how small quantities of polymer can produce large changes in flow. Therefore, an explanation based on the elongational viscosity could be very promising in this regard. Before a mechanism can be established, however, two things must be studied further. First, the large values of $\bar{\eta}$ that are predicted for dilute solutions must be demonstrated experimentally. Secondly, the stretching rate and flow time during the bursting process must be shown to exceed the critical values needed for the onset of a large elongational viscosity.

Acknowledgement

The authors acknowledge the support of the Office of Naval Research.

References

1. Toms, B. A., Proc. 1st Int. Congress Rheology, Holland (1948), Amsterdam, North Holland, 1949, Part II, pp. 135-141.
2. White, D. A., J. Fluid Mech. 28, 195 (1967).
3. Barker, S. J., J. Fluid Mech. 60, 721 (1973).
4. Fabula, A. G., Ph.D. Thesis, The Pennsylvania State Univ. (1966).
5. Kim, O. K., Little, R. C. and Ting, R. Y., AIChE Symp. Ser. 69, 39 (1973).
6. Ting, R. Y. and Kim, O. K., in Water Soluble Polymers, ed. N.M. Bikales, Plenum, p. 151 (1973).
7. Hoyt, J. W. and Soli, G., Science 149, 1509 (1965).
8. Little, R. C., Ind. Eng. Chem. Fundm. 8, 557 (1969).
9. Shin, H., Sc. D. Thesis, MIT (1965).
10. Little, R. C., J. Colloid Interf. Sci. 37, 811 (1971).
11. Virk, P. S., et al., J. Fluid Mech. 30, 305 (1967).
12. Ting, R. Y. and Little, R. C., J. Appl. Polym. Sci. 17, 3345(1973).
13. Paterson, R. W., Ph.D. Thesis, Harvard University (1969).
14. Flory, P. J., Principles of Polymer Chemistry, Cornell U. Press (1953).
15. Donohue, G. L., Tiederman, W. G., and Reischman, M. M., J. Fluid Mech. 56, 559 (1972).
16. Kim, H. T., Kline, S. J., and Reynolds, W. C., J. Fluid Mech. 50, 133 (1971).
17. Oldroyd, J. G., Proc. Roy. Soc. London A200, 523 (1950).
18. Ruckenstein, E., Chem. Eng. Sci. 26, 1075 (1971).
19. Hansen, R. J., J. Fluid Eng. 95, 23 (1972).
20. Ultman, J. S., and Denn, M. M., Trans. Soc. Rheol. 14, 307 (1970).
21. Everage, A. E., and Gordon, R. J., AIChE J. 17, 1257 (1971).
22. Stevenson, J. F. and Bird, R. B., Trans. Soc. Rheol. 15, 135 (1971).
23. Metzner, A. B. and Metzner, A. P., Rheol. Acta. 9, 174 (1970).

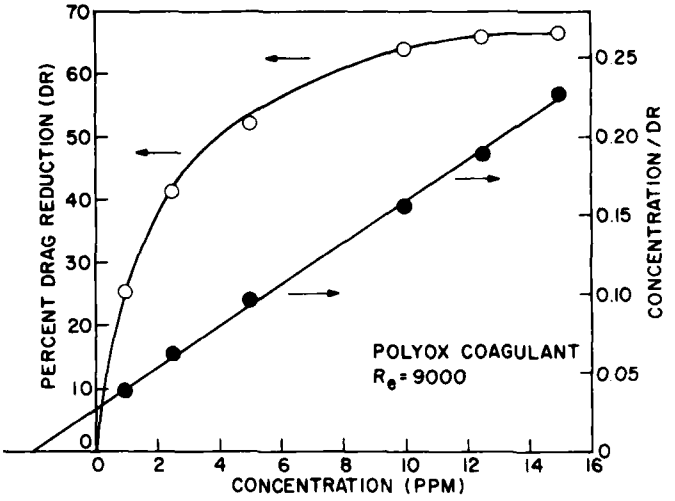

Figure 1: The Concentration Dependence of Drag Reduction of Polyox Coagulant, Showing Conformity to the Universal Drag Reduction Relation.

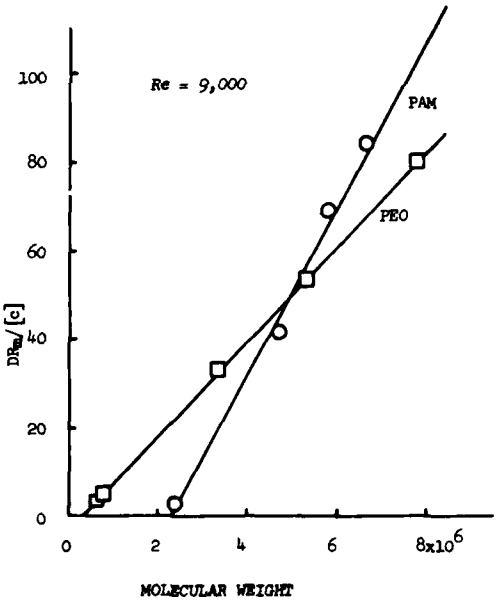

Figure 2: Drag Reduction Effectiveness Index vs. Polymer Molecular Weight

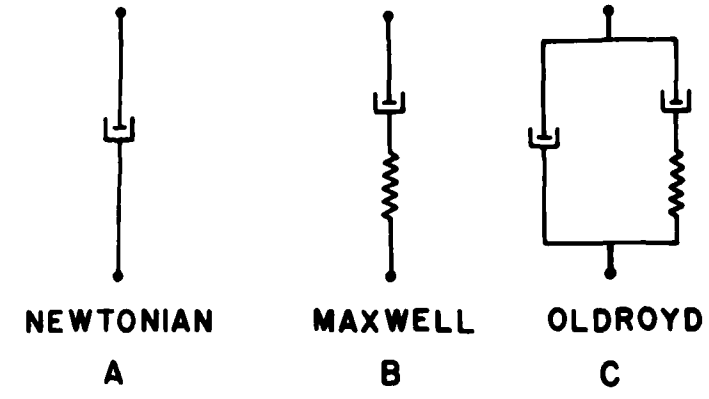

Figure 3: Mechanical Representatives of Fluid Models

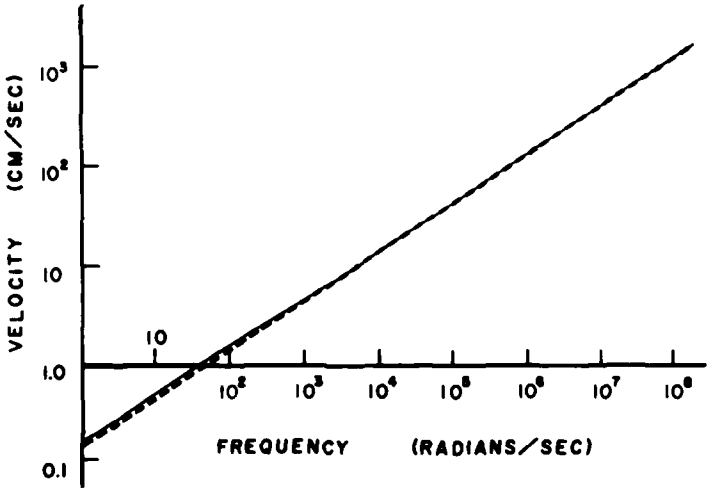

Figure 4: Propagational Velocity of Shear Wave Disturbance as a Function of Frequency.
——— Water, ----- Polymer Solution

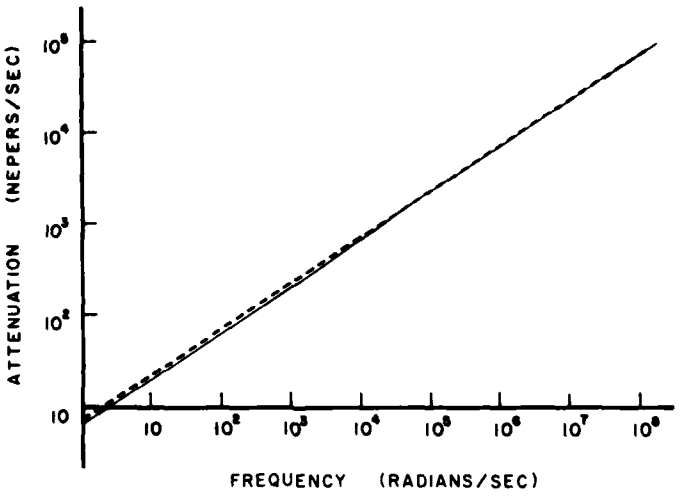

Figure 5: Attenuation of Shear Wave Disturbances as a Function of Frequency. ——— Water, ------Polymer Solution.

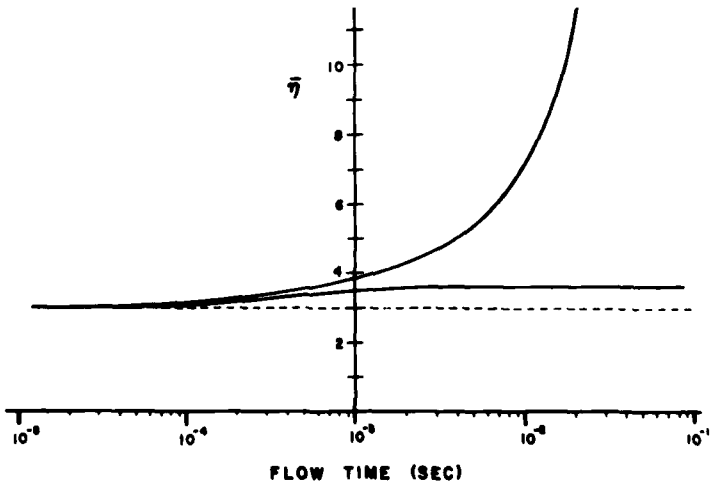

Figure 6: The Temporal Growth of Elongational Viscosity at Different Stretching Rates.

Wettability of Clean Metal Surfaces as Determined with Ultrahigh-Vacuum Techniques

Malcolm E. Schrader

Naval Ship Research and Development Center
Annapolis, Maryland 21402 USA

The physical interaction of liquids with solid surfaces is of fundamental importance to a wide variety of engineering problems. A partial list of these would include:

1. Flow of water through pipes or flexible hoses.
2. Flow of fuel through pipelines.
3. Movement of submerged vehicles or surface vessels through water.
4. Proper initial contact between a liquid adhesive and solid substrate prior to cure of the adhesive.
5. Function of mold release agents.
6. Dropwise condensation of water on condenser coil for efficient energy transfer.
7. Lowering of solid surface temperature required to induce boiling.
8. Hydrodynamic lubrication.

The most widely used method of determining the extent of interaction is by means of the contact angle. Looking at the profile of a sessile liquid drop on a smooth, solid surface the contact angle can be defined as the angle between the solid surface and the tangent to the drop surface at the point of contact. The magnitude of this angle is given by the Young[1] equation which describes the balance of surface forces holding the drop in its equilibrium configuration. The equation

$$\gamma_{LV} \cos\theta + \gamma_{LS} = \gamma_{SV} \qquad (1)$$

where γ_{LV} is the surface tension of the liquid vapor interface, γ_{LS} of the liquid-solid interface, γ_{SV} that of the solid-vapor interface, and θ the contact angle, states that the sum of the surface tension of the liquid-solid interface and the horizontal component of the surface

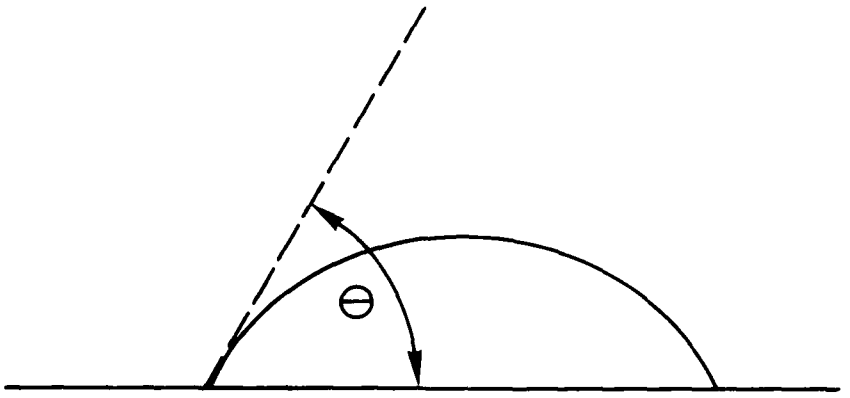

tension of the liquid equals the surface tension of the solid-vapor interface. Transposing,

$$\gamma_{LV} \cos\theta = \gamma_{SV} - \gamma_{SL} \quad (2)$$

so that the right side of the equation is an adhesion parameter, describing the tendency of the liquid to cling to the solid, while the left side consists of experimentally measurable quantities, the surface tension of the liquid and the contact angle. Solid surfaces have been classified into the categories of high and low energy with respect to characteristics affecting their wettability.[2,3] The high energy surfaces include metals, metal oxides, and siliceous glasses, while those of low energy consist mainly of organic materials. As a rule, compounds which are liquid at room temperature spread on high energy surfaces, since their surface tensions are considerably less than the surface energies of these solid substrates.

Girifalco and Good[4] originally proposed a method to predict interfacial tensions of liquid-liquid and liquid-solid systems through use of an interaction term involving the geometric mean of the separate surface tensions of the interacting species.

$$\gamma_{LS} = \gamma_S + \gamma_L - 2\phi(\gamma_S\gamma_L)^{\frac{1}{2}} \quad (3)$$

This would enable the calculation of the right hand side of equation (2) so that the contact angle would be predicted from knowledge of the liquid surface tension. Alternatively, the reaction parameters could be

calculated from measurement of the contact angle. Fowkes[5] proposed to separate the surface tension of each substance into additive components,

$$\gamma = \gamma^d + \gamma^h + \gamma^m \quad (4)$$

so that, for example, the surface tension of water, γ, would be equal to $\gamma^d + \gamma^h$ where γ^d is a component of the surface tension of water resulting from dispersion forces and γ^h the component resulting from hydrogen bonding forces. Likewise, the surface tension of mercury was described as equal to $\gamma^d + \gamma^m$ where γ^d is the dispersion component and γ^m the so-called metallic force component. Assuming that the dispersion component, γ^d, of the surface tension of one substance would interact with only the dispersion component of the surface tension of other substances, Fowkes used the geometric mean of the dispersion components, $(\gamma_1^d \gamma_2^d)^{1/2}$, as an interaction term.

$$\gamma_{12} = \gamma_1 + \gamma_2 - 2(\gamma_1^d \gamma_2^d)^{1/2} \quad (5)$$

By assuming $\gamma = \gamma^d$ for hydrocarbons and that water and mercury each interact with hydrocarbons only via the γ^d component, a γ^d for water and for mercury were calculated, by utilizing the known interfacial tensions of each against one or more hydrocarbons. Utilizing these values of γ^d for water and mercury, Fowkes then calculated an interfacial tension for the mercury-water interface on the basis of the speculative assumption that water and mercury interact with each other in the same manner that each interacts with hydrocarbons. The interfacial tension thus calculated was quite close to the experimentally measured interfacial tension of water and mercury, thus yielding the rather startling conclusion that water and mercury interact by means of dispersion forces only.

The apparent discovery that interaction at the interface of water and mercury involves only dispersion forces led Fowkes to extrapolate this principle to metal surfaces in general.[6] Previous experience with metal surfaces had shown that in the absence of a contaminating organic layer all metals are hydrophilic, i.e., water will spontaneously spread on their surfaces with a zero contact angle.[3] However, the "real" metal surfaces heretofore investigated contain combined oxygen (ranging in nature from a monolayer of chemisorbed oxygen to a thick layer of surface oxide) as a result of their exposure to the atmosphere. These

surface metal oxides are capable of strong hydrogen bonding interaction with water. Fowkes hypothesized that an atomically clean oxygen-free metal surface without this hydrogen bonding capability would interact by means of dispersion forces only, which would be inadequate to yield a zero contact angle. The surface of gold provided a convenient test for this hypothesis, since it is uniquely inert to oxygen and does not form a stable oxide phase.

In 1964 White[7] reported results of observations of the wetting of gold surfaces by water under atmospheric conditions. He obtained dropwise condensation from air saturated with water vapor under conditions of cleanliness during surface preparation and wettability measurement which were adequate to render base metals hydrophilic, i.e., able to spread water. He ultimately reported the contact angle as $60 \pm 5^{\circ}$.[8] In 1965 Erb[9] reported continuous dropwise condensation of water vapor in a gold-plated still at atmospheric pressure. Fused quartz and nonnoble metals were observed to yield filmwise condensation under these same conditions. Shortly thereafter, Bewig and Zisman[10] reported a water contact angle of 0° on a gold disk which had previously been heated to near melting in a flowing atmosphere of hydrogen (at atmospheric pressure) purified of organic contaminants. When the precautions against contamination of the flowing hydrogen were relaxed, the contact angle was no longer zero. The authors concluded that non-zero contact angles reported for water on gold were a result of hydrophobic organic contamination. White,[8] on the other hand, claimed that the zero contact angles observed by Bewig and Zisman resulted from hydrophilic contamination introduced during heating of the sample and by the embedding of alumina abrasive during previous sample polishing. In 1970[11] Bernett and Zisman reported the results of measurements of the contact angle of water on gold made under conditions designed to eliminate the possibilities of hydrophilic contamination which had been suggested by White and Erb. To avoid surface segregation of metallic impurities, the surface was not heated during preparation. The surface was polished with magnesia followed by leaching with hydrochloric acid to remove any residual embedded abrasive. A contact angle of 0° was found for water on this gold surface.

The contact angle of methylene iodide on glass had previously been investigated using ultrahigh vacuum techniques in surface preparation followed by in situ measurement of the contact angle by means of a vapor phase transfer procedure.[12] The latter consisted of admitting suitably purified vapor to the system, condensing the vapor in the sample chamber by means of a cold finger, and depositing a drop on the sample surface through magnetic manipulation. The contact angle was then read by means of a goniometer eyepiece mounted on a telescope. The purpose of the ultrahigh vacuum technique was to eliminate all traces of water in order to obtain and measure contact angles of methylene iodide on truly anhydrous surfaces.

In 1970 results were reported on the use of this technique of vapor phase transfer in ultrahigh vacuum to determine the contact angle of water on gold.[13] Water, of course, was substituted for methylene iodide, and the objective of eliminating organic contamination replaced that of eliminating traces of water from the sample surface. This was made possible by the complete absence of any organic components in the all metal and glass ultrahigh vacuum system. Contamination-free gold surfaces were prepared in this system by heating polished gold disks to successively high temperatures in the presence of oxygen followed by vacuum, or by evaporating gold films on smooth substrates in situ. The gold disk method was repeated in a conventional vacuum system for purpose of comparison.

A striking feature of the results was the hysteresis of the water contact angle which was observed during the various stages of surface activation of the gold disk. The hysteresis effect was observed in a number of different ways. (a) Freezing out the water vapor in the vacuum system after the drop was on the gold surface. As the drop evaporated, a receding angle was observed. Manipulations of the vapor pressure in vacuum eliminated the possibility that this was due to the effect of vapor pressure on the contact angle. (b) Observing the contact angle change with time. The drop may continue to spread for many hours. (c) Agitation of the drop. This caused immediate partial spreading

Upon raising the temperature and time of heating of the gold disk in air followed by evacuation, the receding angle decreased to zero, while the advancing angle decreased to about 20-30°. With more activation (increased heating) the advancing angle decreased further, while the receding remained zero. In the conventional vacuum system (Table I),[13] a limit was reached in the decrease of the advancing angle. Further activation either raised the angle or ceased to lower it. In the ultrahigh-vacuum system (Table II)[13] on the other hand, increased activation decreased the advancing angle to zero degrees.

Table I: Contact Angles on Gold Disk in Conventional Vacuum System (Reprinted with permission from reference 13. Copyright ACS).

Surface activation	Drop no.	Advancing angle, deg	Drop history after initial reading: time lapse from previous reading or mechanical agitation	Receding angle, deg
Vacuum, 100°, 3 hr	1	29	---	0
		19	Mechanical agitation	
Air, 570°, 1 hr, followed by vacuum, 580°, 1 hr	1	20	---	14
		18	Mechanical agitation	
	2	28	---	
Air, 580°, 2 hr	1	25	---	---
		14	Mechanical agitation	
	2	23	---	
		11	Mechanical agitation	
Vacuum, 600°, 1.5 hr	1	22.5	---	0
		11	Mechanical agitation	
	2	35	---	
		27	Mechanical agitation	
		20	10 min	
		15	30 min	
Air, 720°, 2 hr	1	30	---	---
		28	1 min	
		19	Mechanical agitation	
	2	48	---	
		37	Mechanical agitation	
Vacuum, 700°, 2 hr	1	28	---	---
		22	3 min	
		22	7 min	
		6	Mechanical agitation	
	2	26	---	
		11	Mechanical agitation	

Table II: Contact Angles on Gold Disk in Ultrahigh-Vacuum System (Reprinted with permission from reference 13. Copyright ACS).

Surface activation	Drop no.	Advancing angle, deg	Drop history after initial reading: time lapse from previous reading or mechanical agitation	Receding angle, deg
Vacuum, 560°, 2 hr	1	31	---	0
		16	Mechanical agitation	
Air, 1 Torr, 550°, 1.5 hr	1	6	---	---
	2	5	---	
Air, 710°, 2 hr, followed by vacuum, 710°, 1 hr	1	2	---	---
		0	1 Min	
	2	3	---	
		0	5 min	---
Air, 715°, 2.5 hr followed by vacuum, 715°, 2.5 hr	1	5	---	
		0	5 min	
	2	6.5	---	
		2	1 min	
		1	5 min	
		0	30 min	

For the case of gold films evaporated *in situ*, the contact angle of water on a gold film (Table III)[13] evaporated onto the surface of a polished fused silica disk was zero.

Table III: Contact Angles on Gold Film Evaporated in Ultrahigh-Vacuum System (Reprinted with permission from reference 13. Copyright ACS).

Run no.	Substrate	Film no.	Drop	Advancing angle, deg	Time after deposition of drop, min
1	Polished silica disk	1	First	Spread with low angle	---
			Subsequent	0	1
		2	First	10	1
				0	6
2	Polished silica disk	1	First	Spreading at low angle	1
				0	2
			Subsequent	0	1
3	Polished graphite disk	1	First	Spread at 5	---
			Second	8	1
				0	5

The system was evacuated again and another layer of gold deposited on top of the original. The contact angle was zero once more. A few minutes was sometimes required for the drop to reach the equilibrium zero value.

In another experiment the gold was deposited on a polished graphite surface. A zero contact angle was again observed a few minutes after deposition of the water drop. The contact angle of water on the graphite disk surface which was shielded from the gold vapor flux was approximately 22^{o}.

The existence of contact angle hysteresis as a result of contamination or heterogeneity on a smooth surface has been discussed by a number of authors.[14] The hysteresis observed in the work on gold can be attributed to the presence on these surfaces of both hydrophilic and hydrophobic areas, or site clusters. Increased surface activation resulted in an increased ratio of hydrophilic to hydrophobic areas, with an accompanying decrease in both advancing and receding angles, until a zero receding angle was obtained. At this point the average surface free energy less that of the liquid-solid interface was sufficient to overcome that of the water and keep it spread. The advancing angle was nevertheless still relatively high due to the inability of the drop periphery to advance across hydrophobic regions. The situation may be pictured on the basis of hydrophilic "islands" in a hydrophobic "sea." As the surface was activated further, the hydrophobic area continued to diminish with an accompanying decrease in the advancing angle until the hysteresis disappeared as the advancing angle reached zero.

It is clear from a comparison of the conventional high-vacuum and ultrahigh-vacuum experiments that the gradual increase in ratio of hydrophilic to hydrophobic area which occurs upon heating can be interpreted in terms of a gradual removal of hydrophobic organic contamination from the real gold surface. For the case of the measurements in conventional high vacuum, the activation procedure of high temperature oxidation and evacuation gradually cleans the surface, until there are sufficient uncontaminated hydrophilic areas to yield a low or zero receding angle, and an advancing angle of $20\text{-}30^{o}$. A point is reached at which additional activation is ineffective and may even result in

additional contamination. This is due to the fact that the conventional high vacuum is not an ultraclean system. Once the system is evacuated, the residual organic vapors have ready access to the gold surface, unimpeded by the presence of air. When the surface is partially cleaned, a steady state is established at which the rate of contamination equals the rate of vacuum clean up. However, in the ultrahigh-vacuum system which consists solely of metal and glass, there are no organic vapors to recontaminate the gold. The high temperature oxidation-evacuation procedure consequently continues to clean the surface until the hysteresis disappears and the advancing as well as receding contact angle is zero.

The inability of the conventional high-vacuum system to clean the gold surface is not observed for the case of a polished fused-silica surface. In the latter case preliminary heating to 200^{o} is adequate to yield a zero contact angle with water at room temperature. Using water contact angles as a measure of cleanliness, it is apparent that it is far more difficult to remove organic contamination from a gold than from a fused-silica surface. It is clear, then, that a set of conditions which is sufficient to decontaminate one particular surface will not necessarily succeed for a different type.

There is a possible objection to an interpretation of these results in terms of removal of organic contamination. When an impurity in a solid is capable of lowering the surface tension of the clean solid surface, the impurity will tend to migrate to the surface when the temperature is sufficiently high to allow diffusion to take place.[15] Assuming that the surface of real gold is hydrophobic rather than hydrophilic, the ultrahigh vacuum results for the solid gold sample could be explained in terms of hydrophilic impurities diffusing to the surface during the heat cleaning process, causing hysteresis at first, followed by a zero advancing angle as the surface becomes completely contaminated with the hydrophilic impurities. This explanation is not a very plausible one since the gold is 99.999+% pure and complete segregation, in a limited time, of impurities from a rather large volume to the surface would be necessary to contaminate a monolayer. Furthermore, for the case of the conventional high-vacuum results it would have to be

assumed that the hydrophilic impurities which make their way to the surface subsequently become contaminated by the residual organic vapors, thus preventing the ultimate attainment of a zero advancing angle. Nevertheless, the possibility cannot be completely ruled out on the basis of the solid disk experiments alone. However, the method involving evaporation and condensation of a gold film in situ completely bypasses this problem of surface segregation,[16] since the deposited film is very thin and furthermore is not heated.

For the case of any metal other than gold, an uncontaminated real surface would contain chemically combined oxygen, either as a built up surface oxide or as a chemisorbed monolayer. The attainment of a surface which is clean (oxygen free) as well as uncontaminated with organic material, would then entail a procedure such as ion bombardment to remove any chemically combined oxygen already present, followed by maintenance of a suitable ultrahigh vacuum to prevent oxygen from recombining with the surface before the measurement is completed. Of course, for the case of a film evaporated in situ, the ion bombardment is not necessary. In the present work, where water vapor is introduced for the measurement, extensive degassing of the water source is not necessarily sufficient to avoid introduction of a sufficient number of oxygen molecules to chemisorb to a few square centimeters of an active metal surface. For the case of metals in general, therefore, a special gettering technique[12] would have to be devised to ensure measurement on an oxygen-free surface.

The surface of gold, however, is unique among all metals in its relative lack of affinity for oxygen. It is the only metal which does not form a bulk oxide which is thermodynamically stable at room temperature. While this does not preclude the existence of a chemisorbed monolayer on the gold surface, available literature[17-19] indicates that such a monolayer will not form at room temperature, even at high oxygen pressure and much longer periods of time than the duration of these wettability experiments on evaporated gold films.

Investigation of the contact angle of water on clean metal surfaces was subsequently extended to active metals which form surface oxides, or chemisorbed oxygen monolayers, when exposed to oxygen.[20] In particular, the possibility was considered that clean metals do indeed interact

physically with water due to dispersion forces only. To understand why this can be so despite the observed contact angle of 0^{o} for water on gold, it was noted that the prediction that gold would be hydrophobic really involves two assumptions. First, that water will interact with the surface of clean gold according to the geometric mean rule by means of dispersion forces only. This assumption was basic to Fowkes' approach to the wettability of high-energy surfaces. Second, that γ^{d} for gold is too small to give sufficient interaction with γ^{d} of water to cause spreading. This means that γ^{d} of gold must be less than 236 ergs/cm^{2} if γ^{d} of water is taken as 21.8 ergs/cm^{2}. The second assumption, which is not basic to Fowkes' theory, is necessary to make gold a suitable test case. The only independent justification for this second assumption comes from a theoretical calculation by Fowkes[6] relating γ^{d} to the Hamaker constant (A_{12}), which in turn is calculated from data on the stability of gold sols in aqueous solution. This procedure has been criticized by Gregory,[21] who pointed out that "most interfacial interactions will involve nonadditive effects which would not contribute to longer range forces such as those between colloidal particles." It is nevertheless of considerable interest to determine if the method is useful at least as a semiempirical approach in predicting experimental results on the wettability of clean metal surfaces. Hamaker constants for gold particles in aqueous medium are calculated by Reerink and Overbeek[22] from data by Westgren[23] and Tuorila,[24] with the calculated values of A_{12} ranging over an order of magnitude from 0.05×10^{-12} and 0.1×10^{-12} erg calculated from Westgren's data to 0.6×10^{-12} erg from Tuorila's experiments. Fowkes obtains his maximum value of 120 ergs/cm^{2} for γ^{d} of gold from the latter value of A_{12}. More recently, however, a value of 4.1×10^{-12} erg for the Hamaker constant of gold has been reported by Derjaguin, Muller, and Rabinovich,[25] which yields a value of 464 ergs/cm^{2} for γ^{d}. Since this latter result extends the range of calculated γ^{d} values for gold well over 236 ergs/cm^{2}, the possibility may be considered that gold yields a zero contact angle with water as a result of the γ^{d} interaction alone.

Now, constants representing dispersion interactions have been calculated for some elements and compounds. The calculation is performed utilizing data, for example, from atomic scattering experiments or re-

fractive index measurements to determine parameters in London's ation which allow the calculation of the dispersion force constant. Among the elements, investigation has centered around the inert gases and alkali metals. In all cases, the dispersion or London constant increases going down any column in the periodic table. This is not surprising since the London constant is proportional to the square of the polarizability, and the latter quantity increases with increasing atomic size in any given column. Consequently, in the column copper-silver-gold, one would expect gold to have the largest London constant, silver next, and copper the least. This would also be the order of the Hamaker constants and the γ^d values for the case of gold and silver, where the atomic densities are essentially equal. The case of copper, with a larger atomic density than silver or gold, is harder to predict. However, if its London constant is sufficiently small in magnitude compared to that of silver, its γ^d will also be smaller. If γ^d of silver or copper falls below 236 erg/cm^2, a finite contact angle should be observed if the interaction is exclusively geometric mean of dispersion components.

The main experimental problem in measuring the wettability of clean copper and silver consisted of admitting water vapor without any accompanying trace of oxygen. The extreme precautions taken to accomplish this consisted of the following.[20] (1) Degassing the liquid water into the sorption pump by momentarily opening a valve and then closing it as the top water layer started to freeze from evaporation. This operation was performed 60 times. (2) The water was exposed to a chamber evacuated to the ultrahigh vacuum region by means of the ion pump. This operation was performed seven times. The water reservoir remaining after treatment according to this and the previous step served as the original source of water vapor throughout all the experiments with copper and silver. For some of the experiments with copper, the following step was added. (3) Prior to admittance to the sample chamber for contact angle measurement, water vapor from the degassed liquid was adsorbed onto clean (oxygen-free) germanium powder in an intermediate chamber and allowed to equilibrate for at least 1 hr (in experiment 4 the germanium was in the sample chamber manifold). The germanium had been previously cleaned by heating in vacuo at 700°,[26] and was regenerated after each run. Clean germanium rapidly

chemisorbs a monolayer of oxygen. The efficiency of the germanium powder was monitored in a separate experiment by deliberate adsorption of oxygen (after one of the 700° cleanings) which was measured by pressure difference with a thermistor pressure sensor. The amount of oxygen chemisorbed was approximately equal to that which would have been dissolved in the entire water reservoir if it were in equilibrium with the atmosphere. Since the reservoir was actually thoroughly degassed and since, furthermore, only a small portion of it vaporizes into the vacuum chamber for contact angle measurement, the capacity of the germanium powder far exceeded that necessary to completely free the water vapor of any possible oxygen residue.

The contact angles of water on copper for the various methods of removing possible residual oxygen from the water are listed in Table IV.[20]

Table IV: Contact Angle of Water on Deposited Copper Films under Various Conditions (Reprinted with permission from reference 20. Copyright ACS).

Experiment	Conditions	Contact angle, deg
1	H_2O thoroughly degassed	0
2	H_2O from 1 reused after frozen storage in chamber partially located in bakeout zone	20
3	O_2 admitted to drop of 2	20
4	Degassed H_2O exposed to clean Ge powder in sample chamber manifold	0
5	Degassed H_2O equilibrated with clean Ge powder in upper dosing chamber prior to admission to sample chamber manifold	0

The results of one through five were obtained before the quadrupole mass spectrometer was installed in the system. The experiments were consequently run in such a fashion as to successively eliminate possibilities of introducing oxygen contamination to the copper surface. The purpose was to obtain oxygen-free introduction of water vapor with as short and uncomplicated a procedure as possible. A reproducible hydrophobic con-

tact angle at any stage would of course indicate success in oxygen removal while simultaneously demonstrating the hydrophobicity of clean copper. On the other hand, continued zero angles would be inconclusive until the complete absence of oxygen could be independently demonstrated, at which point the hydrophilicity of clean copper would be established. It can be seen that with only one exception, the contact angle of water was 0^{o} throughout, culminating in the experiments where clean powdered germanium, of proven efficiency, was used to getter any possible residue of oxygen. In the lone experiment where a nonzero contact angle (20^{o}) was observed, the failure of a dose of clean oxygen to lower the angle indicated that the hydrophobicity was not due to the presence of a clean, oxygen-free surface, but rather to contamination which apparently resulted from organic ambients picked up by the recycled water during bakeout.

Upon installation of the quadrupole mass spectrometer in the vacuum system, pertinent portions of the experiments in Table IV[20] were repeated for the purpose of monitoring the ambients present at various stages of the experiments. The water utilized for contact angle measurements was monitored both by analyzing the atmosphere above frozen water and by leaking vapor from the liquid state. No indication of oxygen was found in the water reservoir after the 67 cycle degassing procedure, with or without additional purification with germanium powder. Exposure of the metal parts of the vacuum system, germanium powder, or evaporated copper to traces of water vapor tended to evolve hydrogen and sometimes carbon monoxide. The interaction of water vapor with deposited copper was found to produce hydrogen and carbon monoxide in varying amounts depending upon the conditions of evaporation.

The results of the determination of the contact angle of water on evaporated silver are given in Table V[20]. It can be seen that all

Table V: Contact Angle of Water on Deposited Silver Films (Reprinted with permission from reference 20. Copyright ACS).

Film	Drop	Contact angle, deg
1	1	0
	2	0
2	1	0
	2	0
	3	0

measurements yield a zero contact angle. Analysis of the gases produced by exposure of the first deposited silver film to water vapor at saturation yielded hydrogen and carbon monoxide in approximately equal amounts. The second film, on the other hand, yielded nearly all hydrogen on exposure to water vapor.

It is seen that measurements of the contact angle of water on evaporated films of copper and silver in ultrahigh vacuum fail to yield any evidence that clean, oxygen-free, metallic surfaces are hydrophobic. In fact, it is not completely certain that water can come into contact with these active surfaces without decomposing, since the exposure of clean copper or silver to even small amounts of moisture results in evolution of hydrogen. However, while this may be due to reduction of the water molecule by the surface, it is most probable that the phenomenon results from displacement of weakly chemisorbed hydrogen from the surface by the water molecules.

Since all three solid metals (gold, copper, and silver) thus far investigated yield a contact angle of 0^{o} with water,[13,20] there is no evidence to support the highly speculative proposal[6] that their interaction with water is confined to dispersion forces. Any theory must consequently take into account all possible modes of interaction between water and these high-free energy surfaces.

References and Notes

1. T. Young, Phil. Trans. Roy. Soc. (London) 95, 65 (1805).
2. W. D. Harkins and A. Feldman, J. Amer. Chem. Soc. 44, 2665 (1922).
3. H. W. Fox and W. A. Zisman, J. Colloid Sei. 5, 514 (1950).
4. L. A. Girifalco and R. J. Good, J. Phys. Chem. 61, 904 (1957).
5. F. M. Fowkes, J. Phys. Chem. 67, 2538 (1963).
6. F. M. Fowkes, Ind Eng. Chem. 56 (12), 40 (1964).
7. M. L. White, J. Phys. Chem. 68, 3083 (1964).
8. M. L. White and J. Drobek, J. Phys. Chem. 70, 3432 (1966).
9. R. A. Erb, J. Phys. Chem. 69, 1306 (1965).
10. K. W. Bewig and W. A. Zisman, J. Phys. Chem. 69, 4238 (1965).
11. M. K. Bernett and W. A. Zisman, J. Phys. Chem. 74, 2309 (1970).
12. M. E. Schrader, J. Colloid Interface Sci. 27, 743 (1968).
13. M. E. Schrader, J. Phys. Chem. 74, 2313 (1970).
14. For example, A. B. D. Cassie, Discuss, Faraday Soc. 3, 11 (1948).
15. L. A. Harris, J. Appl. Phys. 39, 1428 (1968).
16. P. W. Palmberg and T. N. Rhodin, Phys. Rev. 161, 586 (1967).
17. N. V. Kul'kova and L. L. Levckenko, Kinet, Katal 6, 765, 688 (1965).
18. B. J. Hopkins, C. H. B. Mee, and D. Parker, Brit. J. Appl. Phys. 15, 865 (1964).
19. W. M. H. Sachtler, G. J. H. Dorgelo, and A. A. Holscher, Surface Sci. 5, 221 (1966).
20. M. E. Schrader, J. Phys. Chem. 78, 87 (1974).
21. J. Gregory, Advan. Colloid Interface Sci. 2, 396 (1969).
22. H. Reerink and J. Th. Overbeek, Discuss. Faraday Soc. 18, 74 (1954).
23. Westgren, Ark. Kemi, Min. Geol. 7 No. 6 (1918).
24. Tuorila, Kolloidchem. Beih. 22, 191 (1926); 27, 44 (1928).

References and Notes

25. B. V. Derjaguin, V. M. Muller, and Ya. I. Rabinovich, Kolliod Zh. 31, 304 (1969).

26. A. J. Rosenberg, P. H. Robinson, and H. C. Gatos, J. Appl. Phys. 29, 771 (1958).

Organotin Polymers For Mitigating Ships' Hull Frictional Resistance

D.E. Gilbert, E.J. Dyckman, and J.A. Montemarano

Naval Ship Research and Development Center

Bethesda, Maryland 20034 U.S.A.

ABSTRACT

The manner in which fouling interferes with the proper functioning of ships' hulls demonstrates the importance of fouling prevention. The principal harm is that fouling effects an increased frictional resistance of the hull to movement in sea water, due in particular to roughening of the hull surface. In addition, fouling on the hull increases the boundary-layer thickness, thereby altering propeller efficiency and further decreasing ship performance. To alleviate this fouling, some novel, antifouling organotin polymers (OTPs)* of low-pollution-risk have been developed which to date exhibit excellent antifouling performance after 29 months of exposure to severe fouling conditions in Pearl Harbor, Hawaii.

These OTPs are viable candidates for increasing antifouling longevity of hull coatings, thereby maintaining desired ships' performance by mitigating the frictional resistance as the hulls move through sea water. Furthermore, it is probable that incorporation of hydrophilicity into OTPs will result in even superior performance of the antifouling hull coatings, because of the additional mitigation of frictional resistance ensuing from decreased hull surface roughness.

*OTPs have been referred to previously under the acronym OMPs (organometallic polymers).

Fouling of Ships' Hulls

Fouling is the growth of animals and plants on submerged surfaces. Its most widely publicized effect is on the efficiency of ships' propulsion systems. The fouling of ships reduces speed, increases fuel consumption, and results in losses in time and money during the application of remedial measures to ships' hulls. For example, it is conservatively estimated that a fuel reduction of as little as 1.0%, derived from an improved antifouling coating system, would save the Navy approximately 4 million dollars annually on the basis of current fuel prices.

Fouling immediately effects an increase in the resistance of the hull to movement through water - a phenomenon known as frictional resistance. For present purposes, it will suffice to point out that the accumulation of fouling may readily reduce the speed of the ship by several knots. For example, after six months out of dry dock in temperate waters, fouling caused a 50 and 45% increase in fuel consumption in maintaining speeds of 10 and 20 knots, respectively, for a cruiser with a standard displacement of 10,000 tons.[1] This same vessel experienced a loss of maximum speed of 1-1/4 knots. Similarly, a destroyer with a standard displacement of 1,850 tons experienced a 50 and 35% increase in fuel consumption to maintain speeds of 10 and 20 knots, respectively; its loss of maximum speed was 2 knots.[1] In addition to the skin friction effect, fouling on the hull further decreases ship performance by increasing boundary-layer thickness, thereby altering propeller efficacy.[2,3]

Consequently, any improvement in antifouling hull-coating technology will result in substantial savings. Longer-lived antifouling coatings applied to ships' hull accomplish the following:

1. Ships can remain at sea for longer periods with inconsequential reduction in speed or increase in fuel consumption due to fouling.

2. Dry docking loads are reduced.

3. The demands for fuel by the fleet are reduced.

4. Fewer tankers are required to service the fleet.

The time required for ships to foul depends on the efficacy of the antifouling hull coating, which is destroyed by the action of sea water and the breakdown of the coating. Once the coating is damaged, fouling may develop rapidly and cover the unprotected surface within a few weeks. The tendency of ships to foul depends on the time spent in port since the larvae of many fouling organisms have difficulty in attaching to submerged surfaces when the velocity of the water across the surface exceeds one knot.[1] At greater speeds, the growth of some organisms previously attached is also suppressed, and at high speeds the attached organisms may be washed away.

The manner in which fouling interferes with the proper functioning of ships' hulls demonstrates the importance of fouling prevention. The principal harm is that fouling effects an increased frictional resistance of the hull to movement in sea water, due in particular to roughening of the hull surface.

The total resistance of a ship moving at the surface of water is generally considered to be the sum of two components: (1) the frictional resistance and (2) the residual resistance.[1] The frictional resistance results from tangential stresses due to the drag of the water moving parallel to the hull. The residual resistance,* on the other hand, results from the distribution of pressure which develops about the hull because of the waves and eddies caused by the ships' motion.

*It is usual practice to combine the wavemaking and pressure resistances into one term, called the residual resistance.

The condition of a ship's hull, as determined by the character of the paint coating and the degree to which the coating permits corrosion or fouling, may be expected to affect the frictional resistance primarily. When the hull is clean, the value of the frictional resistance relative to the total ship resistance emphasizes the importance of keeping the frictional resistance to a minimum. This point is emphasized further by examining Figure 1 which contains the results of the analysis of the total resistance of the Japanese destroyer YUDACHI.[1] It can be seen that at normal speeds the residual resistance constitutes only a relatively small portion of the total resistance. In the inset of the figure, the frictional resistance is expressed as a percentage of the total resistance at different speeds. At a speed of 10 knots, the frictional resistance accounts for 85 percent of the total resistance; whereas at 26 knots, the

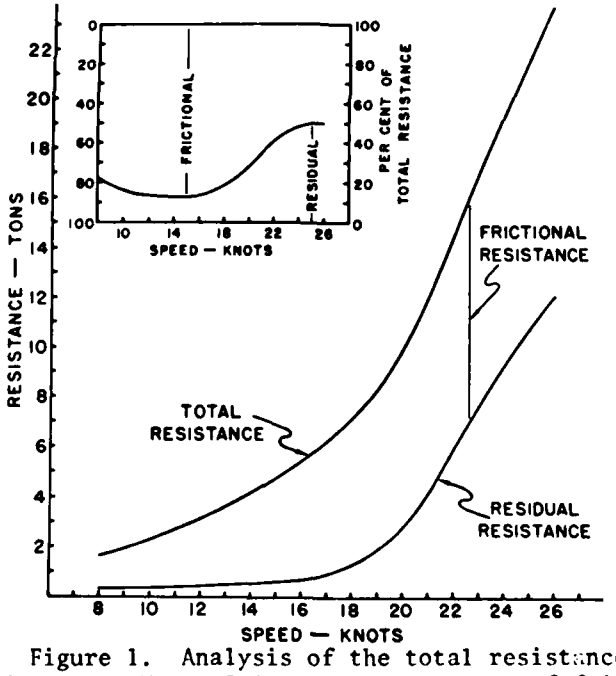

Figure 1. Analysis of the total resistance of the destroyer YUDACHI into its components of frictional and residual resistance at various speeds. Inset. Percentage of total resistance due to frictional and residual resistance at different speeds.

frictional resistance amounts to only 50 percent of the total resistance. Therefore, as speed increases, the percent frictional resistance abates. In addition to fouling affecting frictional resistance, surface roughness[4,5] and slimefilms[1] also increase this resistance. Lackenby[4] found that for new ships, the shaft horsepower required for a given speed increased with the surface roughness. Similarly, Todd[5] has documented an increase in the frictional resistance coefficient of painted friction planes with larger Reynolds numbers or greater surface roughness. A number of observations indicate that the frictional resistance of a submerged surface increases with the immersion time in the absence of macroscopic fouling.[1] This increase is attributed to microscopic fouling - the formation of a slime film.

The purpose of antifouling coatings is to keep the frictional resistance to a minimum for a maximum period of time. The inherent surface roughness of the hull coating becomes important only in the absence of microscopic or macroscopic fouling. Therefore, the final value of an antifouling coating is judged during ship's trials, for example, its sliming and fouling prevention.

Prevention of Fouling

Development of novel, low-pollution-risk, antifouling organotin polymers (OTPs) advance the state-of-the-art in antifouling technology and promise to advance the state-of-the-art of antifouling hull coatings. At present the life of antifouling coatings, based on cuprous oxide, is only from three to eighteen months,[6] mainly due to excessive leaching of the cuprous oxide. Cuprous oxide coatings possess several other disadvantages. They do not prevent algae build-up (grass) along the waterline; they cause galvanic corrosion of bare hull areas; and they are deficient in pigment retention, thus providing ships' hulls with deficient camouflage protection. On the other hand, organotin salts, i.e., bis-tri-n-butyltin oxide, tri-n-butyltin fluoride, and triphenyltin fluoride,

are extremely powerful biocides, being toxic to a wide range of marine organisms. Consequently, organotin salts are the basis of a variety of antifouling coatings. In addition, the use of organotins in antifouling coatings has received additional impetus because these coatings do not accelerate corrosion nor inhibit pigmentation.[6]

Due to the fact that state-of-the-art antifouling technology has not provided a means of controlling the leaching rate of toxic moieties into the marine environment, the Naval Ship Research and Development Center introduced the idea of chemically binding biocidal organotin salts in polymer backbones. It is theorized that OTPs are surface hydrolyzed in sea water to grigger their antifouling effectiveness. Laboratory studies have shown that chemically bound organotin moieties are released at a rate that is dependent on the nature of the OTPs. In an effort to develop antifouling coatings possessing the lowest possible controlled leaching rates, various OTPs were synthesized and, in addition, the rates of release of organotin moieties from these polymers were determined, as well as their antifouling effectiveness. Factors which influence the rate of hydrolysis of OTPs include polymer type, degree of cross-linking within the polymer backbone, the degree of substitution by organotin groups along the polymer backbone, and sea water temperature, salinity, oxygen content, hydrogen ion concentration and turbulence. The service life of low-leaching 20 mil organotin coatings is estimated to be 5 years.[6]

To date, the feasibility of OTPs as antifouling materials has been demonstrated by more than two years of continuous excellent antifouling performance. Patch panel trials for the evaluation of the antifouling performance of OTPs were conducted at Naval Shipyard, Pearl Harbor, Hawaii and at Miami Beach, Florida. The OTPs controlled the growth of marine fouling organisms including bacteria, algae, tubeworms, and barnacles. Exposure indicates that the

optimum antifouling performance may be expected from the OTPs which possess organotin moieties such as tributyltin and/or tripropyltin. For example, poly (trimethyltin acrylate) and poly (triphenyltin acrylate) exhibited low resistance to tubeworm growth, whereas polymers containing tributyltin and/or tripropyltin groups showed excellent antifouling performance. These results agree with previous studies[7] which show that the most effective organotin groups are those which contain 9 to 12 carbon atoms, for example tripropyl or tributyl groups.

Sea water solubility studies show that OTPs, while possessing good antifouling effectiveness, release organotin moieties at a rate of at least one order of magnitude less than a state-of-the-art tributyltin fluoride-base antifouling hull coating. During five weeks of agitation in artificial sea water poly (tributyltin methacrylate/methyl methacrylate) had released 45% less organotin ions than poly (tributyltin methacrylate). This indicates that the release rate of organotins can be controlled by chemically modifying the polymer matrix. Currently, experiments are being conducted to determine the relationship between various polymer matrices and the release rate of organotin moieties.

The success of OTPs can be summarized by: (1) OTPs are proven effective antifouling agents. (2) Chemically binding the toxic organotin moiety in the OTP provides a low leaching rate, thus offering a longer service life and negligible environmental impact. (3) Optimum antifouling performance of OTPs is obtained by chemically modifying the polymer matrix. (4) Incorporation of two or more different types of organotin moieties widens the kill spectrum of the OTPs. (5) OTPs may be synthesized with air pollution exempt solvents.

Next, let us turn our attention from the general consideration of antifouling OTPs to the specific case of incorporating frictional-resistance

properties into these materials. It appears feasible that by reducing the surface roughness of ships' hull coatings the frictional resistance of a ship's hull moving through sea water may be mitigated. This theory is supported by a commercially available hydrophilic acrylic polymer coating which, according to a manufacturer's data, shows a maximum 4% savings in fuel consumption over conventional hull coatings. In addition, NSRDC data show a maximum 3% reduction in frictional resistance using the same coating. It is hypothesized that hydrophilic polymers inhibit turbulent flow near the hull surface and concomitantly retard the onset of hull surface degradation. Based on the aforementioned hypothesis, it is speculated that incorporating hydrophilic groups into the OTPs will permit these antifouling materials to further mitigate ships' hull frictional resistance.

Conclusions

It has been shown by previous investigators that the frictional resistance of the ships' hull moving through water constitutes the major portion of the ships' total resistance, this percent contribution being more significant at lower speeds. The manner in which fouling interferes with the proper functioning of ships' hulls demonstrates the importance of fouling prevention, the principal harm being that fouling effects an increased frictional resistance ensuing from roughening of the hull surface. In addition, fouling on the hull increases boundary layer thickness, thereby altering propeller efficacy and further decreasing ship performance. To alleviate this fouling, some novel, low-pollution-risk, antifouling organotin polymers (OTPs) have been developed which, to date, continue to exhibit excellent antifouling performance after 29 months of exposure to severe fouling conditions in Pearl Harbor, Hawaii.

These OTPs advance the state-of-the-art in antifouling technology. At present, the life of conventional antifouling coating formulations, based on

the physical mixture of cuprous oxide in paint resins, is only from three to eighteen months. This short life is principally due to excessive leaching of the cuprous oxide. To combat excessive leaching and thereby decrease the threat of pollution, the Naval Ship Research and Development Center has introduced the innovative concept of chemically binding biocidal organotin salts in polymer backbones. The success of this concept has been borne out by more than two years of successful antifouling performance at Pearl Harbor, Hawaii. It is theorized that the antifouling efficacy of OTPs is catalyzed by surface hydrolysis in sea water. Laboratory studies have shown that the rate of release of biocidal organotin moieties from OTPs depends on the structure of the polymer. Other factors which influence this rate include: degree of cross-linking within the polymer chain, degree of substitution by organotin groups along the polymer chain, and sea water temperature, salinity, oxygen content, hydrogen ion concentration, and turbulence.

These OTPs are viable candidates for increasing antifouling longevity of hull coatings, thereby maintaining desired ships' performance by mitigating the frictional resistance of ships' hulls moving through sea water. However, it is probable that incorporation of hydrophilicity into antifouling OTPs will result in even superior performing antifouling hull coatings, because of additional mitigation of frictional resistance due to decreased hull surface roughness.

References

1. Woods Hole Oceanographic Institution, Marine Fouling and Its Prevention, United States Naval Institute, Annapolis, Maryland (1967).

2. Kan, S., H. Shiba, K. Tsuchida, and K. Yokoo, "Effect of Fouling of a Ship's Hull and Propeller Upon Propulsive Performance," I.S.P., 5 (41), (1948).

3. Levine, H. G. and S. Hawkins, "Comments on Service Margins for Ships," Robert Taggart Incorporated (1969).

4. Lackenby, H., "Ship Performance and the Effect of Hull Surface Condition," Corrosion Prevention and Control, 91(8), 31 (1962).

5. Todd, F. H., "Skin Friction Resistance and the Effects of Surface Roughness," Transactions of the Society of Naval Architects and Marine Engineers, 59, 351 (1951).

6. Dyckman, E. J., J. A. Montemarano, and E. C. Fischer, "Antifouling Organometallic Structural Plastics," Naval Engineers Journal, April (1974).

7. Luijten, J. A. A. and G. J. M. Van Der Kerk, Investigations in the Field of Organotin Chemistry, Middlesex, England: Tin Research Institute (Oct 1955).

CONCLUDING REMARKS

A. Walz
Technische Universität Berlin

The First Symposium on Fluid-Solid-Surface Interaction at Meersburg, Germany, in May 1972, was principally a public relations effort for a very special and more or less future-oriented field of research activity, which, however, was justified by remarkable initial results. At that time it was not easy to be optimistic about the early application of research based on limited theoretical and empirical results and estimates. It was, however, not difficult to describe and define the positive consequences for the whole field of applied fluid mechanics if this research achieved its main goals. These facts and the availability of highly qualified and experienced teams of scientists warranted the German Government's sponsorship of these research programs for a reasonable period of time.

The First Symposium also started with a secondary objective: to demonstrate the necessity for close cooperation of more or less diverse disciplines, such as continuum mechanics, theoretical physics, solid-state physics, and physical chemistry, to insure a good chance of success.

Analysis of the papers of this Second Symposium has shown that during the past two years some progress has been made in both the completion of the theoretical basis and the solution of technological problems. The following reports are representative of the state of the art at this Second Symposium: the paper by K. Bärwinkel (Dornier System) bridged the gap between continuum mechanics and recent results in the field of gas kinetics. These investigations show that, at realistic altitudes of about 20 km at flight Mach-numbers between 2.5 and 3, reductions in the friction coefficient c_f of about 5

to 10% may be expected. The related momentum accommodation coefficient α_m is, according to Bärwinkel's calculations, about 10^{-2}. Very low values of α_m have been measured on specially prepared gold surfaces by M. Seidl and E. Steinheil. For the same solid-surface and the same flight conditions, the achievable reduction of the energy accommodation coefficient α_E and the relating heat transfer coefficient (as a decisive parameter in energy balances of thermo-fluid dynamics) will be much greater due to the smaller effect of molecular roughness as shown in the analysis of Bärwinkel and confirmed by D. Menzel in his paper presented at the First Symposium.

There is no doubt that these latter results on possible heat transfer reduction by special solid surface preparation may have enormous practical importance. It seems to be possible to keep the surface of high speed flight vehicles cool by treating portions of the surface so that they have small values of α_E.

Preliminary investigations have been started and reported on the problem of liquid-solid surface interaction which predominates in Navy projects. There is a general lack of basic theories in this matter. Liquid-solid surface interaction modes for the molecular contact layer must be quite different from those applicable to gas-solid surface interaction. The concept of "wettability" described in the paper by M.E. Schrader (NSRDC) may play an essential role in these problems.

APPENDIX

Titles of Papers Presented at the First Symposium on Gas-Solid Surface Interaction, 3-5 May 1972, Meersburg, Germany

Simmler, W., German Ministry of Defense. Opening Remarks (in German).

Walz, A., Technical University Berlin, FRG*. The Connection between the Aerodynamic Coefficients of a Flying Body and the Type of Boundary Condition (in German).

Lugt, H.J., Naval Ship Research and Development Center, Bethesda, Md., U.S.A. Laminar Flow Past Bodies under Perfect Slip (in English).

Lehmann, V., Dornier System, Friedrichshafen, FRG. The Connection between Gas-Surface Interaction and the Boundary Conditions of Gas Dynamics (in German).

Pauly, H., Max-Planck-Institut für Strömungsforschung, Göttingen, FRG. Technology and Applications of Molecular-Beam Investigations (in German).

Hollstein, M., et al., Dornier System, Friedrichshafen, FRG. Measurements of Gas-Surface Interaction with an UHV Molecular-Beam Device and with Gas-Friction Apparatus (in German).

Hays, W.J., et al., University of California, Los Angeles, California, U.S.A. Effects of High-Energy Incident Molecular Beams on Surface Characteristics (in English).

Müller, W.J.C., Dornier System, Friedrichshafen, FRG. Theoretical Investigations on the Scattering of Molecular Beams at Solid Surfaces (in German).

Bossel, U., Aerodynamische Versuchsanstalt Göttingen, FRG. Generation of Intense Molecular Beams of Suborbital Energies for Scattering Experiments (in German).

Gebhardt, E., Max-Planck-Institut für Metallforschung, Stuttgart & Rieger, H., Dornier System, Friedrichshafen, FRG. Boundary Phenomena at Solid Surfaces (in German).

---

* Federal Republic of Germany

Rieger, H., Dornier System, Friedrichshafen, FRG. Influence of Solid Properties on Gas-Surface Interaction (in German).

Menzel, D., Technical University Munich, and
Kouptsidis, J., Deutsches Elektronensynchroton Hamburg, FRG. The Mechanisms of Energy Transfer During Impact at Solid Surfaces (in German).

Devienne, F.M., Laboratoire de Physique Moléculaire des Hautes Energies, 06 Peymeinade, France. Application of the Techniques of High-Energy Molecular Beams to the Study of Solid-Gas Interface (in English).

Fromm, E., Max-Planck-Institut für Metallforschung, Stuttgart, FRG. Surface Reactions of Oxygen and Nitrogen with Evaporated Metal Films (in German)

Bärwinkel, K., Dornier System, Friedrichshafen, FRG. Statistical Theory of Adsorption (in German).

Morrison*, S.R., and Hauffe, K., University of Göttingen, FRG. Surface Phenomena of Zinc Oxide Treated with UV Rays (in German).

Seidl, M., Dornier System, Friedrichshafen, FRG. Influence of Properties of Chemisorption and Adsorption on Solid Surfaces by means of Treatment and Doping (in German).

Trepte, L., Dornier System, Friedrichshafen, FRG. Investigation of Oxydation Effects on Cu (in German).

Zei, M.S. and Block, J.H., Fritz-Haber-Institut der Max-Planck-Gesellschaft, Berlin, FRG. Occurrence of Carbonium Ions on Solid Surfaces by Means of Field Ionization Mass Spectrometry (in German).

Schrader, M.E., Naval Ship Research and Development Center, Annapolis, Maryland, U.S.A. Oxidation and Other Contamination of Gold Surfaces (in English).

Christmann, K. and Ertl, G., Technical University Hannover, FRG. CO Adsorption on Mono-crystalline Ag/Pd alloys** (in German).

---

* Visitor from the Stanford Research Institute, Menlo Park, California, U.S.A.

** Detailed publication will appear in Surface Science.

Sarholz, W. and Baresel, D., Robert Bosch GmbH., Stuttgart, FRG. On the Connection Between the Electro-catalytic Activity of Various Hard Materials For the Oxidation of Hydrogen and Formaldehyde and the Symmetry of their Surface Complexes (in German).

Forstmann, F., Fritz-Haber-Institut der Max-Planck-Gesellschaft, Berlin, FRG. Recent Results on the Interpretation of Diffraction Experiments with Slow Electrons (in German).

Gronau, K.H., German Ministry of Defense. Epilogue (in German).